博士論文

Study on Single Photon Emission from III-Nitride Interface-Fluctuation Quantum Dots

（窒化物半導体界面揺らぎ量子ドットからの単一光子発生に関する研究）

平成 29 年 12 月 01 日提出

指導教員　荒川　泰彦

東京大学大学院工学系研究科

電気系工学専攻

37－157084

高　亢

To my wife 杨 纯一

&

My parents

Preface

This thesis presents a part of the research carried out at Institute of Industrial Science (IIS) of the University of Tokyo, where the author was a graduate student in the Department of Electronic Engineering from April 2015 to March 2018.

Professor Yasuhiko Arakawa has supervised the research in this thesis.

In this thesis, original study on single photon emission from III-Nitride interface fluctuation quantum dots are presented.

December 01, 2017

Kang Gao

Acknowledgement

I would like to express my sincere gratitude to my supervisor, Professor Yasuhiko Arakawa, for his constant guidance, encouragement, and support throughout this thesis. His insights and enthusiasm for science will certainly benefit me through my following career.

I am deeply indebted to Professor Mark James Holmes, who was kind enough to guide me to be a real scientist. His excellent insight led me to the proper direction in this work. He opened my eyes on the beauty of experimental physics.

I want to thank Professor Satoshi Iwamoto, for all his concerns and help on my study during the past three years.

I would like to thank other three professors in thesis defense committee for my PhD Degree, Professor Tsutomu Shimura, Professor Kazuhiko Hirakawa, and Professor Masahiro Nomura.

I must thank Professor Munetaka Arita for his excellent fabrication of the GaN interface fluctuation quantum dot.

I need to thank my friend, Mr. Florian Le Roux, who teach me a lot and work with me together in the experiment of temperature dependence study.

I would like to thank Dr. Satoshi Kako, Dr. Masao Nishioka, and Mr. Satomi Ishida for their technical support in the lab.

I want to thank Dr. Renchun Tao and Dr. YuanHsuan Jhang for their kindly help during three years.

I need to thank Miss. Ritsuko Nara and Miss. Miwa Ouchi for their kindly assistant work for my research.

I would like to thank Professor Takeshi Kamijoh, Professor Yasutomo Ota, Dr. Toshio Saito, Dr. Alto Osada, Dr. Masahiro Kakuda, Dr. Jinkwan Kwoen, Dr. Bongyong Jang, Dr. Katsuyuki Watanabe, Dr. Takeyoshi Tajiri, Mr. Koya Otokozawa,

Mr. Yoshihiro Nambu, Mr. Takahiro Doe and other researchers in our lab for their kindly help.

I want to thank Mr. Wenbo Zhan, Mr. Chee Fai Fong, Mr. Hirofumi Yoshikawa, Mr. Ingi Kim, Mr. Kazuhiro Kuruma, Mr. Jueon Park, Mr. Huy Vo Quoc, Mr. Akihito Tamada, Mr. Takeshi Ishida, Mr. Ryota Katsumi, Mr. Fumio Maehara, Mr. Wenbo Lin, Mr. Takuto Yamaguchi, Mr. Yang Mei, Mr. Zhaoyin Sun and other students in our lab. I also would like to thank all the others who have helped me during the past three years.

I must acknowledge the financial support from Japanese Government (MEXT) Scholarship Program for the three and a half years.

Finally, I want to thank my family, for their eternal love.

Abstract

Semiconductor quantum dots have been intensively studied because their atomic-like electric characteristics are expected to bring significant progress in optical and electric device applications. Single photon sources based on semiconductor quantum dots have attracted extensive attention due to their solid-state nature, high emission purities, and a large possible emission wavelength range, thanks to their possible applications in secure communication and quantum information processing. In particular, it has been shown that III-Nitride quantum dots can operate at high temperature and at the wavelength ranging from the Ultraviolet all the way to Infrared due to their large band offsets and wide ranges of bandgaps. However, III-Nitrides quantum dots have their limitations because they suffer from a spectral diffusion induced linewidth broadening (which can result in emission linewidths up to a few meV), compared with their III-V counterpart such as Arsenide. This spectral diffusion occurs due to an interaction between the internal-field induced exciton permanent dipole moment and the fluctuating electric field of charges trapped in relatively large densities of surrounding defects.

The interface fluctuation GaN quantum dots, have been successfully fabricated in recent years through a metal−organic chemical vapor deposition reactor. Thanks to the improved crystal quality with a low density of defects around the quantum dots, such interface fluctuation GaN quantum dots have been shown to exhibit a record narrow linewidth, as low as 87 μeV. This narrow linewidth is thought to be from the suppression of the inhomogeneous broadening down to the order of its limitation. Meanwhile, unprecedented purity of ultraviolet single photon emission has been obtained by such material system. In this thesis, we will focus on the investigation of the optical properties of interface fluctuation GaN quantum dots to achieve high-quality quantum sources.

In the beginning, we present the optical systems to perform the basic photon auto-correlation study by using a macroscopic photoluminescence measurement and Hanbury Brown and Twiss type correlation setup. Time-Integrated and time-resolved measurements of the ultraviolet luminescence can be realized to investigate the single photon emission properties from III-Nitride interface fluctuation quantum dot.

Secondly, we show the temperature dependence of the single photon emission from interface fluctuation GaN quantum dots and discuss their single photon purity decreasing due to the increased spectral contamination from uncorrelated background emission related to quantum-well states. Quantum light emission is confirmed at temperatures up to ~ 77 K, by which point the background emission degrades the emission purity and results in a measured photon auto-correlation $g^{(2)}(0)$ in excess of 0.5. A discussion on the extent of the background contamination is also given though the comparison to extensive data taken under various ambient and experimental conditions, revealing that the quantum dots themselves are emitting single photons with high purity. This result reveals that it is possible to improve temperature characteristics achieved by reducing the volume of measured material- perhaps via the fabrication of mesa-like structures, or by local resonant excitation.

Furthermore, we have measured the exciton recombination time in a GaN interface fluctuation quantum dot using photon auto-correlation measurements. The exciton decay time of such a dot is evaluated to be 2.0 ± 0.1 ns by power dependent single photon dynamics. By comparing this measurement to the literature results of typical III-nitride quantum dots, we find that the lifetime measured for such an interface fluctuation quantum dot compares very well with that for typical Stranski Krastanow GaN quantum dots emitting around the same energy. As both the lifetime and permanent dipole moment depend in effect on the separation of the electron and hole wavefunctions, this result has been used to infer that the relatively narrow emission linewidths of these quantum dots are likely resulting from a comparatively cleaner environment around such quantum dots, not from any inherent difference in the

quantum dots themselves. These GaN fluctuation quantum dots may become an important technical solution for III-nitride based quantum sources, but will also act as a good platform for the study of fundamental properties of III-nitride nanostructures.

Finally, we investigate the temporal evolution of the emission spectrum of an excitonic emission line from a single GaN interface fluctuation quantum dot. The extremely stable emission line shows that the extent of any spectral wandering (long-term spectral diffusion) is much smaller than the energy resolution limit of our system. We develop the typical characteristic spectral diffusion time scale in the single photon emission of a GaN interface fluctuation quantum dot by using photon auto-correlation measurement with the careful spectral selection via the spectrometer and its exit slit connected onto the HBT setup. For the first time, the spectral diffusion time scale in III-Nitride quantum dot system was evaluated be the order of ~20 nanoseconds. We have also presented the excitation power dependence of the spectral diffusion rate, showing the expected increase in rate as the excitation power is increased. It shows that indistinguishable photons may be produced from such quantum dots under excitation with pulse pairs separated by times less than such spectral diffusion time scale.

These results will have important consequences for the generation the high purity of the single photon emitters towards the generation of the indistinguishable photons. This study will be a useful step towards the practical realization of high-quality quantum optoelectronic devices using the technologically important III-Nitride material system.

Contents

1. Introduction

Quantum information science is an exciting new area of study based on the information science depends on quantum effects. It has been proposed and improved in past decades in a large range of quantum technique including quantum computing, [1-5] quantum teleportation, [6-8] and quantum cryptography. [9-12]

Single photon sources play a key role in many quantum technologies. [13-19] After decades of rapid advances, high-quality single photon sources are still required for a range of quantum information processing applications. [20-22] In this thesis, we will focus on the investigation of the optical properties of III-Nitride QDs to achieve high-quality quantum sources.

1.1 Quantum Dots

Quantum dot (QD) is a nanocrystal structure made of different semiconductor materials that is small enough to exhibit quantum properties.

QDs are often referred to as 'artificial atoms' as well. Attributed to the three-dimensional quantum confinement of electrons and holes, QDs are usually believed to be good candidates to improve the performance of the semiconductor optical devices.

As a high-performance laser devices superior to quantum well lasers, semiconductor QD has drawn more and more attention in the recent few decades, since it was theoretically predicted by Arakawa and Sakaki in 1982. [23]

1.1.1 Quantized Energy Levels

Atoms or molecules are easy to expect to have specific discretized energy levels. Crystals, which consists a large number of atoms and have periodic structures, on the other hand, have continuum energy levels.

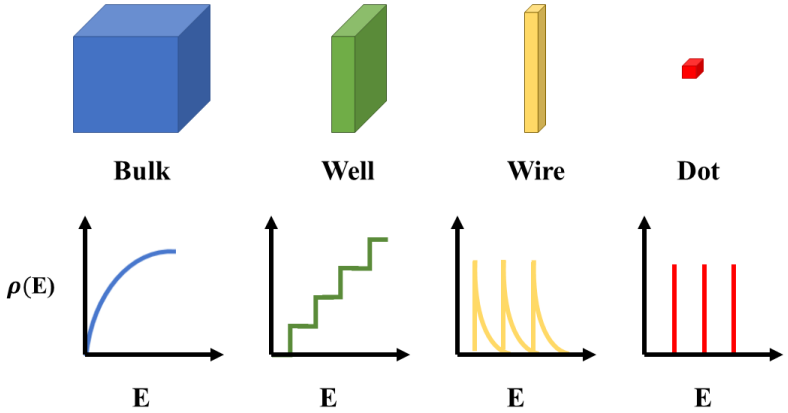

Figure 1-1. The state density of the bulk (3D), quantum well (2D), quantum wire (1D) and quantum dot (0D).

Figure 1-1 demonstrates the comparison of the structure and the state density of the bulk (3D), quantum well (2D), quantum wire (1D) and quantum dot (0D).

Compare with the quantum well structure where the thickness L_X is reduced to the similar order of de Broglie wavelength λ, in the quantum wire structure where the length L_Y and in the QD structure where the length L_Y and the width L_X are also reduced down to the order of the λ, after calculation, the state density of i-dimensional (i=1, 2, 3) quantum structures is expressed as follows:

$$\begin{aligned}
\rho^{(3D)}(\varepsilon) &= \frac{\left(2m/\hbar^2\right)^{3/2}}{\left(2\pi^2\right)}\sqrt{\varepsilon} \\
\rho^{(2D)}(\varepsilon) &= \sum_n \frac{m}{\left(\pi\hbar^2 L_z\right)} H\left[\varepsilon - \varepsilon z(n)\right] \\
\rho^{(1D)}(\varepsilon) &= \sum_{n,l} \frac{\left(m/2\hbar^2\right)^{1/2} \Big/ \left(\pi L_y L_z\right)}{\left[\varepsilon - \varepsilon y(l) - \varepsilon z(n)\right]^{1/2}} \\
\rho^{(0D)}(\varepsilon) &= \sum_{n,l,k} \frac{1}{\left(L_x L_y L_z\right)} \delta\left[\varepsilon - \varepsilon x(k) - \varepsilon y(l) - \varepsilon z(n)\right]
\end{aligned} \tag{1-1}$$

where $\hbar$ is Planck's constant, m is the electron effective mass, ε is the energy measured from the conduction-band edge, $H(\varepsilon)$ is a unit step function with $H(\varepsilon > 0) = 1$ and $H(\varepsilon < 0) = 0$, and $\delta(\varepsilon)$ is the delta function. $\varepsilon x(k)$, $\varepsilon y(l)$ and $\varepsilon z(n)$ respectively represents the quantized energy levels with the quantum numbers n, l and k. In the case of that the barrier is relatively high enough, the quantum levels are given by:

$$\begin{cases}
\varepsilon z(n) = \left(\hbar^2\pi^2/2m\right)\left(n/L_z\right)^2 \\
\varepsilon y(l) = \left(\hbar^2\pi^2/2m\right)\left(l/L_y\right)^2 \\
\varepsilon x(k) = \left(\hbar^2\pi^2/2m\right)\left(k/L_x\right)^2
\end{cases} \tag{1-2}$$

As proposed above, the delta function-like density of states of a QD is believed to have a great potential to improve semiconductor laser performance. Two most common improvements are ultralow threshold current density and higher operating temperature.

Also, the QD has a strong ability in many kinds of applications, not only as the semiconductor QD lasers but also as others such as the single photon source, the light-emitting diodes, the infrared photodetectors, the solar cells, the biochemical analysis and the entanglement devices. [24]

1.1.2 Optical Performance

Most usual method to investigate the physics of the QDs is to detect them optically. The theoretical tool in our measurement setup is the photon excitation on the QD by lasers and to probe its micro-photoluminescence.

As shown in figure 1-2, the two most popular ways to excite the QD are the above-bandgap and resonant excitation.

In above band excitation, the laser is tuned above the bandgap of the matrix. The electron-hole pairs are generated in the environment of the QDs. The capture of these carriers occurs first by the wetting layer or quantum well structure. Then they will fall into the higher excitation states of this QDs and keep falling to the ground state of the electron and hole of the QD. After this process the recombination of the electron and hole occurs and a photon emits out which is the principle of the single photon generation from a single QD.

The above band excitation is usually considered as an easy excitation method because it is relatively efficient.

On one hand, this kind of excitation, which is so-called ‘Non-Resonant Excitation’ allows us to excite the QD in a large volume of the matric acts as absorber.

On the other hand, this method allows a non-accurate tuned wavelength of the excitation laser. In principle, the laser which photon energy larger than the bandgap can

be used to excite the QD (although in the practical measurement the difference of the laser photon energy and the QD emission energy should also in consideration).

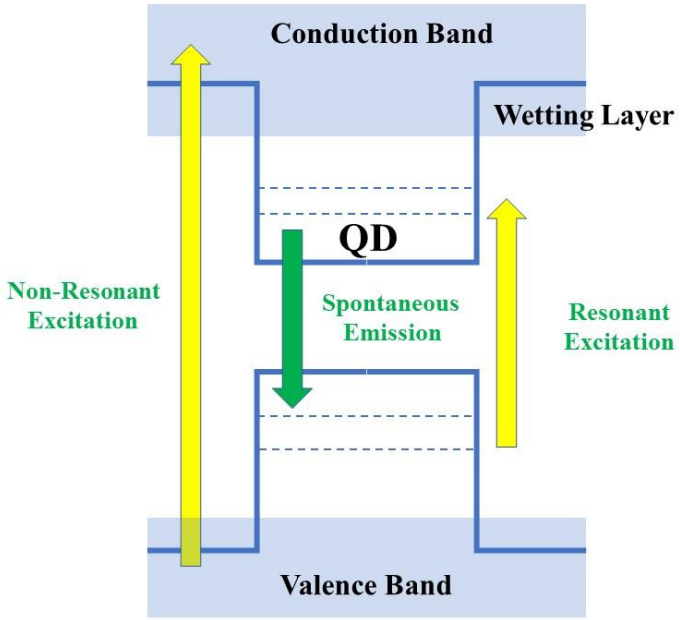

Figure 1-2. Schematic energy-level diagram of the above-bandgap and resonant excitation of the QD.

The resonant excitation is always required the excitation laser tuned to a higher transition within the QD, as shown in figure1-2, which leads to a demand for higher excitation power than the above-band excitation.

It also can be called as photoluminescence excitation, by tuning the emission wavelength of the excitation laser. In the spectrum of such excitation method, a background tail of the absorption is usually unavoidable to appeared that extends down from the wetting-layer absorption edge. [25]

1.2 Single Photon Sources

Single photon source (SPS) is a light source that emits light as single photons as shown in figure1-3. It is distinct from the coherent sources (such as lasers) and the thermal light sources.

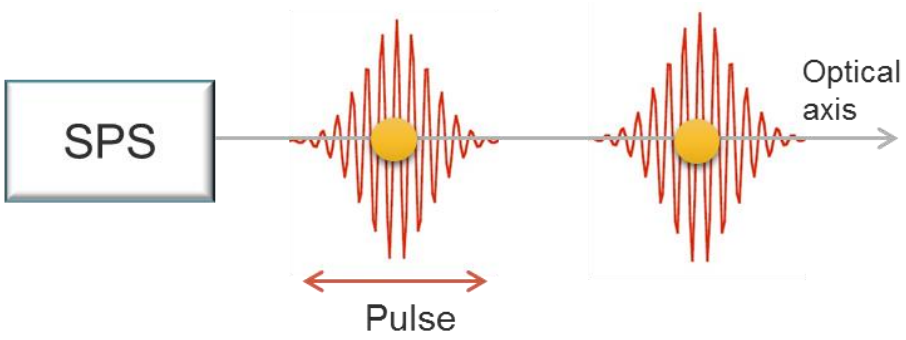

Figure 1-3. The single photon emission from single photon source.

Figure 1-4 shows that several different types of materials are able to achieve single photon emissions, such as color center defects in diamonds, single atoms, single-walled carbon nanotubes and QDs. [26-29]

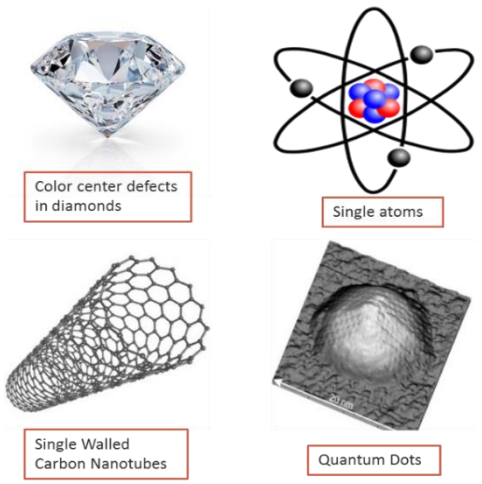

Figure 1-4. Several candidates of single photon sources (color center defects in diamonds, single atoms, single-walled carbon nanotubes and QDs). [26-29]

There are many applications for single photon source, especially for a high-quality one, such as the quantum key distribution, quantum repeaters, quantum computer and quantum information processing.

An ideal single photon source can emit one and only one photon at one time, and it exhibits quantum mechanical characteristics. The most important one of these is the photon anti-bunching as in figure 1-5.

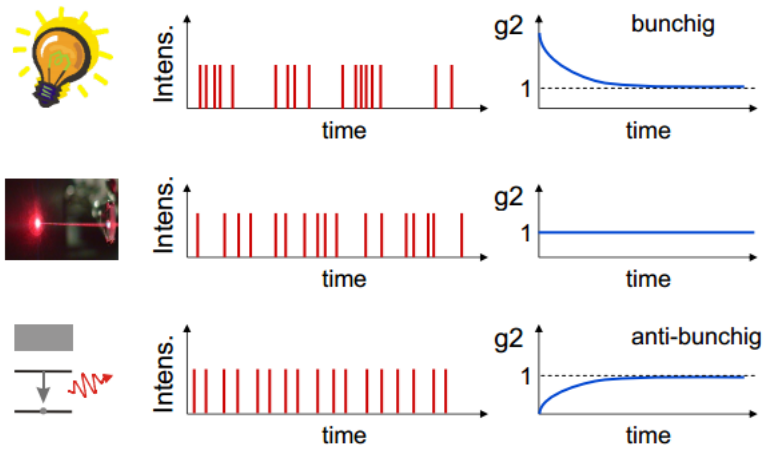

Figure 1-5. The differences of the single photon source, coherent sources, and the thermal light sources.

1.2.1 The Second Order Auto-Correlation and Hanbury-Brown & Twiss Measurement Method

To confirm the single photon source, the output is usually spectrally filtered and guided to Hanbury Brown and Twiss interference system, as shown in figure 1-6 [30,31], containing two single photo detectors (usually they are PMTs-photomultiplier tubes) separated by a beam splitter (usually it is 50/50 to get more efficient detection) operating in the emission wavelength range for the emitter.

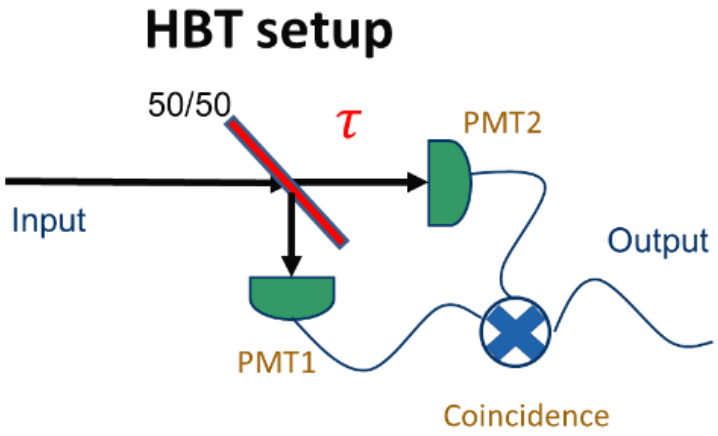

Figure 1-6. The setup of the detection of the single photon source (HBT setup). PMT, photomultiplier tube. 50/50, 50/50 beam splitter. [30, 31]

Coincidence histogram as a function of the time delay for the two optical arms, τ , the coincidence system between single photon detectors in the two arms is used to evaluate the statistics of the single photon candidates. The histogram follows the second order auto-correlation function,

$$g^{(2)}(\tau)=\frac{\langle I(t)I(t+\tau)\rangle}{\langle I(t)\rangle^{2}} \tag{1-3}$$

Where I(t) is the intensity of the emission at the time of t. Then this equation can be derived continually as:

$$g^{(2)}(0)=\frac{\langle a^{+}a^{+}aa\rangle}{\langle a^{+}a\rangle^{2}}=\frac{\langle n(n-1)\rangle}{\langle n\rangle^{2}}=\left(1-\frac{1}{\bar{n}}\right) \tag{1-4}$$

Where a^{+} is the creation operator, a is the annihilation operator, n is the photon number operator, and $\bar{n}$ is the average of the photon number.

It is clear to see that $g^{(2)}(0)=0$ when $\bar{n}=1$, and $g^{(2)}(0)>0.5$ when $\bar{n}>2$.

In particular, if the measurement result meets the inequality as: $g^{(2)}(0)<0.5$, that confirms the detection of a single photon state $|n=1\rangle$ (a photon number of 1, Fock State) from a single photon source because it represents the photon anti-bunching. The smaller of the second order correlation function $g^{(2)}(0)$, shows that is in fact a higher purity of the single photon source.

1.2.2 Single Photon Emissions from Quantum Dots

A quantum dot consists of a low bandgap semiconductor into a nanoscale size structure embedded within a high bandgap semiconductor [32,33], as in Figure 1-7a.

This kind of structure leads to a 3-dimensional electronic confinement because of the difference of the bandgap as shown in Figure 1-7b in 1- dimensional. Originally, holes are in the conduction band electrons are inside the valence band. Because the optically active QD confines electrons and holes to a relatively small area, as our discussion in Section 1.1.1 that their energy levels of the QDs are considered quantized.

An electron can be excited by the excitation, and reach to the conduction band, leaving a hole in the valence band. The QD traps the electron-hole pairs, and leads to an excitonic state. This exciton will radiative decay and formed the emission of one (usually a single) photon.

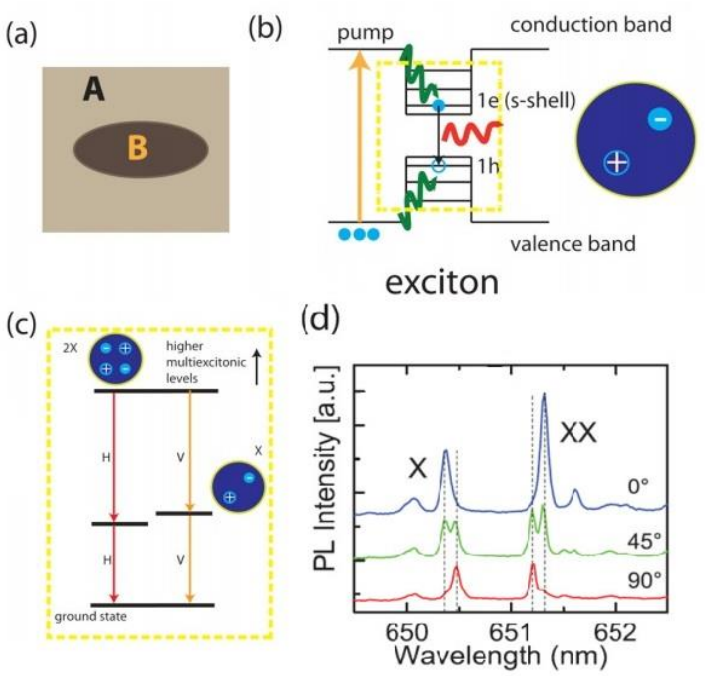

Figure 1-7. (a) A QD consists of a nano-size structure of a lower bandgap semiconductor embedded in another semiconductor with a relatively high bandgap. (b) The electronic diagram of the QD. (c) The fine and level structure for the X and XX (exciton and bi-exciton) in the QD. (d) Splitting spectrum from III-V QDs. (a), (b), (c) [32], (d) [34].

In the experiment, the QD under excitation is usually firstly raising up to a bi-exciton state (XX)with 2 electrons, and 2 holes, shown in Figure 1-7c, or raising even upper to a higher multi-state (more than 2 holes and electrons).

The asymmetries of the QD lead to actually a splitting because of the different electrons and holes spin states of the QD. In the spectrum, two (even more) frequencies for polarized light in horizontally and vertically directions will appear for this reason. [32-34]

The first report of the single photons triggered by a QD was given by Santori et al. in 2001 from Stanford University. [35]

They try to emit single photons under optical excitation by a pulse laser of a single

QD and spectral filtering to remove all but the last emitted photon.

Their self-assembled InAs QDs were grown by molecular beam epitaxy (MBE) at a high temperature to allow alloying with the surrounding GaAs. After the process of electron-beam lithography and dry etching. More fabrication details can be found elsewhere. [36]

The density of the QDs inside the smallest mesas contain was reduced down to the average in a single of the mesas, contains less than one QD.

The experimental setup is shown in Figure 1-8b. The sample was cooled down to the temperature of 5 K in a cryostat. The excitation laser was a mode-locked Ti-sapphire laser with the repetition frequency of 76 MHz.

Photoluminescence from the self-assembled InAs QD was collected and directed to focus on a small pinhole to selected as small as 5μm region onto the surface of the sample for measurement.

The QD emission as directed to a (CCD) charge-coupled device camera to measure the emission spectrum, or a spectrometer, or an HBT system to measure the photon auto-correlation of the QD emission.

In order to measure photon auto-correlation, two photon counters were connected to the start and stop channel of a time interval counter.

Even the detections of the photon counters are not such efficient, the photon auto-correlation histogram can get by the electronic pulses from start and stop signal with relatively longer accumulation time.

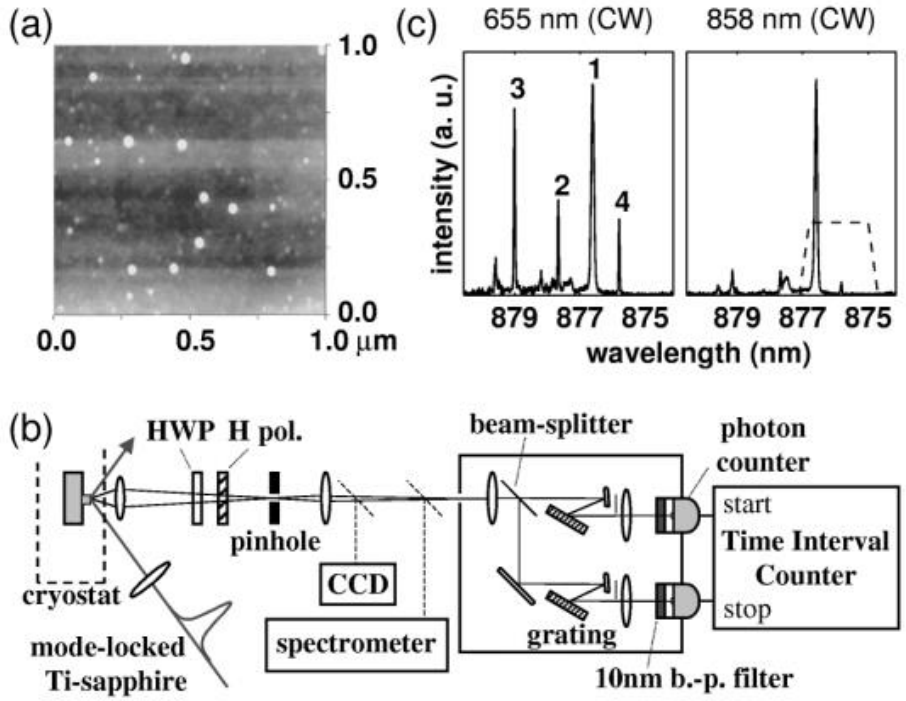

Figure 1-8. (a) Atomic force microscope (AFM) image of a studied InGaAs self-assembled QD. (b) The experimental system with the excitation part in the left, photoluminescence collection optics path in the middle, and HBT system in the right. (c) QD emission spectrum with above-band excitation in the left and resonant excitation in the right. [35]

In their previous study, they find the mesa itself contains a ground state photon with its emission wavelength of 876.4 nm.

By the above GaAs bandgap excitation using a continuous-wave (CW) excitation laser, the photoluminescence from the sample contains some narrow emission peaks were shown as figure 1-8c in the left as recorded in Ref [37].

These kinds of narrow emission peaks can be explained to come from the QD inside the mesas.

Furthermore, they tuned the wavelength of the laser to realize the resonant excitation. At this situation, the peaks 3 and 4 in the right of figure 1-8c disappeared,

which shows, in fact, they come from the charge states of the QDs. [38]

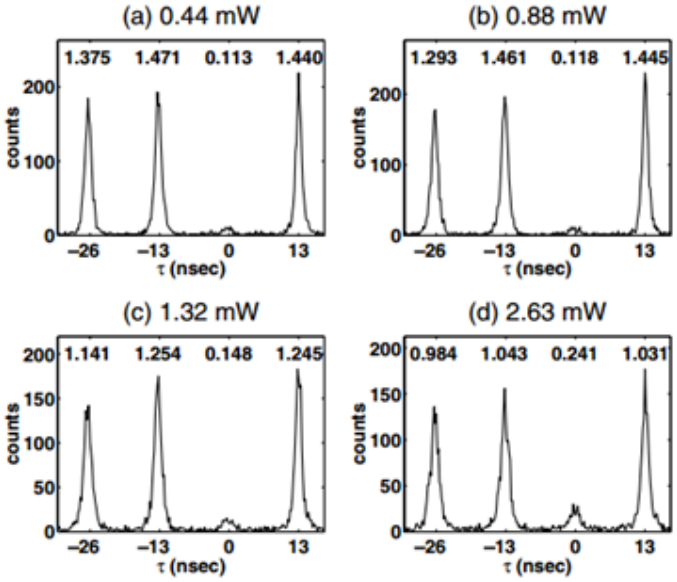

Figure 1-9. Photo auto-correlation histograms of the a selected InGaAs self-assembled QD under various laser power. [35]

Photo auto-correlation histograms under different excitation laser power as shown in figure 1-9 lead to a lower value down to $g^{(2)}(0)=0.095$ after the correction by the dark count from the background. Which confirms the clear single photon emissions with antibunching.

1.3 Advances of Current Single Photon Emissions from Quantum Dots

With the QD generated by many different materials, they show various properties when they are used to build a single photon source setup. As the following table:

Material System	λ (nm)	τ (ns)	$T_{max}(K)$
InAs/GaAs	~850–1000	~1	50
InGaAs/InAs/GaAs	~1300	~1.1–8.6	90
InP/InGaP	~650–750	~1	50
InP/AlGaInP	~650–750	~0.5–1	80
InAs/InP	1550	~1–2	50–70
GaN/AlN	~250–500	~0.1–1000	200
InGaN/GaN	~430	~8–60	150
CdTe/ZnTe	~500–550	~0.2	50
CdSe/ZnSSe	~500–550	~0.2	200
CdSe/ZnSSe/MgS	500–550	~1–2	300

Comparison of different QDs and their properties.

Including the emission lifetime τ, emission wavelength λ, and the maximum operation temperature with single-photon emission T_{max}. [32]

Recently the III-V Nitride QDs have been proved the great potential to emission single photons at the higher temperature than the data this table.[39-43] We will discuss it in detail in Chapter 2.

1.3.1 The Telecom Band Pure Single Photon Sources

From the beginning of the study of the fiber transformation by Kao, [44] the optical fiber information communication plays a crucial role in today's life.

Optical fiber communications typically based on the optical sources in telecom

windows. The original band (with a range of wavelength of 1260–1360 nm) and conventional band (with a range of wavelength of 1530–1565 nm) are the most important telecom bands.

It has been well-known that the In-V QDs are good candidates to generate telecom band single photon sources. It has been reported that the original band single photon emissions can be generated by using InAs/InP and InAs/GaAs systems. [45-47] However, the InAs/InP QD with a double-cap procedure had been shown the advantage of obtaining high-quality at c-band.

Recently, T. Miyazawa et al. achieved the highest purity of the telecom band of the single photon source. [48] They used self-assembled InAs QD grown on InP (100) substrate using 'double-capping' method [49] as shown in figure 1-10.

The photoluminescence from an InAs/InP QD was collected into a single-mode fiber.

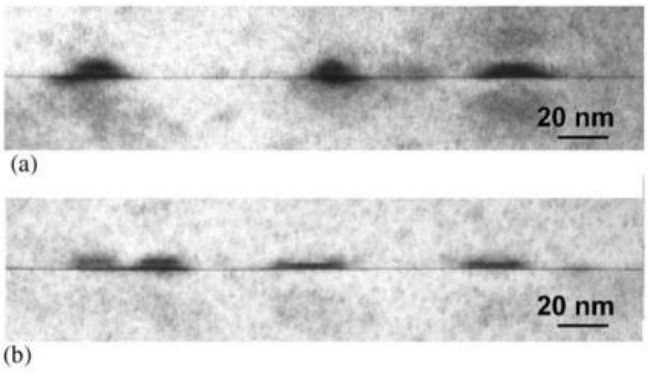

Figure 1-10. Cross-sectional images (a) the normal procedure;
(b) with the double-capping. [48]

Superconducting single-photon detector (SSPD) was used in the photon auto-correlation from such a single 'double-capped' InAs/InP QD. [49] (as shown in figure 1-10.)

The resonant excitation was used directly to the e1h0 state to improved the single photon purity following the K.P calculation results. [50]

As a result, they successfully suppress of the $g^{(2)}(0)$ down to $g^{(2)}(0) = 0.003$ at the resonant excitation wavelength and photon emission wavelength at 1538 nm., which is inside the conventional band as shown in figure 1-11.

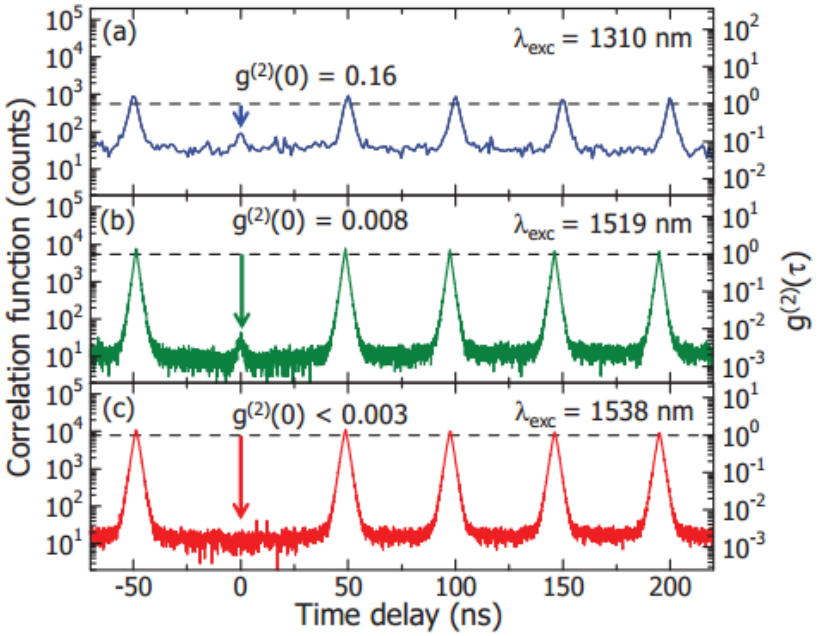

Figure 1-11. Photon auto-correlation of emission from exciton state under various excitation wavelength of 1310, 1519, and 1538 nm. [48]

Moreover, in the advances of this work, even higher pure single photon emission has been obtained by T. Miyazawa et al. [51]

They used an advanced method of quasi-resonant excitation (QRE)to excite the higher excited states. This method can much more highly suppressed the two or multi-photon emission states from a single QD, which leads to obtaining the even higher purity of the single photon emission. [52,53]

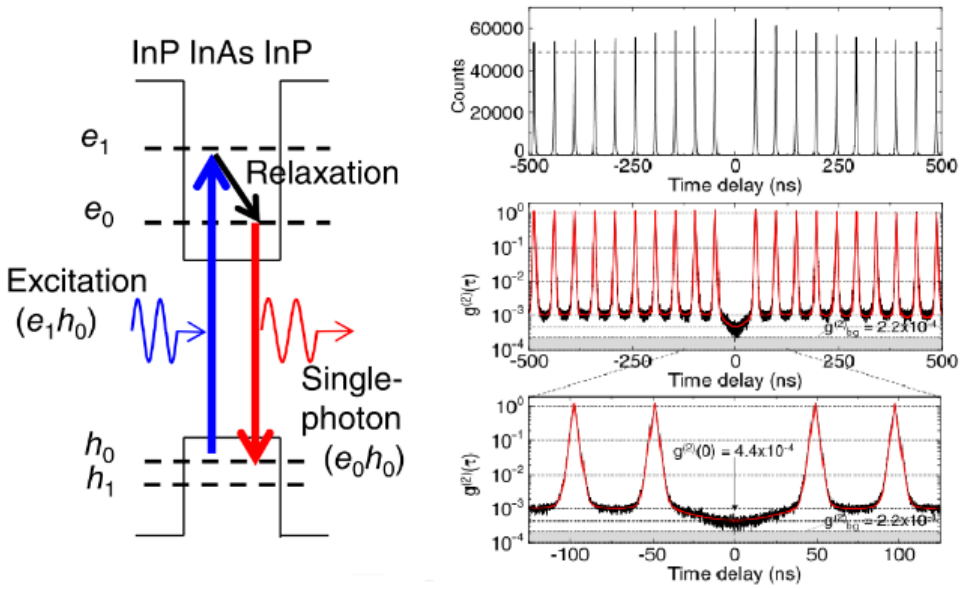

Figure 1-12. Left, Schematic illustration of quasi-resonant excitation method Right, Photon auto-correlation of a single InAs/InP QD emission under quasi-resonant excitation method. [51]

As shown in figure 1-12, the measured $g^{(2)}(0)$ from a single InAs/InP QD has already reached as low as $(4.4\pm0.2)\times10^{-4}$ measured by two high performance superconducting single photon detectors, without background correction. [51]

1.3.2 The High Efficient Single Photon Sources

The low efficiency of the generation of the single photon still effects the practical applications of single photon sources.

There are several different types of structures to achieve a highly efficient single photon sources. For example, the QDs in trumpet-like and needle-like photonic wires[54], the QDs embedded in a micro-pillar device,[55] the QDs in a Bragg bullseye

DBR structure[56] and so on.

Here we will take two examples of the efficient structures to briefly demonstrate their mechanism.

J. Gerard et al made a single photon source from a signle InAs QD in photonic wires. A high pump efficient single photon emission was obtained from such structure. [54, 57, 58] In order to optimize this structure, a QD was imbedded in a pillar micro-cavity structure. [58]

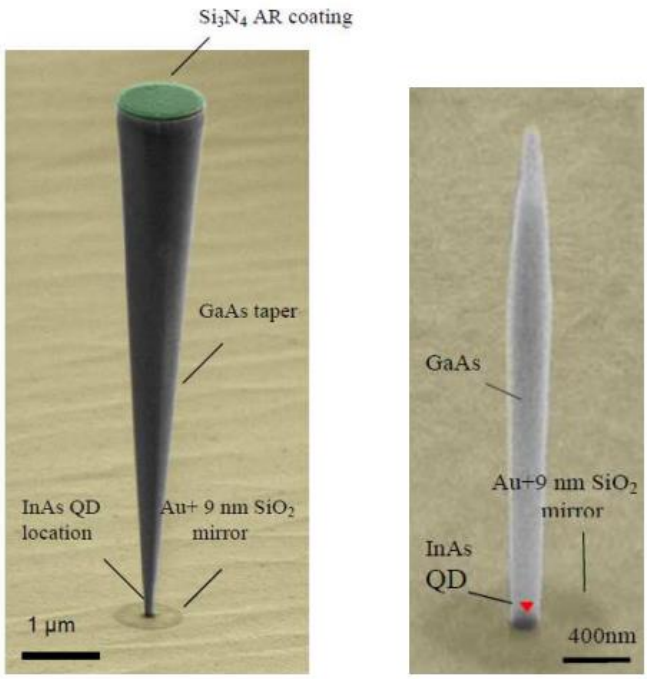

Figure 1-13. SEM image of trumpet and needle-like single photon emitters based on a QD in a photonic wire, with a bottom mirror. [54, 59, 60]

Single photon sources based on an InAs QD embedded in a needle-like photonic wires [54] trumpet-like photonic wires, [59, 60] as shown in figure 1-13, have been realized by the different choice of the mask and etching condition during the fabrication process of e-beam lithography and reactive ion etching.

The single photon emissions from such structures have been investigated by micro-photoluminescence and photon auto-correlation experiments, at a low operation

temperature of 4K using pulsed laser excitation. High collection efficiencies can been obtained from both of these two structures. The efficiency from the needle-like structure is 0.72 photon per pulse, while the efficiency of the trumpet-like structure is 0.75 photon per pulse. Meanwhile, both of them maintain the high purity single photon emission with a $g^{(2)}(0) < 0.01$.

Photonic wires provide us a possible solution to control the spontaneous emission of single photon sources. High efficiency above 0.75 photons per pulse has been realized in InAs QD based single photon emission.

Furthermore, second order bullseye distributed Bragg reflectors structure has been fabricated to be useful for increasing the collection efficiency of single photon emission from Arsenide QDs. [56, 61]

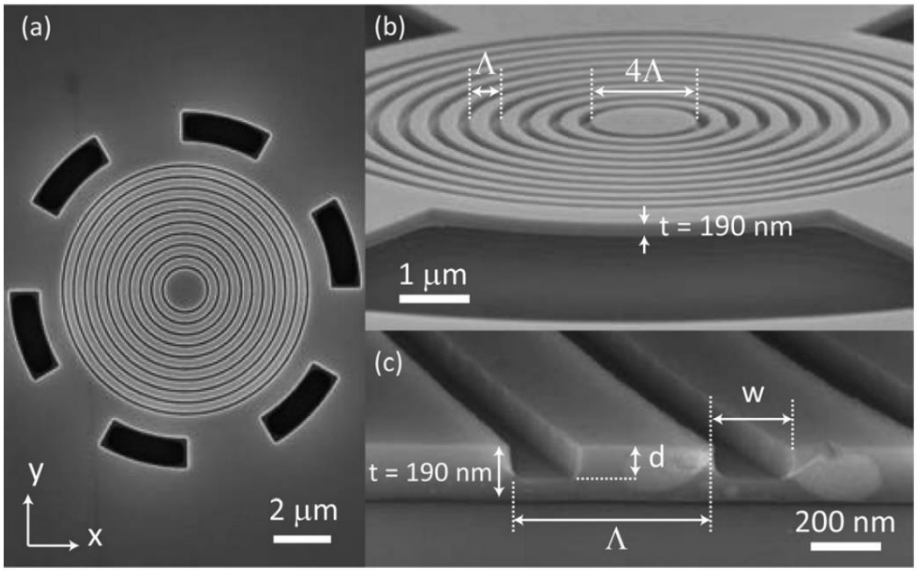

Figure 1-14. Top, side and cross-sectional images of the efficient circular Bragg bullseye DBR structure. [56]

M. Davanc et al reported an efficient and relatively broadband second order bullseye distributed Bragg reflector structure within a single InAs QDs.

From their simulation results, this structure allows a high extraction efficiency more than 80% of the photon emission from the imbedded InAs QDs. And their fabricated devices provide a ~10% collection efficiency with a numerical aperture of 0.42. Meanwhile, the Purcell rate enhancement also leads to a reduction of the emission lifetime down to less than 25%.

1.4 Research Aim and Goals

III-Nitride QDs base single photon sources have attracted a lot of attention thanks to their remarkable optical and physical properties. Current III-Nitride QDs still have their limitation towards to the high purity of the single photon emitters, indistinguishable photons, and bright quantum optical sources.

Recently, a novel GaN interface fluctuation QDs with narrow emission linewidth and high purity single photon emission has been reported. [62] However, the optical properties of such QD have yet to be studied to date.

In this thesis, we will focus on the single photon emission properties of such novel GaN interface fluctuation QDs to provide us a solution to the practical realization of high-quality quantum optoelectronic devices, using the technologically important III-Nitride material system.

1.5 Scope of Thesis

This thesis focuses on the investigation of the optical properties of III-Nitride QDs to achieve high-quality quantum sources.

Chapter 2 will describe the attractive properties and current limitation of the III-Nitride QDs based single photon emission and the sample (the interface fluctuation GaN QD) we used in this thesis.

Chapter 3 will describe the optical systems to perform the basic photon auto-correlation study by using a macroscopic photoluminescence measurement and Hanbury Brown and Twiss auto-correlation system.

The main part of my experimental and theoretical results are found in Chapters 4 to 6.

Chapter 4 will describe the temperature dependence of the single photon emission based on such interface fluctuation GaN QDs and discuss their single photon purity decreasing due to increased spectral contamination from uncorrelated background emission related to quantum-well states.

Chapter 5 will describe the exciton recombination time of the studied single QD without the influence from its photoluminescence background through the measurement of excitation power dependence of single photon dynamics. we estimate the exciton recombination time of the studied single QD without the influence from its photoluminescence background. It provides further evidence that the relatively narrow linewidths exhibited by such QDs are due to the “cleaner” environment of the QDs, not the smaller dipole moment.

Chapter 6 will describe the typical characteristic spectral diffusion time scale in the single photon emission of a Nitride QD, for the first time, which we find to be of nanosecond order. We also investigate the excitation power dependence of the diffusion rate. It shows that indistinguishable photons may be produced from such QDs under

excitation with pulse pairs separated by times less that such spectral diffusion time scale.

Furthermore, in the appendix, for application to III-nitride materials and considering fabrication issues, we will present a design of a bullseye-like structure based on radial 5λ/4 Nitride-Air gap DBRs around a central waveguide structure on a planar mirror to efficiently out-couple photon emission into the desired direction. By using FDTD method to simulate the structures, it shows that we can achieve an optimized extraction efficiency of ~70% with a wavelength range ~50nm for collection in an NA of 0.7.

The thesis will be concluded in chapter 7 with a summary and outlook.

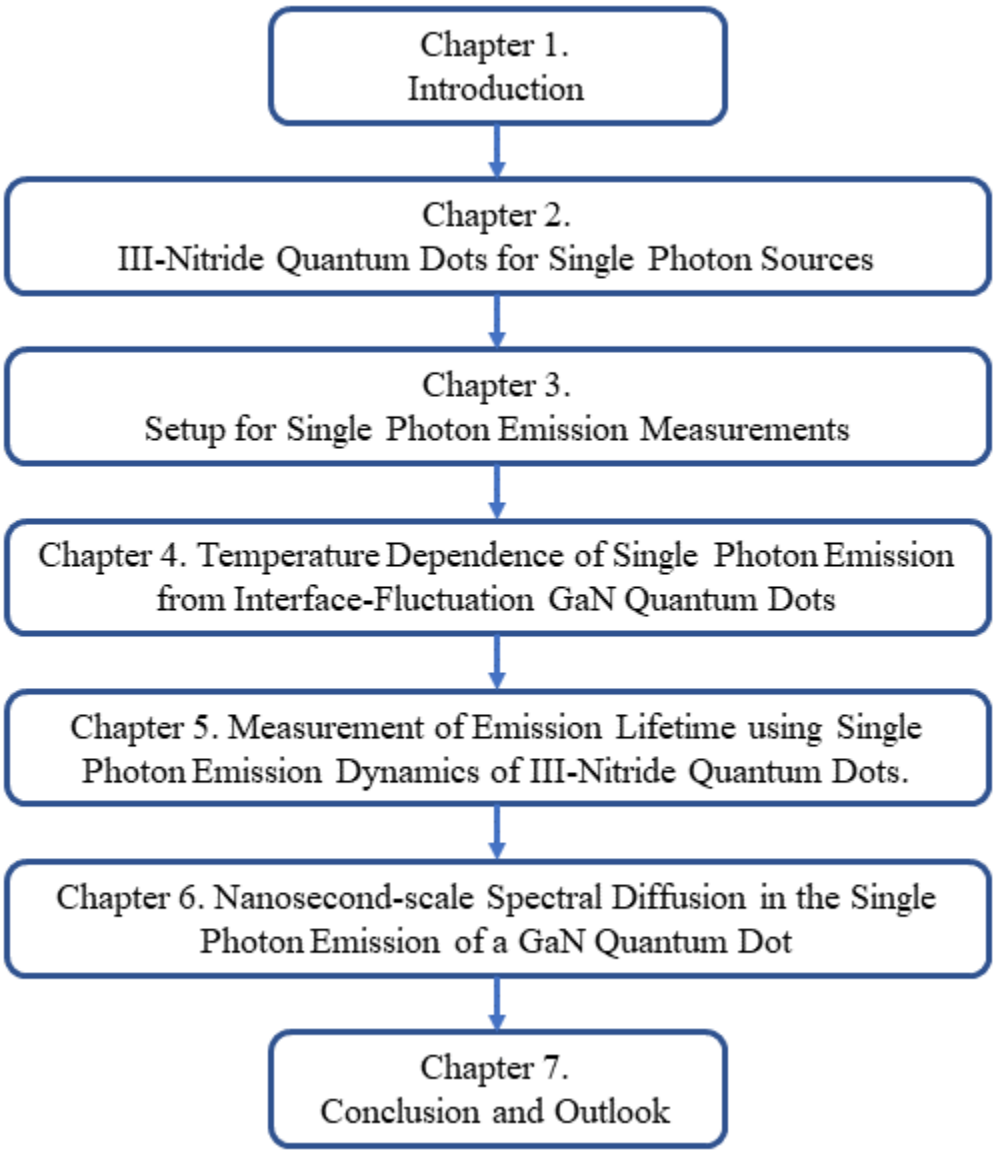

Figure1-15 Flow of this thesis.

Figure1-15 is the flow of this thesis. Chapter 1 to 3 introduce the reader to the fundamentals of III-Nitride QDs and the experiment methods used. Chapter 4 to 6 detail the experimental and theoretical research achievements.

2. III-Nitride Quantum Dots for Single Photon Sources

In general, during the past decade, III-nitride based semiconductors have become more and more initial materials in a huge field in the daily life of human being. Such as its great achievement of the blue LED which helps Isamu Akasaki, Hiroshi Amano, and Shuji Nakamura to win the Nobel Prize in 2014. [63]

Various materials during the fabrication of the QDs (such as Arsenides, Nitrides, Phosphides) caused big differences in their physical and optical properties. These properties not only affect greatly in their single photon emission characteristics, but also lead to very different practical application filed. It also made the evaluation methods and systems have large differences.

In the past decade, III-Nitride QDs have a large number of improvements for the daily life of human being, [64-72] because of their lots of attractive properties, for example their wide emission wavelength range and their probabilities to operate single photon emission in high temperature up to room temperature and even higher to 350K.

However, III-Nitride QDs also have their own limitation that leads to bad influence to their characteristics. For example, their relatively worse Single Photon Purity and their broadening linewidth resulting from the spectral diffusion comparing with other material such as Arsenide QDs. [22, 51, 73-75]

In this chapter, we will focus on the recent progress of the investigation of the properties of III-Nitrides QD.

2.1 Nitride Semiconductors

III-nitride based quantum dots have become promising candidates for single photon sources due to several advantages such as their wide range of emission wavelengths [76-79] (owing to a wide range of available material bandgaps), their ability to operate at relatively high temperatures due to their sufficient exciton confinement, [39-43] and recently, the possibility of high purity single photon emission. [62]

However, III-Nitrides have limitations because they suffer from a spectral diffusion induced linewidth broadening (which can result in emission linewidths of a few meV) [80-82]. This spectral diffusion occurs due to an interaction between the internal-field induced exciton permanent dipole moment [83, 84] and the fluctuating electric field of charges trapped in relatively large densities of surrounding defects [85, 86]. It will be discussed in detail later, and here a brief introduction of the crystal structure of III-Nitride will be provided in the following part.

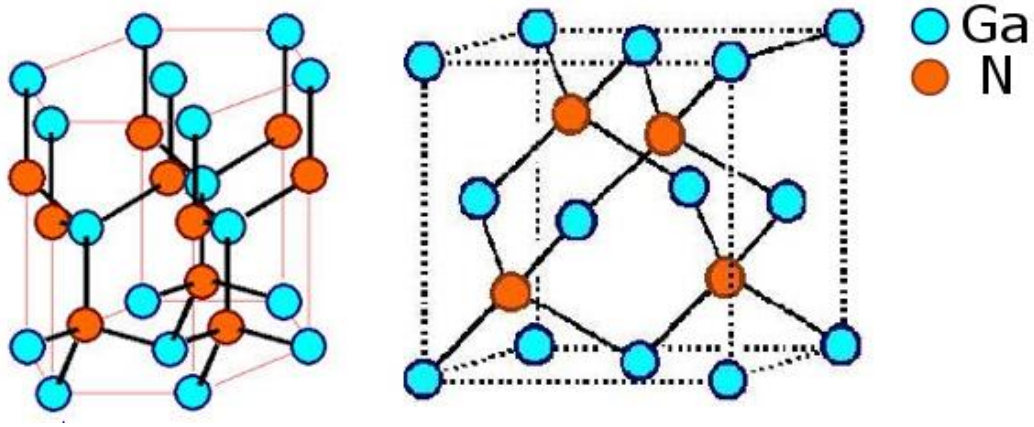

Figure 2-1. The hexagonal Wurtzite structure (left) and cubic ZincBlende structure (right) of GaN. [87]

There are two different structures usually formed by III-Nitride semiconductor materials. They are Wurtzite and ZincBlende, as shown in figure 2-1. Those structures are strongly depended on the physical properties of during their grown.

Firstly, in these two structures, interfacing two different materials of semiconductors to form III-Nitride QDs spontaneously creates a polarization with the interaction on the lateral interfaces. [88]

The wurtzite structure is more common one. The wurtzite structure for bulk III-Nitrides is thermodynamically stable in district tough conditions. The zincblende structure of III-Nitrides has been stabilized by epitaxial growth of thin films on the (011) crystal planes within the cubic substrates. [89]

If we focus on the most thermodynamically stable structure, the wurtzite structure, it is easy to find from figure 2-1 that there is no centrosymmetry. The large piezo-electric constants have been reported resulting from this non-centrosymmetric in wurtzite III-Nitrides. [88]

During the fabrication of the wurtzite QDs, as they are grown on a substrate which leads to a lattice mismatch with the Nitride material, t the piezo-electric polarization was induced by the structural strain. That leads to a strong built-in-field of the wurtzite QDs (~MV cm^{-1}). [90, 91]

Because of the quantum-confined Stark effect, which demonstrates the influence of the electric field on the energy level, the strong built-in-field leads to the changes in the structure energy levels of the wurtzite III-Nitride QDs. That causes the spatial separation of the electrons and holes induced by the electric field, which made radiative decay times (the emission lifetimes) of the exciton extended to the level from the nanoseconds to the microseconds. [92]

On the other hand, in the ZincBlende crystal structure, their observable properties are different from the wurtzite QD.

As shown in figure 2-1, the centrosymmetric of the ZincBlende crystal structure leads to a relatively weak piezo-electric constant [93] compared with wurtzite crystal structure.

For that reason, their radiative decay times (the emission lifetimes) reduce a little

bit shorter (a few hundred picoseconds). [94]

2.2 Attractive Properties from III-Nitride Quantum Dots

In this section, we will introduce two of the attractive properties from III-Nitride QDs: their wide emission wavelength range and high-temperature single photon emission operation.

2.2.1 Wide Emission Wavelength Range

The III-Nitride semiconductors have a recognized potential for widely emission range from the UV all the way to the IR. It is coming from their (InN, GaN and AlN)wide direct bandgaps as shown in figure 2-2. (~6.2 eV for AlN, ~3.5 eV for GaN, and ~0.7 eV for InN. [95])

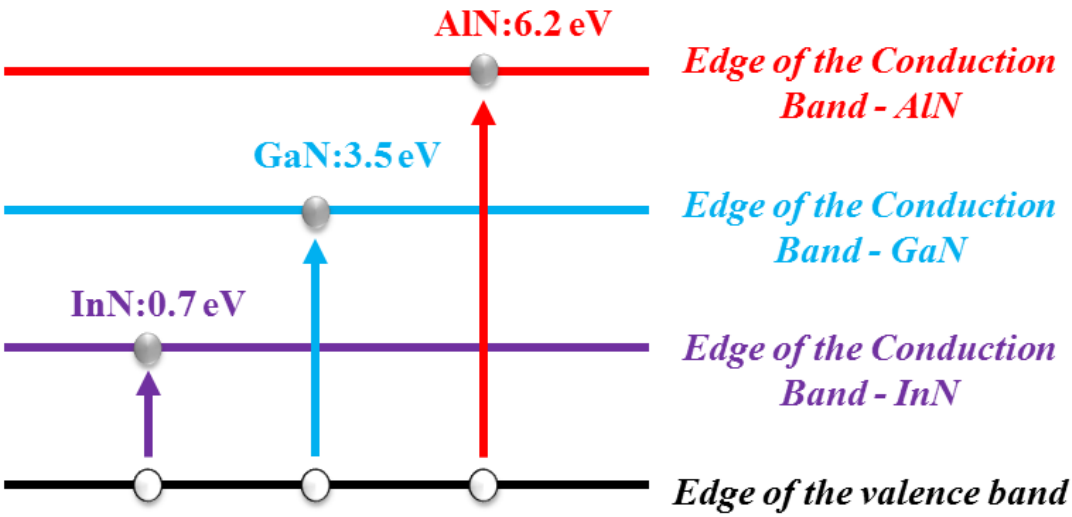

Figure 2-2. The extended range of III-Nitride semiconductors bandgap energy values.

According to these characteristics, people did a lot of efforts to control the emission color (in another word, that is the same as wavelength) from the III-Nitride semiconductors.

Figure 2-3 and 2-4 provide us an example of tuning of the emission range from blue to red. [77]

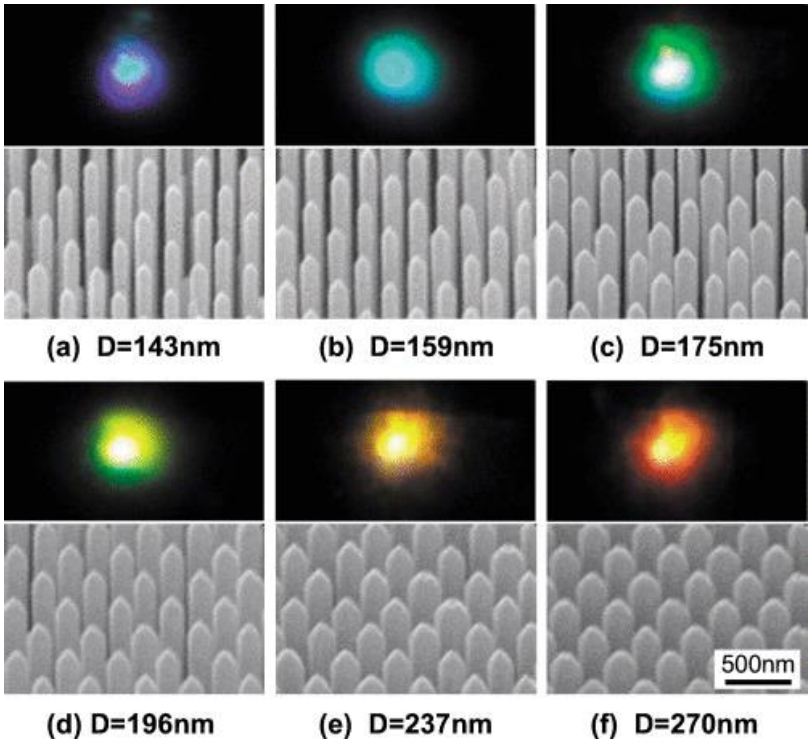

Figure 2-3. SEM and emission color from nanocolumns under excitation of He-Cd laser. [77]

In their experiment, InGaN/GaN multiple quantum well arrays with nanocolumn were growth by rf-plasma-assisted molecular beam epitaxy.

The diameters of the nanocolumn from 137 to 270 nm area. Micro-PL spectra of these nanocolumn arrays was measured at room temperature, selectively exited by an InGaN semiconductor laser (emission wavelength of 405nm). And the excitation power

density is relatively high to 15.2 kW/cm^2.

It is easy to find their color-control var the size of the nanocolumn that the emission wavelength increases while increasing the diameter of the nanocolumn. And this kind of change become from the In compositions of InGaN/GaN nanocolumns by considering the piezoelectric, spontaneous polarization, and quantum carrier-confinement effects. More fabrication detail can be found in Ref. [77].

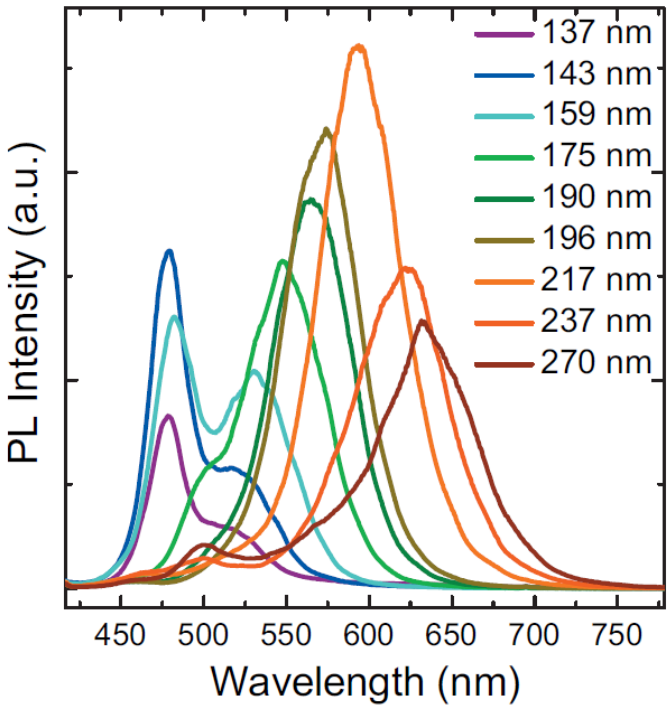

Figure 2-4. PL spectra of InGaN/GaN nanocolumns for patterns with different diameters from 137 to 270 nm. [77]

In this work, they provide an explanation of such color changing mechanism that the emission wavelength shifting in different diameter nanocolumn size is due to the beam shadow effect of the neighboring nanocolumns and the diffusion length difference of Ga and In adatoms on the sidewall.

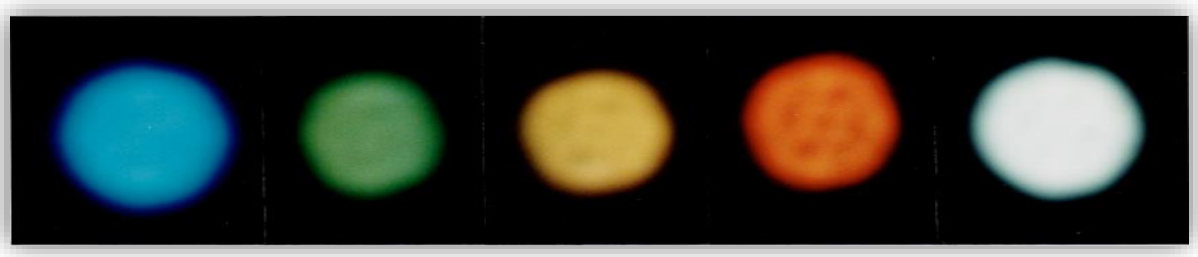

Figure 2-5. Photographs of the light emitted at room temperature from GaN/AlN QDs under excitation of an unfocused HeCd laser. [78]

In another group from France[78], GaN QDs have been grown in an AlN matrix on Si (111) by molecular-beam epitaxy.

As shown in figure 2-5, the QD emission can be continuously varied in different colors by controlling the QD size. Here the excitation source is an He-Cd laser without focusing with a large spot about 3 mm^2, according to a relatively low excitation power density of ~0.3 W/cm^2.

Moreover, the mixing of different QD sizes leads to multi-wavelength photon emission in white light.

In addition, the operation temperature is also a key parameter which effects emission photon energy of III-Nitride QDs.

S. Sergent et al [82, 94] observed excitonic recombination in a single zinc-blende GaN/AlN QDs with a large band offset and binding energy up to the room temperature (300K).

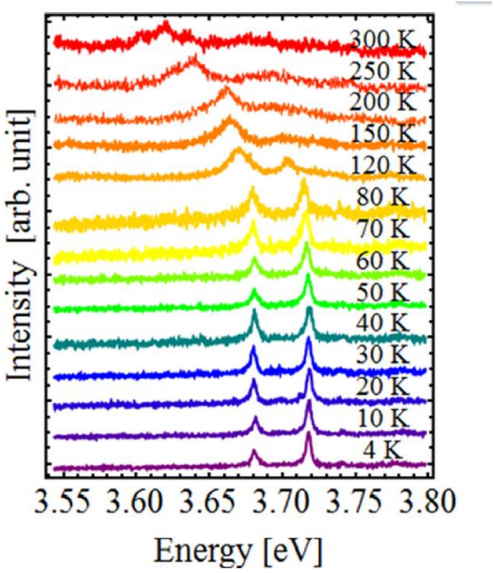

Figure 2-6 Normalized micro-PL spectra of two individual QDs measured in the same mesa at various temperatures. [82]

These single zinc-blende GaN QDs was fabricated by the droplet epitaxy growth mode. Fabrication detail can be found elsewhere. [96]

The sample is held in a flow He-cooled cryostat so that we can control the operating temperatures that from 4K up to 300K to study its optical properties by micro-photoluminescence. The QDs are under non-resonant excitation by a frequency-quadrupled continuous-wave laser with emitting wavelength at 266 nm.

As shown in figure 2-6, a clear red shit can be found while increasing the temperature. It is resulting from the temperature dependence of the shrinkage of the bandgaps of the materials.

Meanwhile, such droplet epitaxy zinc-blende GaN QDs are similar to the typical SK QDs [39, 92] with fast radiative recombination lifetimes and narrow spectral linewidths down to 0.6 meV (which is still much more than the interface fluctuation

GaN QDs, we will discuss it later).

However, a much more interesting thing from this research these dots even show better prospects for high-temperature single photon emission as single QD micro-photoluminescence has been observed up to 300K and the low QD density limits the spectral contamination of background from its surrounding environment. And this is another attractive property of III-Nitride QDs we will introduce in the following section.

2.2.2 High Temperature Single Photon Emission Operation

As the introduction in Chapter 1, recently, it has been recognized that the III-Nitride QD shows a significant potential to solve the problem of the high operating temperature, thanks to the improvement of the martial quality. [41-44]

In 2006, S. Kako et al reported a triggered single-photon emission from GaN QDs up to the temperature of 200K. [40] In this study, the hexagonal Stranski–Krastanov GaN/AlN QDs were made by metallorganic chemical vapor deposition on a (0001)-oriented 6H-SiC substrate. They have been grown on top of a 100 nm AlN buffer layer and then a 100 nm AlN cap layer covered them. More grown condition details can be found in ref. [97]

The QDs samples have been etched and detected using a micro-photoluminescence method, in order to isolate individual single QD emission in its spectrum. The sample has been processed by electron-beam lithography.

The size of the mesas is reduced into the range from 0.2 to 2 μm. It can be expected that a lower QDs density in the smallest mesas.

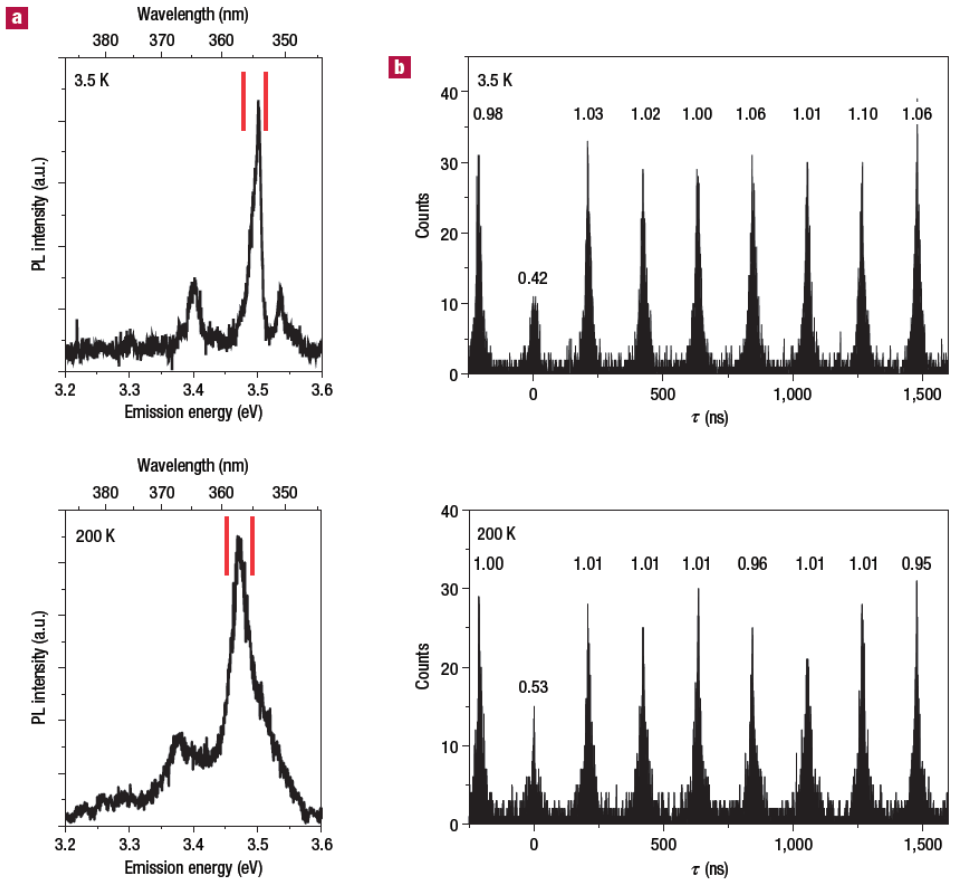

Figure 2-7 Photon auto-correlation measurement using pulsed excitation. Upper, photoluminescence spectrum and auto-correlation histograms under pulsed excitation at the temperatures of 3.5 K. Lower, photoluminescence spectrum and auto-correlation histograms under pulsed excitation at the temperatures of 200 K. The spectral window in the auto-correlation measurement is between the solid lines inside the spectrum after spectrometer. [40]

In order to evaluate the single photon emission, Photon auto-correlation of such QD was measured under pulsed excitation with the 4.74 MHz repetition rate.

As the red slit in figure 2-7a, a spectral window was selected by the spectrometer at two different temperatures of 3.5 K and 200 K. And the according auto-correlation histograms were performed in figure2-7b.

Although, it is clear that the emission spectral getting worse not only the emission

line broadening but also the contamination of background while raising the temperature from 3.5K to 200K. We can still get the low $g^{(2)}(0)$ of around 0.5 as shown in the figure 2-7b.

This research guides us that it will be necessary to get a further reduction of linewidth to improve the two-photon reduction efficiency, for the achievement of the high temperature single photon emission in the short wavelength region. Whatever, this demonstration in 2006 is an important step to realize a higher temperature operation single-photon sources in the UV region.

As the first time of room temperature single photon emitting, M. Holmes et al. had reported that the single photon emission from an AlN/GaN site-controlled nanowire QD in the 300K. [41]

The structures were grown by metal−organic chemical vapor deposition (MOCVD). More fabrication detail can be found elsewhere. [41, 98-100]

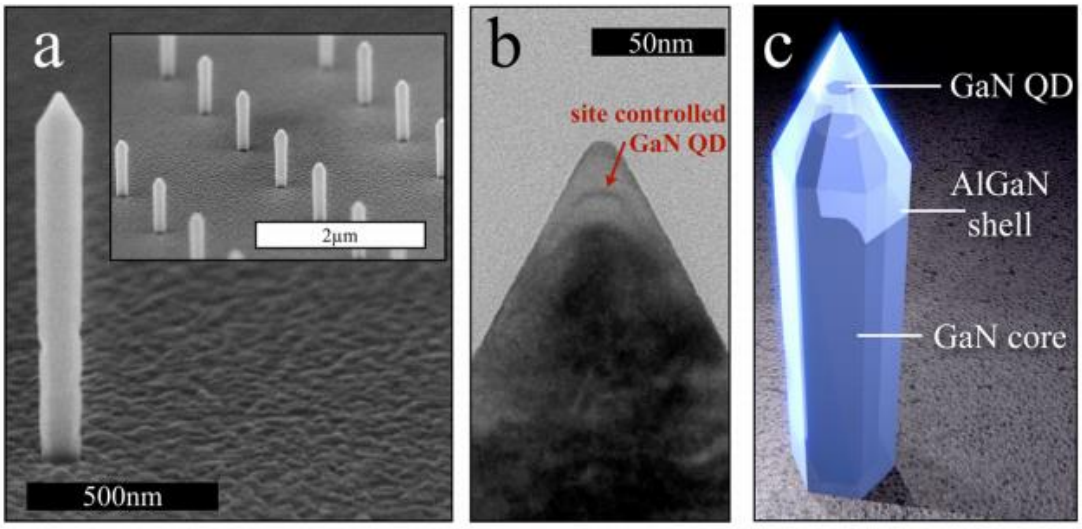

Figure 2-8. Images of AlN/GaN site-controlled nanowire-QD. (a) Scanning electron microscopy (SEM) image of AlN/GaN site-controlled nanowire-QD. (b) Transmission electron microscopy (TEM) image showing the detail of the formation of a single AlN/GaN site-controlled nanowire-QD near its tip. (c) Schematic of a nanowire containing a single AlN/GaN QD. [41]

Scanning electron microscopy, transmission electron microscopy images, and a schematic diagram of the structure of AlN/GaN site-controlled nanowire-QD were presented in figure 2-8.

The sample of AlN/GaN site-controlled nanowire-QD is under non-resonant excitation with an ultrafast pulsed ultraviolet laser. Their emission spectrum from such a single QD measured by micro-photoluminescence at the temperature of 3.9, 150, up to 300K can be found in figure 2-9.

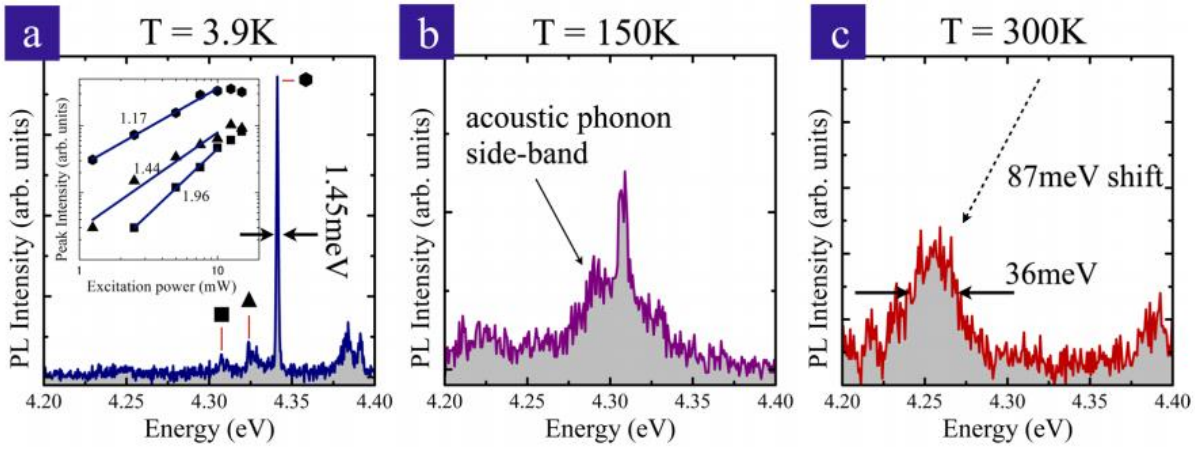

Figure 2-9 Emission spectrums from an AlN/GaN site-controlled nanowire-QD.

(a) The temperature of 3.9K and excitation power of 5 mW.

(b) The temperature of 150K and excitation power of 10 mW.

(c) The temperature of 300K and excitation power of 15 mW.

The emission linewidth is broadening from 1.45 meV up to 36 meV with a red-shift of 87 meV. [41]

It is clear to find a red-shift by 87 meV while raising the temperature from 3.9K to 300 K. Meanwhile, its emission linewidth is broadening from 1.45 meV up to 36 meV. It can be explained by the temperature dependent shrinkage of the bandgaps of the materials. [101]

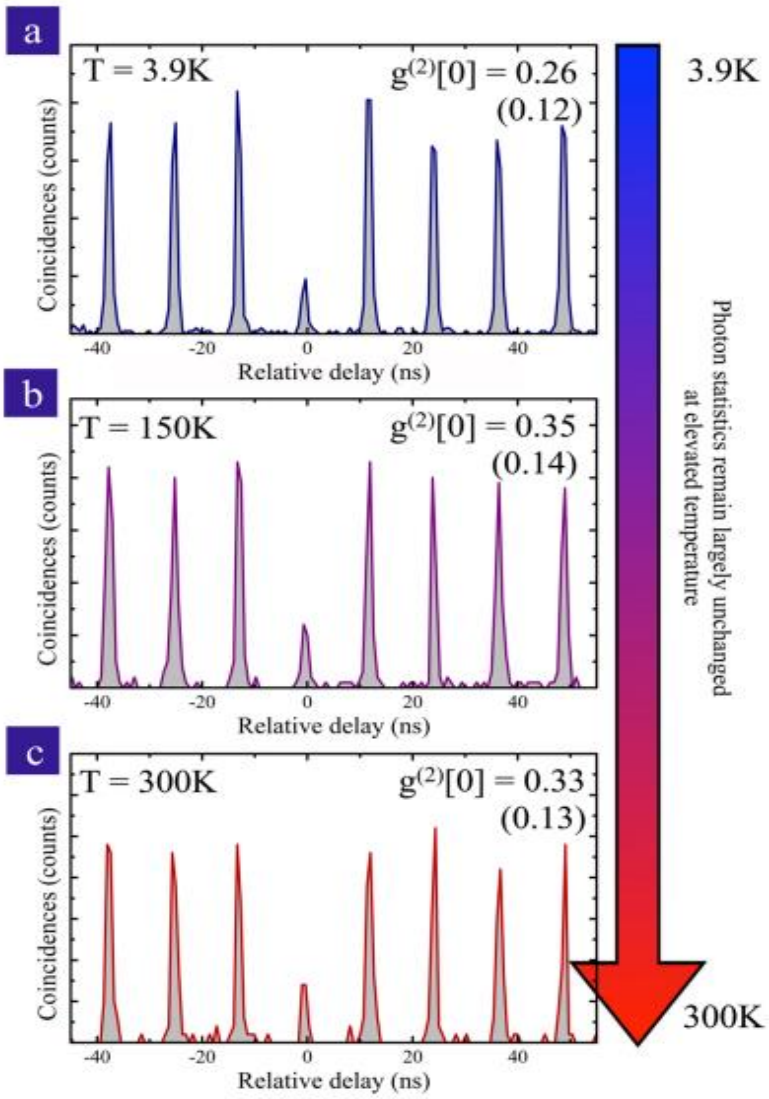

Figure 2-10 Photon auto-correlation that reveals the single photon emission from an AlN/GaN site-controlled nanowire-QD with the operation temperature from 3.9K up to 300K. [41]

The photoluminescence from the AlN/GaN site-controlled nanowire-QD was directed to the HBT setup. As the results shown in figure 2-10, it reveals the single photon emission from 3.9K up to 300K. This is the first time that human being achieves the room temperature single photon emitting!!

The important point of this study is that exciton confinement at room temperature

is realized thanks to the wide bandgap semiconductor material of III-Nitrides QD.

Moreover, the site-controlled QD results in the reduction of the QD density. That made the isolation of single QD emission from the environment is possible.

Finally, the QD, which has the quantized energy levels, lead to the exciton energy separation, preventing the contamination of the emission spectrum up to the room temperature of 30K.

As the following work of this room-temperature single photon emission, M. Holmes et al. continued his work on the AlN/GaN site-controlled nanowire QD and realized the even higher operation temperature (up to 350K) single photon emission. [42]

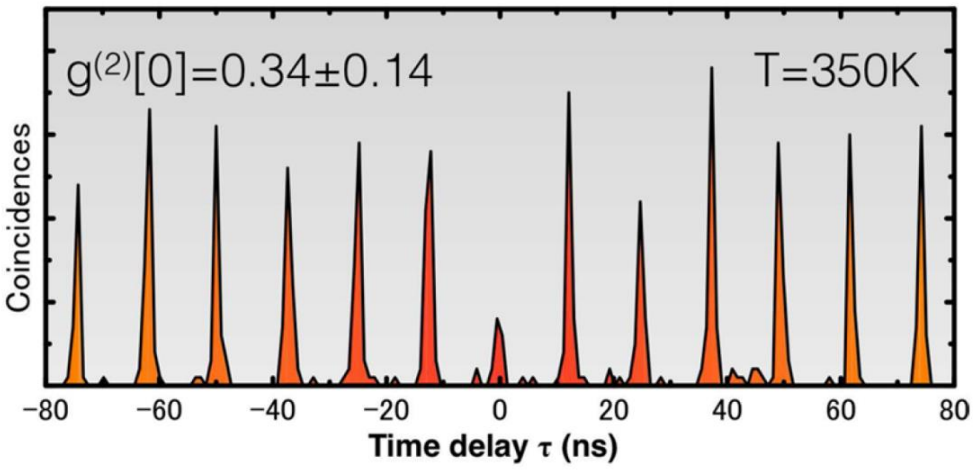

Figure 2-11 Photon auto-correlation histogram of single position-controlled GaN nanowire QD. [42]

In this experiment, under the above-bend pulsed laser excitation with a wavelength of 247nm (excitation photon energy of 5 eV), the selected single position-controlled GaN nanowire QD emits the photon energy at the range of 4.0eV - 4.6 eV, in the color of deep ultraviolet.

As shown in figure 2-11, the measured $g^{(2)}(0)$ of 0.34 representing the single

photon emission at the temperature of 350K.

2.3 Material Limitation of III-Nitride Quantum Dots

Just as the saying goes, every coin has its two sides.

III-Nitride quantum dots also have their own limitation that affects their practical applications.

2.3.1 Broadening emission linewidth

The emission linewidth broadening from III-Nitride QDs (which can usually reach to the order of a few meV) due to its spectral diffusion suffering from spectral diffusion.

As the discussion in [80], the spectral diffusion occurs due to an interaction between the internal-field induced exciton permanent dipole moment [83, 84] and the fluctuating electric field of charges trapped in relatively large densities of surrounding defects, [85] we will discuss it in detail in Chapter 5.

C. Kindel et al made a study on the origin of the relatively large emission linewidth. [81] Their work summarized a statistically significant number of spectrums observed from wurtzite GaN/AlN QD.

The studied self-assembled wurtzite GaN/AlN QDs was fabricated by metal-organic vapor deposition. More detailed in growth conditions can be found elsewhere. [97]

Under the above-band excitation by 266nm continuous wave frequency-quadrupled solid-state laser, micro photoluminescence from a huge number (more than 200) of single GaN/AlN QDs was collected and detected by a spectrometer with a charge coupled device (CCD).

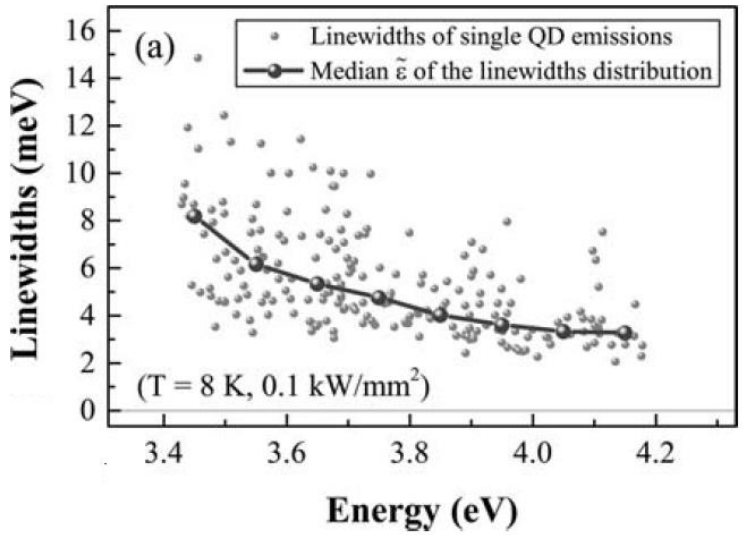

Figure 2-12. A huge number (more than 200) of emission linewidths from single GaN/AlN QDs. [81]

As shown in figure 2-12, a large number (more than 200) of emission linewidths from such single wurtzite GaN/AlN QDs have been shown as a function of emission photon energy.

It is clear that with the increase of the emission energy, a reduction trend of the reduction of the emission linewidths happened and the average of the linewidths was in the order of several meV.

Furthermore, S. Sergent et al reported a similar study focusing on the single zinc-blende GaN/AlN QDs. [82]

The studied self-assembled zinc-blende GaN/AlN QDs were grown by droplet epitaxy. The micro photoluminescence spectrums from such zinc-blende QDs were detected under the above-band excitation from a continuous-wave laser with a wavelength of 266 nm.

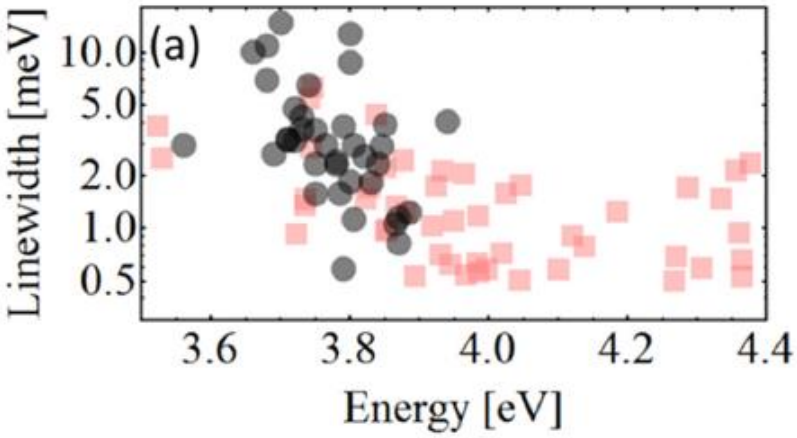

Figure 2-13. Homogeneous linewidths of single droplet epitaxy zinc-blende GaN/AlN QD and Stranski Krastanow zinc-blende GaN/AlN QD in low temperature with a low power of continuous wave excitation laser. [82]

The homogeneous linewidths extracted from serval zinc-blende GaN/AlN QD emissions were shown in figure 2-13, with the comparison of the single Stranski Krastanow zinc-blende GaN QDs. [94]

Moreover, M. Holmes et al made a model to explain the mechanism of the emission linewidths by investigating the emission properties from an AlN/GaN site-controlled nanowire QD in the 300K. [41, 80]

They used the Michelson interferometer with a piezo tuned arm to measure the various course delays to increase the resolution of the measurement of the emission linewidth from the QD.

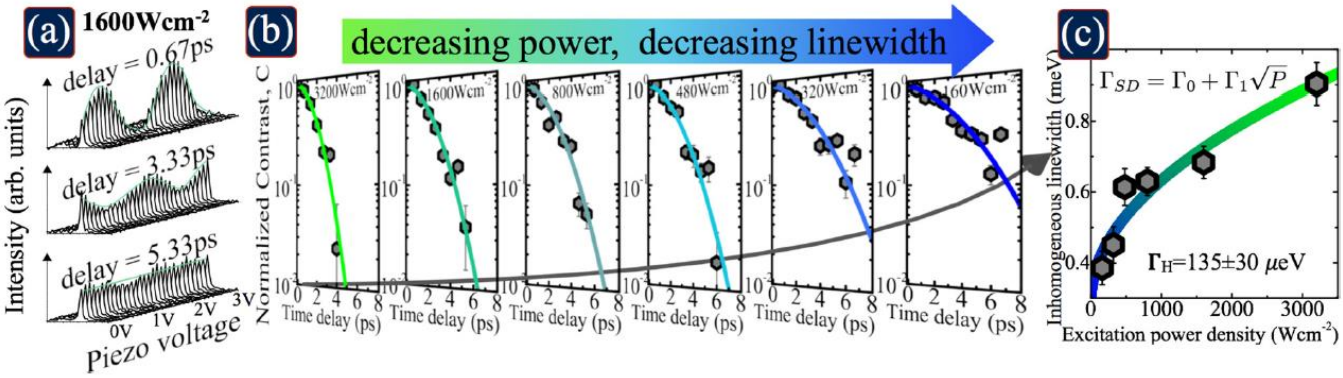

Figure 2-14. (a) Interference fringe with Michelson interferometer.

(b) Decay in fringe contrast with excitation power.

(c) Inhomogeneous linewidth under various excitation power. [80]

As shown in figure 2-14, the inhomogeneous linewidth from the emission of an AlN/GaN site-controlled nanowire QD has been investigated by Michelson interferometer. And the emission linewidth decreased with reducing the excitation laser power.

The measured interference fringe was fitted by a Fourier transform of a Voigt function:

$$C(\tau) = \exp\left[-\left(\frac{\tau}{\tau_{SD}}\right)^2 - \left(\frac{\tau}{\tau_H}\right)\right] \tag{2-1}$$

where C represents the interference fringe contrast, τ is the path difference in the two arms of Michelson interferometer.

τ_{SD} and τ_H are the time scale of the spectral diffusion and homogeneously broadened of the photon emission. And the homogeneous Lorentzian emission linewidth and inhomogeneous Gaussian emission linewidth can be envaulted as:

$$\Gamma_{SD} = \frac{2\sqrt{\ln 2}}{\pi \tau_{SD}} \quad \text{and} \quad \Gamma_{H} = \frac{1}{\pi \tau_{H}} \tag{2-2}$$

By measuring the inhomogeneous Gaussian line shape, it can be found that the inhomogeneous linewidth nonlinear increased while raising the excitation laser power. Their relationship has been formed as $\Gamma_{SD} = \Gamma_0 + \Gamma_1 \sqrt{P}$. The measured spot data and the fitting curve in figure 2-14c fitted well under this equation.

Moreover, they also provide a model to explain the spectral diffusion is related to the statistics numbers of charge traps localized states surrounding the studied QD as shown in figure 2-15. We will discuss the spectral diffusion in more detail in chapter 6.

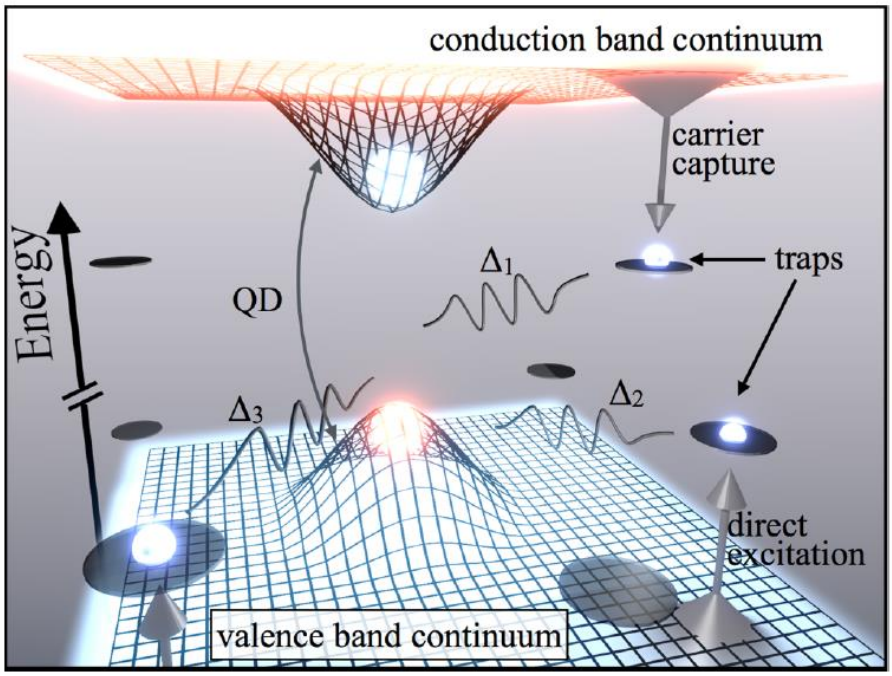

Figure 2-15 Schematic image of a few number of charge traps localized surrounding the single QD. [80]

2.3.2 Single Photon Purity

As the introduction in Chapter 1, the single photon sources need to emit one and only one single indistinguishable single photons at one time for the practical applications.

The measured second-order correlation $g^{(2)}(0)$ represents the purity of the single photon emission. As the equation (1-4), the higher purity of the single Fock n=1 state, the lower $g^{(2)}(0)$ can reach. That also means the lower rate of the second-photons or multi-photon states. The key factor to reach high purity of the single photon emission is to reduce the possibility of the two-photon and multi-photon. In another word, it needs a much cleaner QD emission spectrum.

Concerning the purity of the spectral condition of the III-Nitrides semiconductor and the broadening emission linewidth compared with Arsenides QDs, the reported raw $g^{(2)}(0)$ values from the III-Nitrides QDs are usually large from Arsenides QDs.

S. Deshpande et al reported lowest reported measured $g^{(2)}(0)$ value from a III-Nitrides QD without background correction before our results. (for the emission background in the spectrum and response time of the detector in HBT setup, we will discuss it in Chapter 4) [43]

Their InGaN/GaN QDs were grown by plasma-assisted molecular beam epitaxy on GaN-on-sapphire templates.

In the measurement of auto-correlation, their sample was excited by the injection of electrical current. The auto-correlation histogram was shown in figure 2-16, and their lowest reported measured $g^{(2)}(0)$ value is clear as low as $g^{(2)}(0)=0.11$.

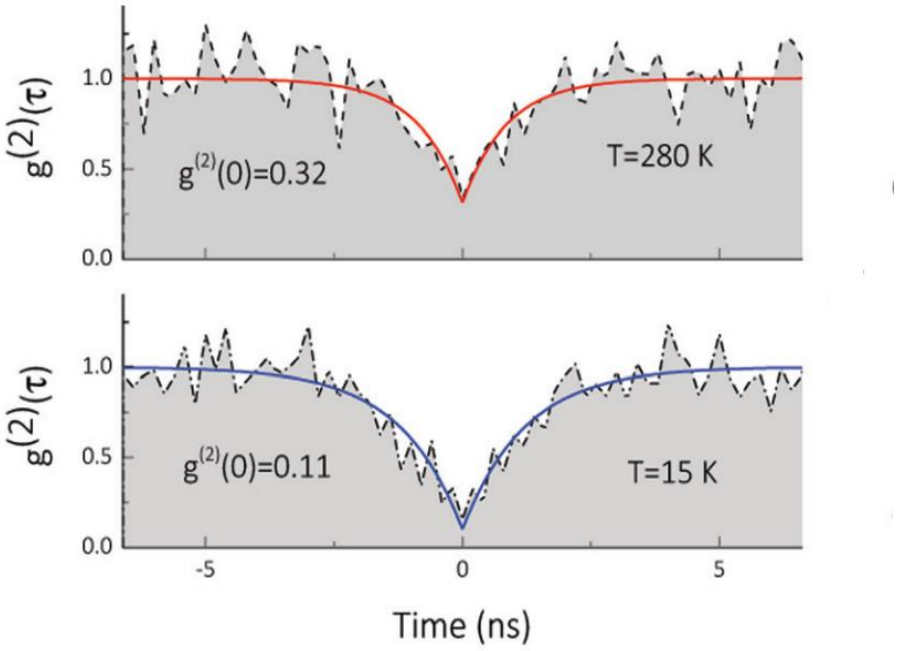

Figure 2-16 Photon auto-correlation results measured under continuous electrical excitation. Lower, at the temperature of 15 K under electrical injection density of 6.67 A/cm^2. Upper, at room temperature (280K) under electrical injection density of 1 A/cm^2. [43]

G. Schmidt et al reported another work with lowest $g^{(2)}(0)$ value after background correlation.[102]

The studied GaN islands-like QDs were fabricated from GaN layer growth by metal-organic vapor phase epitaxy on an AlN/sapphire template.

The photon auto-correlation histogram of a single emission line at 4.203 eV was performed at low temperature of 8K as shown in figure 2-17. The excitation source used here is a 256-nm wavelength continuous-wave laser.

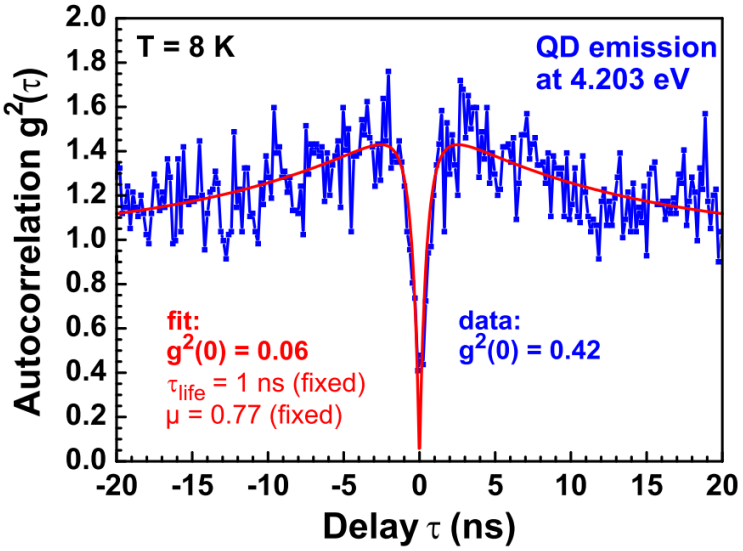

Figure 2-17. The photon auto-correlation histogram of a single emission from GaN islands-like QD at 8K. [102]

Their experiment result revealed a measured $g^{(2)}(0)$ value of 0.42 (lower than 0.5) confirmed a single photon emission. Their deconvoluted $g^{(2)}(0)$ value after background corrected is as low as 0.06 is the lowest results before our result, which reveals that the probability of the high purity single photon emissions from III-Nitride semiconductor system.

2.4 Interface Fluctuation GaN Quantum Dots

In this thesis, we will focus on the sample of interface fluctuation GaN QD, which were successfully grown and fabricated in recent years. It has improved crystal quality with a low density of the surround defect of the GaN QD.

This so-called interface fluctuation comes from that during their growth through a metal−organic chemical vapor deposition reactor.

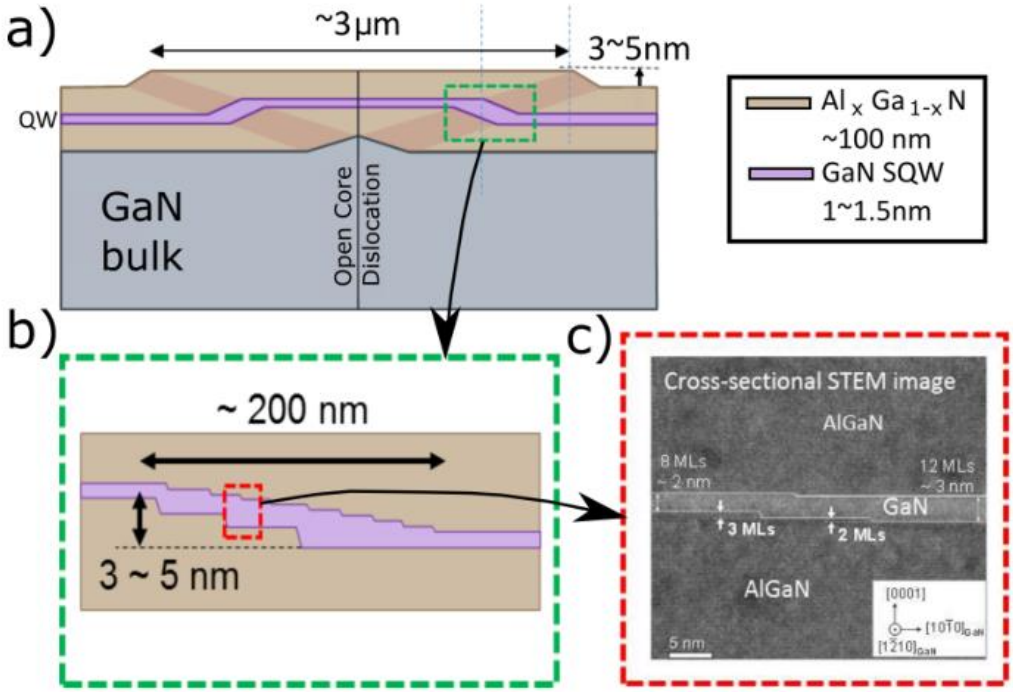

Fig. 2-18. (a) schematic of an interface fluctuation GaN QD,
(b) zoomed in a schematic of the micro-steps,
(c) cross-sectional STEM image. [62]

As shown in figure 2-18a and b, A thin GaN layer (with the thickness of 1-1.5nm) was fabricated between two thick (with the thickness of ~100nm) AlGaN layers on a GaN bulk template.

Between the different layers, the random fluctuations in layer height localized on

the interfaces of the semiconductor materials are formed. Figure 2-18c shows a cross sectional STEM image of one of the fluctuations on the interface of the GaN to InGaN layers.

These kinds of irregularities inside the structure can be recognized as some quantum dot-like structures which is possible to confine the carriers.

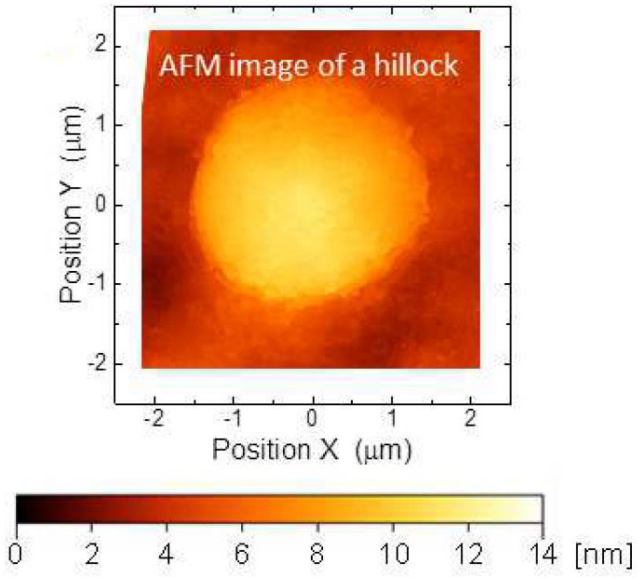

Figure 2-19. Atomic force microscopy image of the hillocks-like structure in the interface fluctuation GaN QD sample. [62]

On the surface of our sample, a hillocks-like structure can be observed, as the atomic force microscopy image shown in figure 2-19. The confinement of the exciton is believed to be localized at the position right under the edge of the micro-steps.

A low density of the defects around the QD-like structures is achieved by the high quality of the crystal, due to the high-temperature growth process.

As mentioned before, the relatively broadening emission linewidth due to the spectral diffusion is the current limitation of III-Nitride QDs system. Thanks to the low density of the defects around this QD. A recorded narrow emission line from II-Nitride

QDs has been obtained. [62]

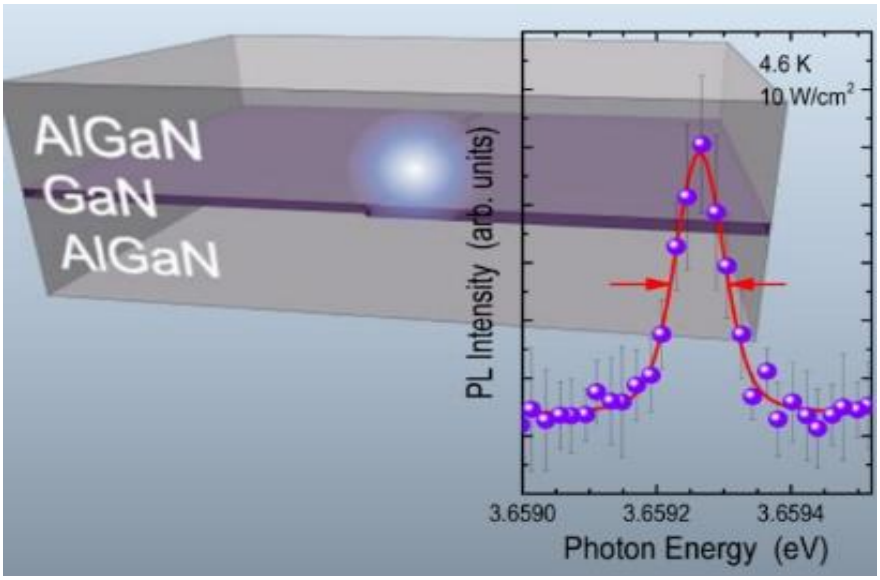

Figure 2-20 A schematic of a GaN interface fluctuation QD. Inset figure is the emission profile from such QD at 4.6K with a Gaussian model fitting. [62]

As shown in figure 2-20, the narrowest linewidth, as low as 87 μeV, from III-Nitride materials has been reported and the inhomogeneous broadening has already assessed the order of its an upper limitation. [62]

Meanwhile, a recorded pure single photon emission from III-Nitride semiconductor materials has been generated from such kind QD, with a $g^{(2)}(0)$ as low as 0.02. We will discuss it later in detail in chapter 4.

3 Setup for Single Photon Emission Measurements

In order to investigate the single photon emission properties, micro photoluminescence and auto-correlation mothed were used here.

There are mainly two systems I used in my experiment, the side excitation setup which is suitable for the emitters in the range of ultraviolet, and Vertical Excitation setup for the visible measurement. Both of them are used for the III-Nitride semiconductor materials.

In this chapter, I will introduce the measurement mothed and these two optical systems, especially more detail in the side excitation setup which is more focus on the III-Nitride interface fluctuation quantum dot.

3.1 The Two Excitation Setup Used in this Study

3.1.1 Side Excitation Setup for UV Measurement

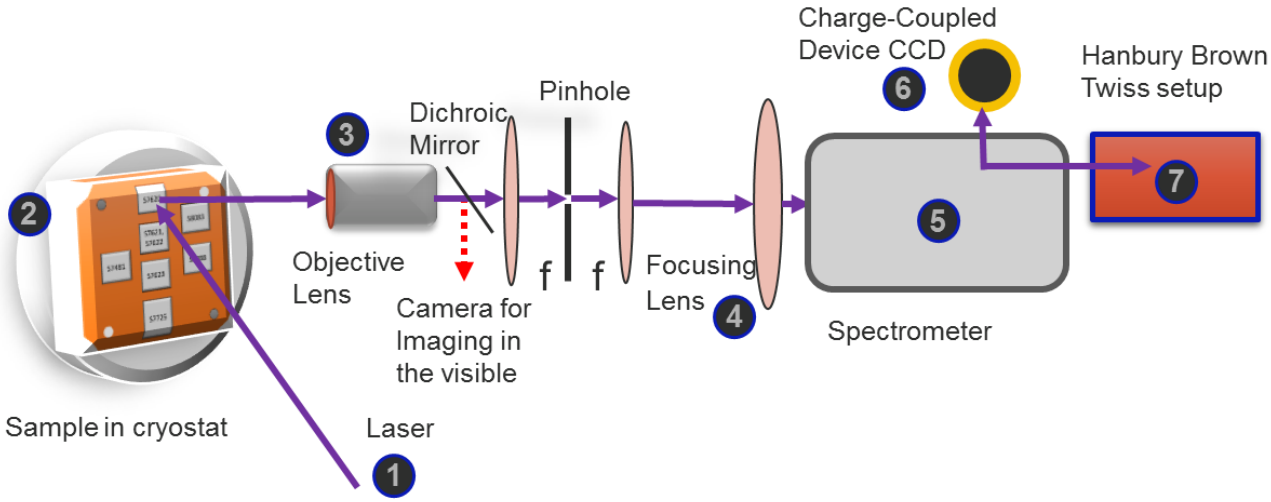

Figure 3-1. The side excitation setup is used for ultra violet single photon detection.

Figure 3-1 shows our side excitation UV setup to achieve the micro photoluminescence and auto-correlation measurement from the III-Nitride semiconductors ranging in the short wavelength. The experiment for the interface fluctuation GaN quantum dots is basically done in this setup. So, we will mainly focus on the introduction of this side excitation setup.

The numbers in the figure 3-1 represent the different components in the system.

Part 1 in figure 3-1 is the excitation lasers focusing onto the surface of the sample in the experiment as the figure 3-2. Considering the emission range in the short

wavelength, two lasers with high photon energy levels were controllable used here in this setup.

One is a tunable Ti: Sapphire pulsed laser with the emission wavelength range from 700~900 nm as shown in the left of figure 3-2. In our experiment, two non-linear Lithium Borate crystals were used to generate the third order harmonics beam. The emission wavelength of the Ti: Sapphire pulsed laser was set to be 800nm in common, leads to the wavelength of the third order harmonics of 266nm.

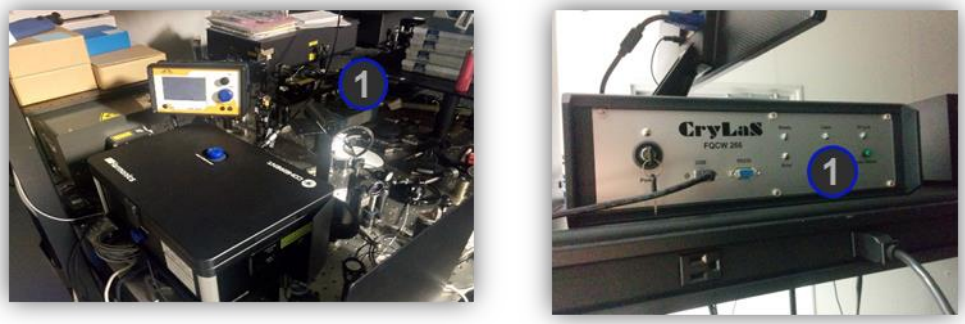

Figure 3-2. Two lasers used in the side excitation UV setup.
Left, Ti: Sapphire pulsed laser. Right, diode pumper continuous wave laser.

The other one is the diode pumper continuous wave (CW) laser with 266nm emission wavelength (CryLas, FQCW266) as shown in the right of figure 3-2.

A mounted continuously variable ND filter was set into the optical path after the laser output to control the excitation laser power.

Figure 3-3. The cryostat and objective lens.

Part 2 in figure 3-1 is the cryostat where localized our studied sample, and Part 3 if the objective lens which helps us to collect the photoluminescence from the sample. The picture of these two parts can be found in figure 3-3. We will provide more information of these two parts in Section 3.2.

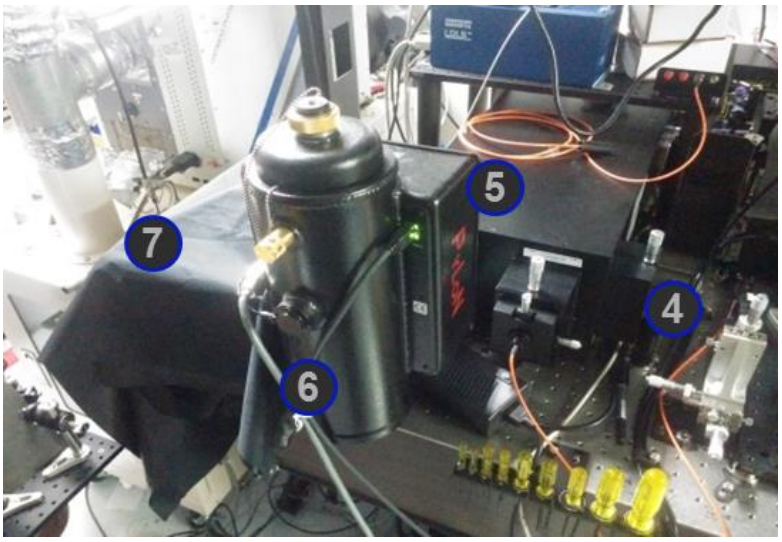

Figure 3-4. The detection part of this setup. Including the focusing lens, spectrometer, an nitrogen cooled charge-coupled device (CCD), and Hanbury Brown Twiss system.

The detection part of this setup was shown in figure 3-2 and figure 3-4. Part 4 is a lens with 10cm focus length, which focuses the luminescence into a spectrometer. Part 5 is the 75cm-length spectrometer (Princeton Instruments SP-2760-U). Part 6 is a nitrogen cooled charge-coupled device (CCD) and part 7 is our home-made Hanbury Brown Twiss system. More detail of these part will be discussed in the following part of this chapter.

3.1.2 Vertical Excitation Setup for Visible Measurement

We built another setup using Vertical Excitation which is suitable for the visible optical observation for III-Nitride semiconductors. As shown in figure 3-5.

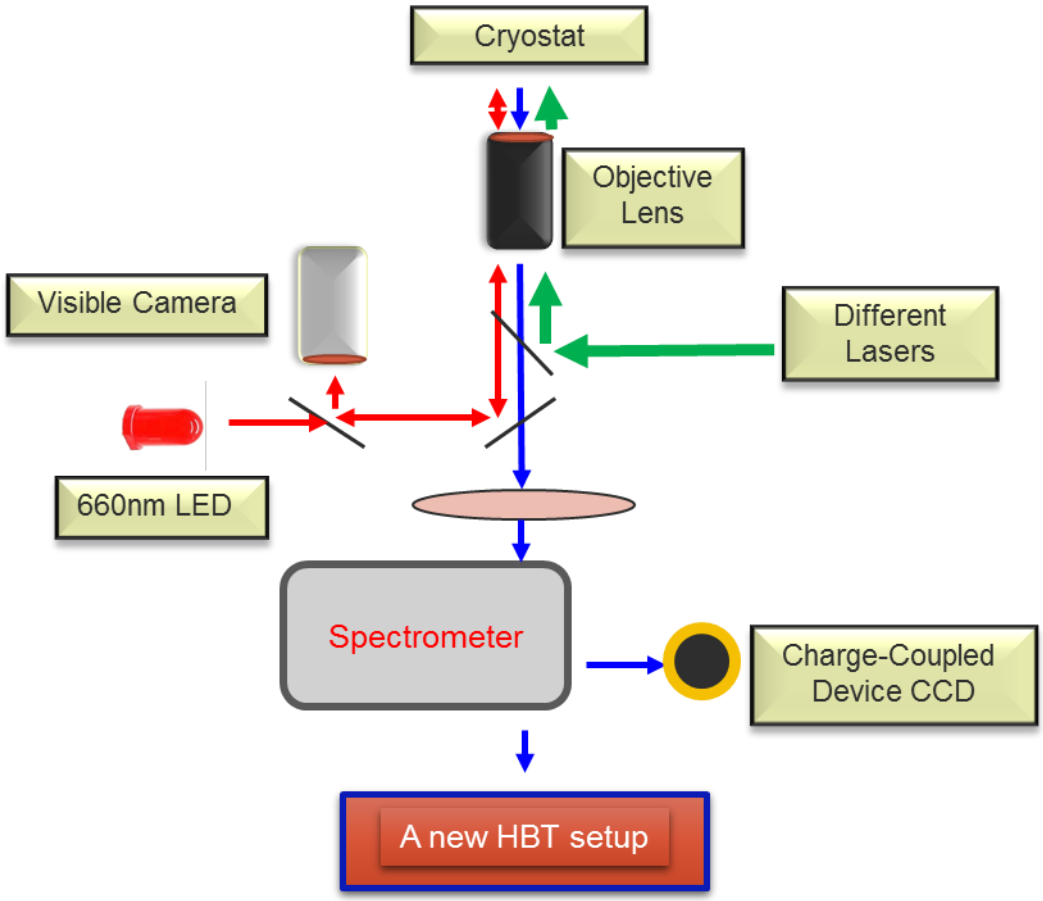

Figure 3-5. The vertical excitation setup is used for visible range single photon detection.

As the difference in their name, the excitation beams from different lasers was guided into the same path of the observation path (in the inverse direction). Which help us to excite the sample in the vertical direction.

Meanwhile, more option of the excitation lasers provided in this setup including the second and third order harmonics generated by the Ti: Sapphire pulsed laser, and serval continuous wave (CW) lasers in different emission wavelengths (325nm, 355nm, 375nm and 400nm). The optical paths for all of these lasers were well designed and aligned so that they can be easily change to excite the sample in cryostat by pushing the button on the controller for the respective flappable mirror within the respective optical path.

One more difference to the side excitation setup is the spectrometer here is only 35cm-length, which part we dream to improve in the following.

3.2 Measurement Technique

3.2.1 Sample Preparations

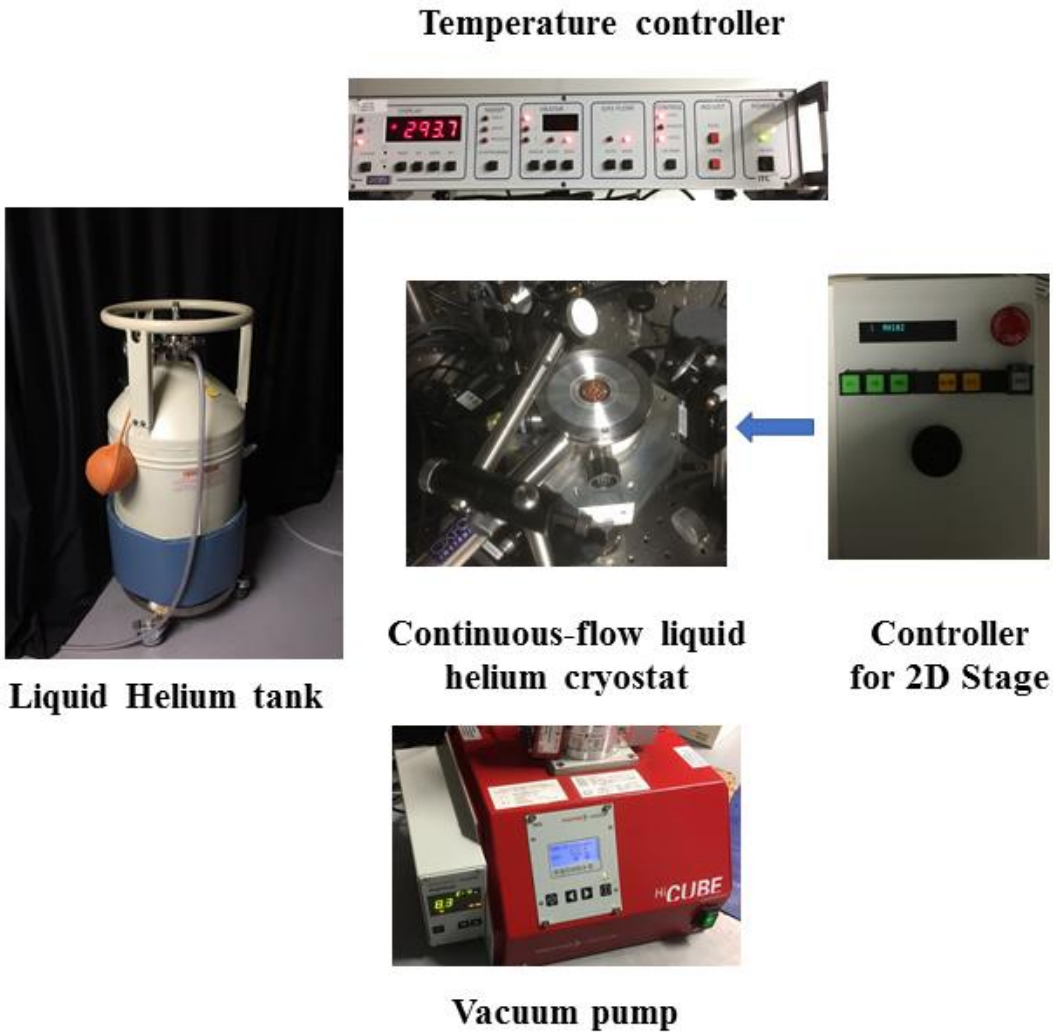

Figure 3-6. Equipment system in our setup for the sample preparation.

Figure 3-6 is several equipment systems used in our side excitation UV setup.

In the middle is the continuous flow liquid helium cryostat, which is localized on a 2-dimension stage. By using its electrical controller as shown in the right, mapping onto the sample to search good single photon candidate is available.

The left figure shows one of the 65-liter liquid helium tanks (C-65 or CD-65 is usually used here) to cool down the sample. With the temperature controller (Oxford Instruments Cryogenic Temperature Controller, ITC503 and 502) as shown in the top figure, we can set and maintain the temperature of the sample mounted inside the cryostat in a big range from 4.6K to the room temperature of 300K.

A vacuum pump (HiCube80Eco) was used to pump down the pressure inside the cryostat to provide a clean vacuum environment surround our quantum dot. The pressure is pumped down the order of 10^{-4} bar during the experiment.

3.2.2 Micro-Photoluminescence

The micro photoluminescence was performed in our study. In the side excitation UV setup, two objective lenses were chosen to collect the emission from the sample. The objective lens was localized on an electric controlled stage to find the right height of the lens to focus the optical path in the experiment.

One of them is a Mitutoyo M Plan UV with the magnification x50 and numerical aperture (NA) of 0.40. The other one is an Olympus LUCPlanFL N with a higher numerical aperture of 0.60 and magnification x40.

These two lenses help this setup to provide a relatively wide UV wavelength range from 330-350nm, which is available for our investigation of the interface fluctuation GaN quantum dots sample.

A dichroic mirror after the lens was used to separate the UV and visible light.

The visible light which is coming from a 660nm LED and reflected from the

surface of the sample is guided to a visible camera to do the navigation of the quantum dot, which we will introduce in 3.5.

The UV light is the photo luminescence from the sample, which will direct to a spectrometer. The spectrometer used in the side excitation setup is 75cm-length (Princeton Instruments SP-2760-U) within 600,1200 and 2400 lmm^{-1} grating. Usually, 600 and 1200 lmm^{-1} grating are used to navigate the sample. 2400 lmm^{-1} grating is used to do the further investigation after finding so of the quantum dot candidate due to their narrow linewidth.

The spectrometer has two exit slits. One on the front edge of the spectrometer is attached onto a nitrogen cooled charge-coupled device (CCD) to do the time-integrated measurements. The other one on the side of the edge of the spectrometer is attached onto our home-made Hanbury Brown Twiss system to do the time-resolved experiments.

3.3 Time-Integrated Measurements

In the side excitation setup, the time-integrated measurement of the photoluminescence was performed using a nitrogen cooled charge-coupled device (CCD) arrays.

We used a software called Winspec on a computer connected to the CCD to control the mirror inside spectrometer to direct the photoluminescence to the front edge (we can also control it the side edge to do the time-resolved measurements).

CCD can record the emission spectrum after the diffraction by our selected grating inside the spectrometer. Usually, we will set the integration time to 1 second. Meanwhile, we need to be careful to avoid the saturation of the CCD arrays to keep it working as normal.

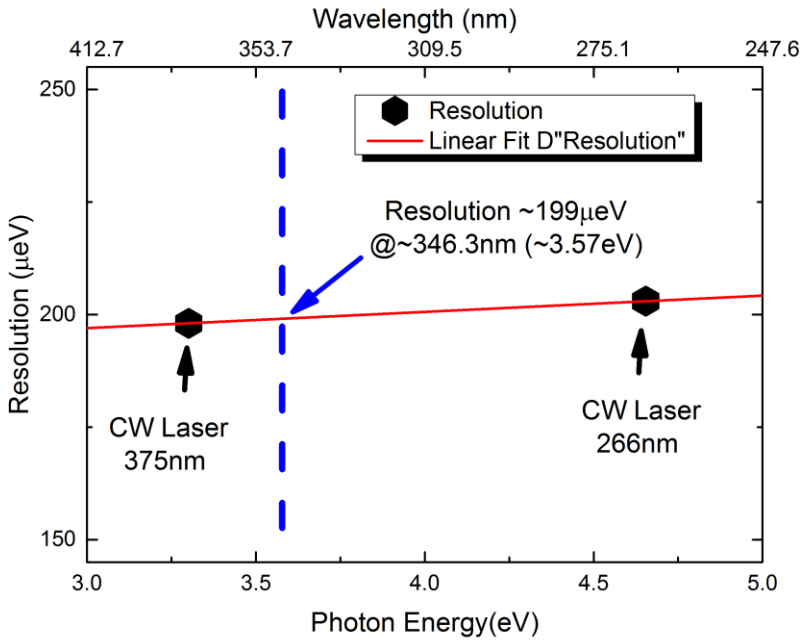

Figure 3-7 Resolution limit of our system. Measured by the laser scatter from 266nm and 375nm CW lasers.

In order to investigate the narrow emission linewidth from the interface fluctuation quantum dots (less than 1meV in common). The spectral resolution limit of our system is important to ensure our results.

The resolution limit of our system has been measured as shown in figure 3-7. We Measured by the laser scatter from 266nm and 375nm CW lasers far reduced by an ND filter. Here the CW laser linewidth is thought to in the narrower order of our photoluminescence, and the spots in figure 3-7 shows the linewidths of these two lasers as a function of their photon energy. By a linear fit, the measured data we can evaluate Resolution limit of our system around the quantum dot emission wavelength (346.3nm) is ~200 μeV, which is smaller than our studied quantum dot.

3.4 Time-Resolved Measurements

In the side excitation setup, the time correlated single photon counting was performed using a PC-mounted Becker & Hickl GmbH card (SPC-130-EM).

The radiative decay time measurement and the photon auto-correlation measurement are performed in this time correlated counting system.

3.4.1 The Hanbury-Brown & Twiss Setup and Auto-correlation Measurement

The Hanbury-Brown & Twiss system in the side excitation UV setup was built with our previous co-worker, Mr. Florian Le Roux. [103]

Two Hanbury-Brown & Twiss systems in two mentioned setups are similar. A brief introduction will be given here.

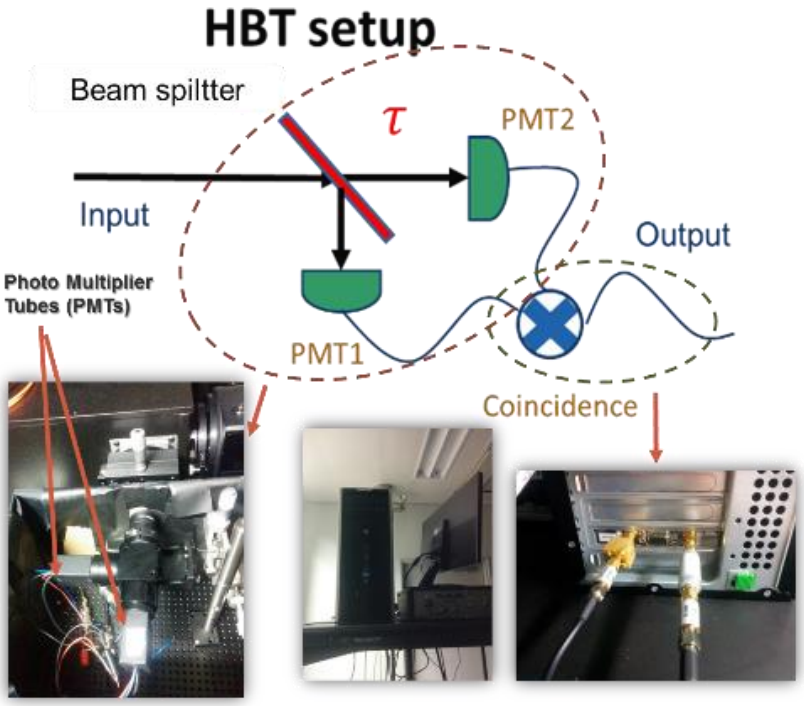

Figure 3-8 A home-made HBT measurement setup.

The Hanbury-Brown & Twiss system consists two photomultiplier tubes (Hamamatsu H10682-210) and a beam splitter as shown in figure 3-8.

Photoluminescence diffracted by the grating inside the spectrometer is guided to the beam splitter. It has been detected and transformed electrical signals. After the transmission through BNC cables, these signals injected into the start and stop channels of the PC-mounted counting card to do the coincidence.

Because the order of the lifetime from the quantum dot is in the range of microseconds to picoseconds. [32] The Time response distribution affected by the whole optical setup is a key parameter to evaluate our experiment result.

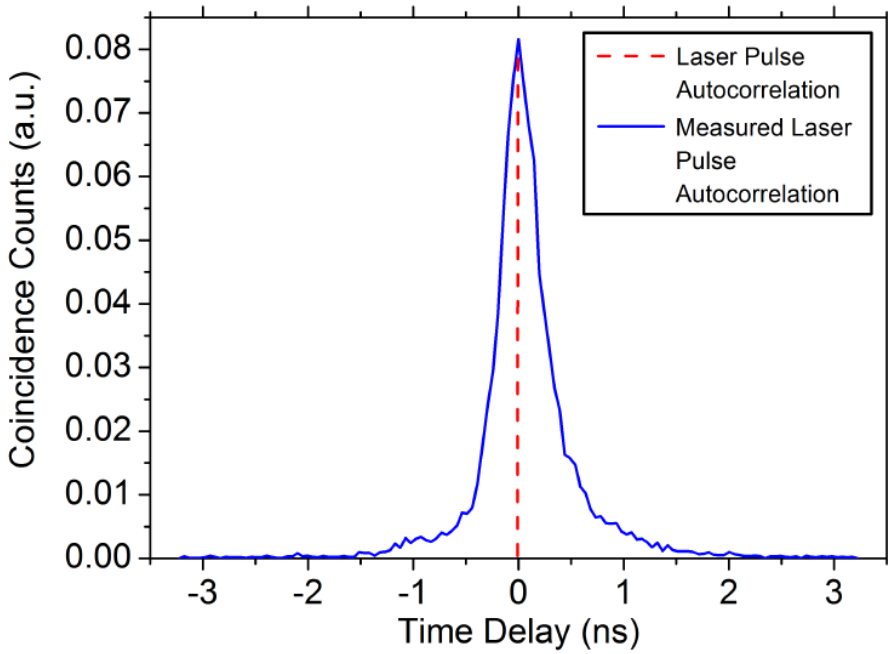

Figure 3-9. Time response distribution of the optical setup.

Red line: Theoretical pulsed laser auto-correlation.

Blue line Measured pulsed laser auto-correlation broadening by the time response.

[103]

Intensity auto-correlation from the Ti: Sapphire ultrafast pulsed laser (as we motioned in section 3.1) was used to investigate the time response of this system. Here the pulse width of Ti: Sapphire laser is short enough (as short as 200 fs) to be estimated as a delta function.

Pulsed laser intensity auto-correlation can be found in figure 3-9. The red line is theoretical pulsed laser auto-correlation, and the blue line is the measured pulsed laser auto-correlation broadening by the time response. [103]

As a result, the time response of our side excitation setup can be evaluated to the order of hundreds of picoseconds, representing the fact that our system is sensitive enough for our following measurement.

3.4.2 Radiative Decay Time Measurement

As a common method, pulsed excitation was used to evaluate the radiative decay time, which can be also done by our HBT setup.

Here we used the Ti: Sapphire ultrafast pulsed laser (with a repetition frequency of 80MHz) to excite the sample, and use only one of the PMTs (either is fine) to measure the luminescence. The signal from this PMT will be connected to the start channel of the photon counting system. Meanwhile, the stop channel is connected to the time signatures of the pulsed laser.

At this situation, the photon counting is recording the coincidence of the time differences between the laser pulse and the photon emission. After the accumulation of the coincident counter of the two electric channels, we can get the decay curve as shown in figure 3-10. [92]

However, it is clear that the background luminescence from the environment of the quantum dot (in the figure it is the wetting layer) will lead to an addition decay curve. This is the current limitation of this radiative decay measurement method.

In chapter 5, we will provide another method to investigate the exciton decay time of the interface fluctuation quantum dots by its excitation power dependence of single photon dynamics under CW excitation.

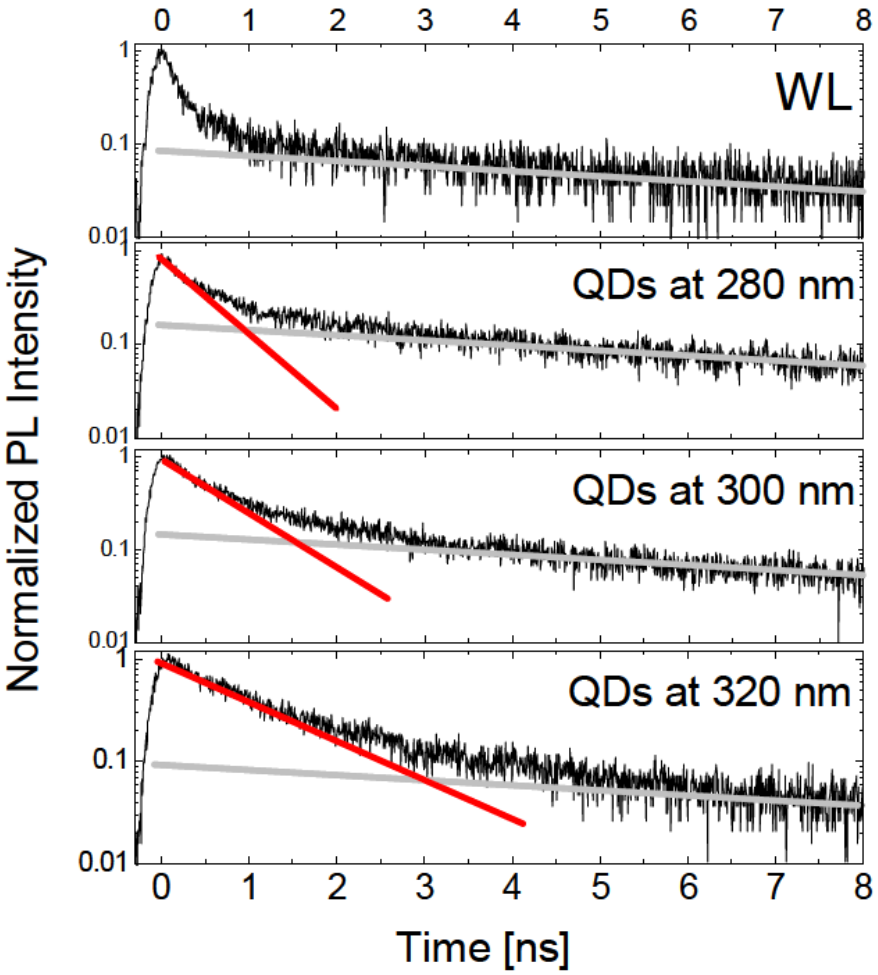

Figure 3-10. Photo wavelength depend time-resolved radiative decay curves of GaN/AlN self-assembled quantum dots. [92]

3.4.3 Auto-correlation Under Different Excitation Sources

Both pulsed laser and CW laser can be used to excite the sample. However, the auto-correlations under this two excitation sources are different.

In this section, we will introduce the performance of them and the consideration within the single photon detection.

One case is the pulsed auto-correlation as shown in figure 3-11 for an example. [104] The repetition of the peaks in the histogram is the same as the repetition of the excitation laser pulse. The widths for each of the peaks are related to the radiative decay time of the emitters.

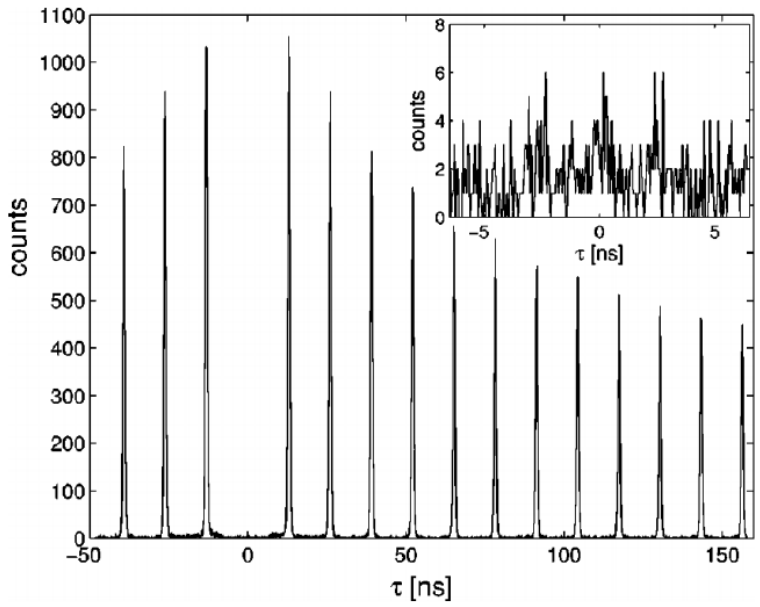

Figure 3-11. An example of auto-correlation histogram under pulsed excitation. [104]

As a result, the emission time should be considered before doing the laser excitation single photon detection. Which should be in the smaller order than the pulsed laser repetition time (in here it is 12.5ns) to avoid the combination of the neighboring peaks.

During the analyzation of the measured data, usually, we will select a time window which a width between the peaks width and the repetition time of the setup to isolate each one of the peaks. As a result, the measured $g^{(2)}(0)$ is always calculated as the

accumulated counts in the center peak (while time delay equals 0) divided by the average of all the other peaks.

The other case is the CW auto-correlation as shown in figure 3-12 for an example. [105] A dip in the middle (when delay time equals 0) of the histogram due to the single photon emission.

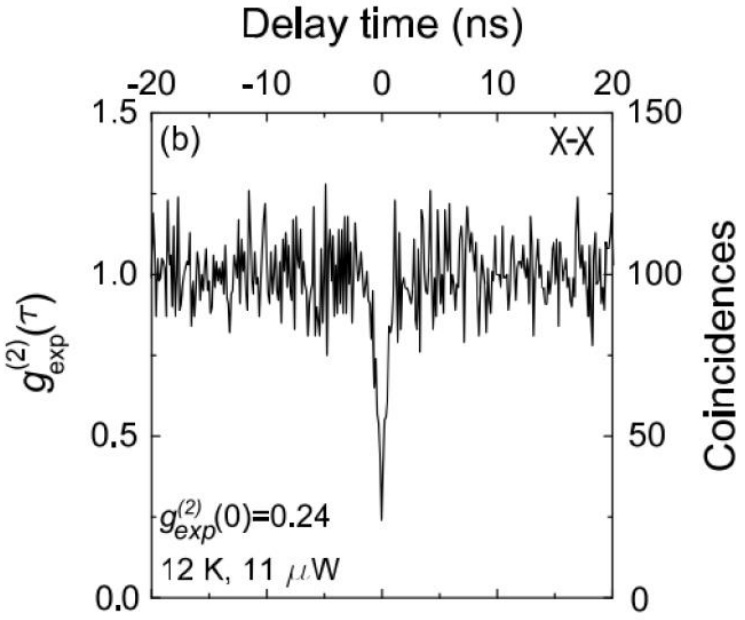

Figure 3-12. An example of auto-correlation histogram under CW excitation. [105]

In order the extract the measured $g^{(2)}(0)$ normalized measured auto-correlation data can be fitted as a typical exponential function:

$$g^{2}(\tau)=1-(1-g^{(2)}(0))\exp(\frac{-|\tau|}{t}) \tag{3-1}$$

Where t is a time constant of the excited emitters, we will discuss this constant in details in Chapter 5. τ is the time delay, $g^{(2)}(\tau)$ is the normalized coincident

counts as a function of time delay.

The widths for antibunching dip are resulting from the convolution of the actual second order auto-correlation function and the time response of the optical setup. Furthermore, in order to get accurate $g^{(2)}(0)$, a long acquisition time is thought to be necessary to reach relatively high average counts (which is usually no less than 30 in our experiment).

3.5 Mapping the Sample

After preparing the sample loading in the cryostat, we need to scan its and try to find some good single photon emitters onto the sample.

Usually, we need to acquire the photoluminescence while scanning the different place of the sample. And try to find some delta-function-like narrow emission peak on the spectrum by using the 300 or 1200 lmm^{-1} grating in the spectrometer and the charge-coupled device.

3.5.1 Visible Mapping Technique of the Sample Surface

As shown in figure 3-1, we used a 660nm LED and a camera for imaging the surface of the sample. In the optical path, a dichroic mirror is used for this visible line. After finding good single quantum dot candidates, usually we change to the 2400 lmm^{-1} grating inside the spectrometer and try to optimize the observation.

Figure 3-13. Sample image and marks on the scream connected to the visible camera.

In order to help us to record the position of the quantum dot and find it easily if we plan to do more investigation of it again. We would prefer to draw some marks on the scream connected to the visible camera, as shown in figure 3-13. Those marks always meet the image of the patterns or microstructures on the surface of the sample.

3.5.2 Isolation of a Single Emitter

In the experiment, the excitation laser was focused into a small spot to excite only a small range of the sample to depurate the emission spectrum. Furthermore, in order to improve the isolation of the single emitter, an additional optical isolation system was built after the objective lens to isolate the detection area of the sample surface, as shown in figure 3-14.

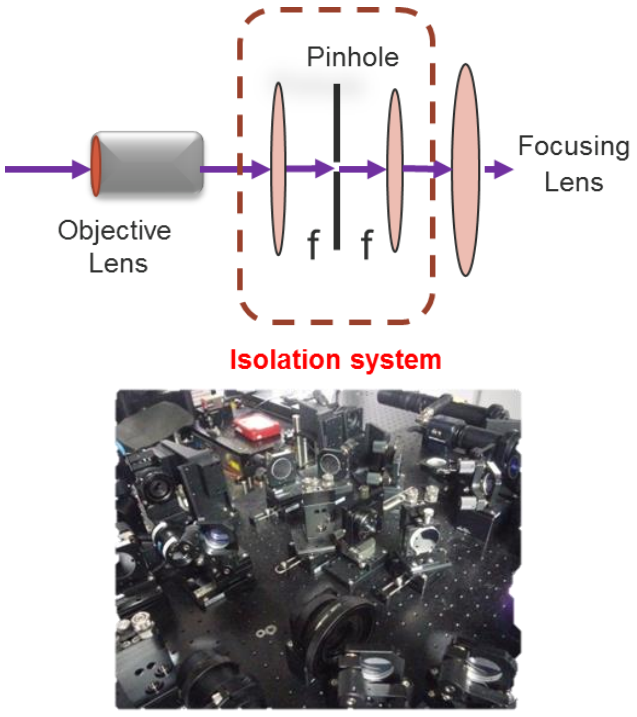

Figure 3-14. The isolation system of the in the optical setup. Upper and lower, Schematic diagram and the picture of the isolation system.

Upper in figure 3-14 is the schematic diagram which can also be found as parts of figure 3-1. This system contains a pinhole in the middle of two lenses (in experiment two concave mirrors are used instead of the lenses to save the room of the whole setup) right at the position of their focal points. Filtered spatially by the pinhole, a notable reduction of the detecting pried has been obtained (from the order of 200*100μm^2 down to 2*2μm^2). This system efficiently eliminates spectral contamination by reducing the background emission from environment surround the selected quantum dots.

4 Temperature Dependence of Single Photon Emission from Interface-Fluctuation GaN Quantum Dots

In this chapter, we will focus on the investigation of the single photon emission from the interface fluctuation GaN quantum dot [62] and its performance under different operating temperature conditions. To evaluate its temperature characteristics that could be achieved high purity single photon emissions. This work cooperated with Mr. Florian Le Roux, and it has been published in *Scientific Reports* 7, 16107 (2017). [106]

4.1 Motivation: How Purely can we Measure Single Photon Emission from III-Nitride Quantum Dots?

Second-order auto-correlation coincidence $g^{(2)}(0)$ is an important parameter that reveals how pure of the measured single photon state, in another word, it reveals the quality of the sing photon sources.

In Chapter 2, we introduce that one of the current limitations for the single photon emissions from III-Nitride quantum dots is their relatively low purity compared with other materials such as III-Arsenide. It is well known that the spectral contamination from the emission background usually affects the purity of single photon emitters.

Meanwhile, the operation temperature is thought to be a factor that affects the background emission. Spectral contamination is usually unavoidable while increasing

the temperature of the emitters.

In this chapter, we will investigate the introduce the high purity from single photon emission from a recently fabricated interface fluctuation GaN quantum dot [62], which exhibit a recorded narrow linewidth in III-Nitride semiconductor system. Furthermore, we will introduce the different single photon emission purities from such a single quantum dot as a function of its operating temperature, and reveal the relationship among the operation temperature, the spectral contamination of the photoluminescence and the purity of the single photon emission from our studied single quantum dot.

4.2 Temperature Dependence of Single Photon Emission

In this experiment, we used our side excitation UV setup to try to find pure single photon emitters from interface fluctuation quantum dot. More detail of this setup can be found in Chapter 3.

The sample was held inside of a continuous-flow liquid helium cryostat, and the operation temperature was controlled by a temperature controller, cooling down to a relatively low temperature. A diode-pumped solid-state CW laser at a wavelength of 266nm was guided onto the top surface of the sample. A 40x objective lens was used to collect photoluminescence from the sample the operational in the near UV (NA=0.6).

By mapping the sample, we found serval photon luminescence spectrums with nice sharp QD-like emission peak from our interface fluctuation quantum dot sample, which proves their possibility to emit single photons.

Moreover, we used our home-made HBT system to measure auto-correlation and get serval antibunching dip, which clearly shows the single photon emissions, as 2 examples shown in figure 4-1. [103]

The images on the left side of figure 4-1 are the spectrum and auto-correlation result of one single dot candidate with ~339nm emission wavelength. The images on the right side are the spectrum and auto-correlation histogram of another single candidate with ~337nm emission wavelength.

It is clear that both of them are in fact emitting single photons because their $g^{(2)}(0)$ are evaluated lower than 0.5 (fitted $g^{(2)}(0)$ of the 339nm dot is 0.47, while fitted $g^{(2)}(0)$ of the 337nm dot is 0.34).

However, compared with reported lowest [43,102] $g^{(2)}(0)$ from III-Nitride quantum dots, these values need to improve to get much purer single photon emission by searching another good candidate and the optimization of its excitation conditions.

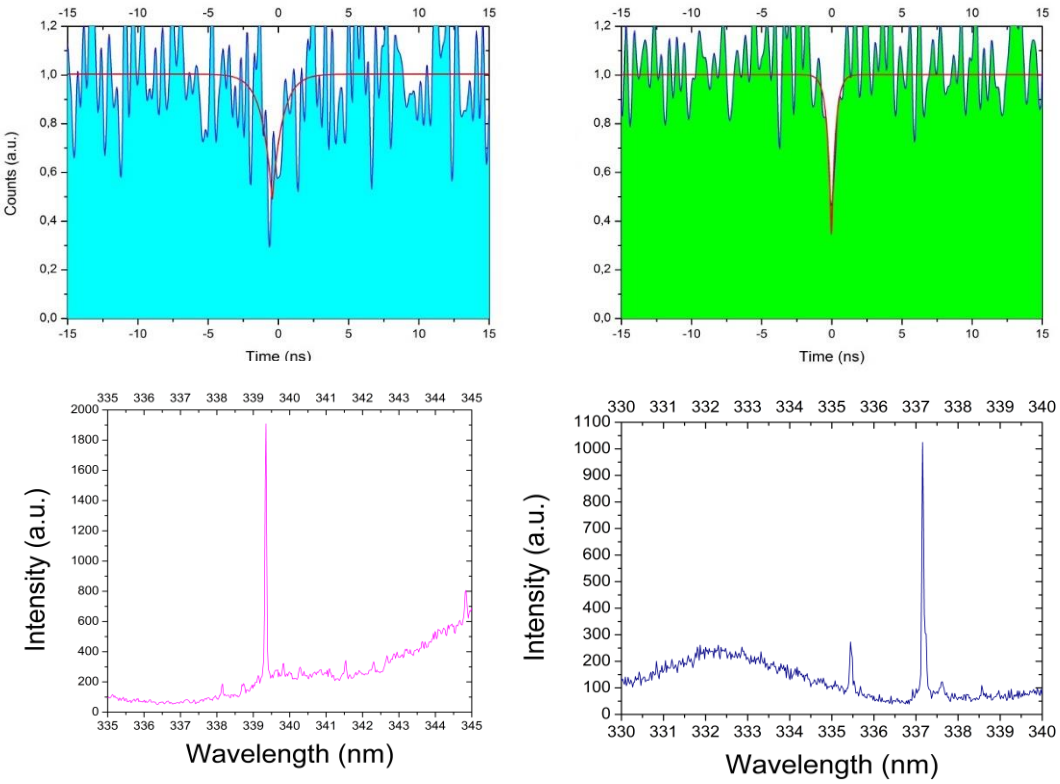

Figure 4-1. Two single photon emitters from the interface fluctuation quantum dots. [103]

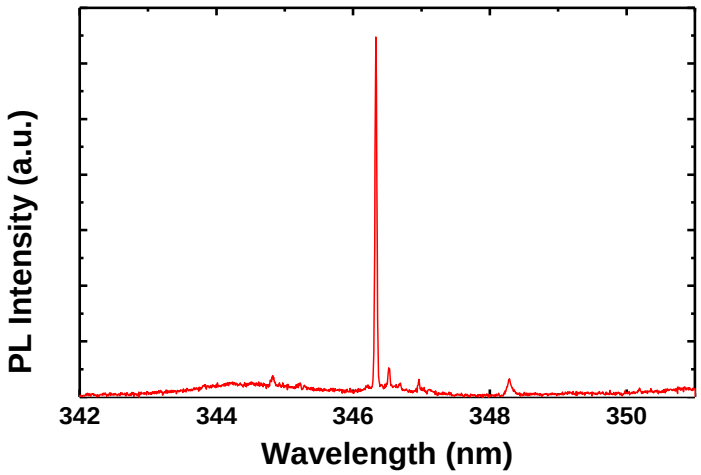

Figure 4-2. Another single photon emissions from the interface fluctuation quantum dot. [103]

Finally, we found a good candidate as its spectrum showing in figure 4-2 (more measuring detail will be discussed later). We selected it as the study platform of our following research due to its narrow linewidth, stable emission line, and other properties we will discuss later.

4.2.1 Emission Spectrum under Various Temperatures

Here we would like to investigate the influence of the temperature on the purity of single photon emissions. Firstly, we got the temperature dependence of the emission spectrum and made a comparison of them.

After cooling the sample down to a low temperature (4.6K), we kept liquid helium continuously flowing to the cryostat, and then turned on the heater inside the cryostat connected to the temperature controller. By setting operation temperature on the temperature controller, the photoluminescence from such selected quantum dot in different temperature conditions were collected by the UV objective lens. The spectrums were obtained by the CCD attached onto the front exit slit of the spectrometer. We selected the 2400 lmm^{-1} grating inside the spectrometer to get higher spectral resolution due to its relatively narrow linewidth.

The measured spectrums under 10K, 30K, 50K and 77K were recorded as figure 4-3. The spectrum in each of the figures was got when the peaks intensity is at the saturation point while increasing the excitation CW laser power.

From figure 4-3, we can basically find a trend om the spectrums. That is the height of the emission peak dropped while increasing the operation temperature. However, at the same time, the emission background keeping increasing. This is the key point of this study, we will discuss the mechanism of this phenomenon and its influence to the single photon emission later.

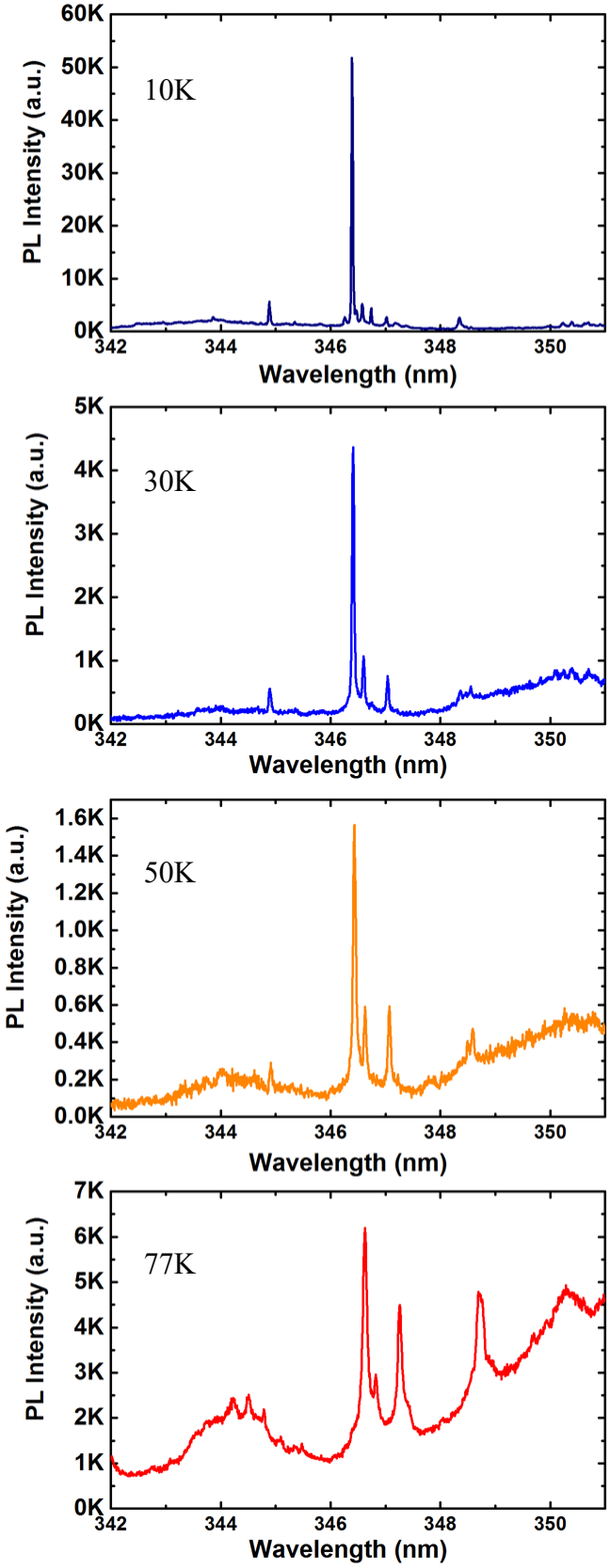

Figure 4-3. The emission spectrums under 10K, 30K, 50K and 77K from an interface fluctuation quantum dot. [103, 106]

4.2.2 Temperature Dependence of Auto-correlation Measurement

After measuring of the emission spectrum of corresponding temperature, the photoluminescence was directed to the side exit slit of the spectrometer, in another word, we guided the emission into our home-made HBT setup to measure the auto-correlations.

Photon auto-correlation measurement results from such selected single interface fluctuation III-Nitride Qs from 10K to 77K and the emission spectrum profiles corresponding to each of them are performed in figure 4-4. [106] Where T in the figures is the operation temperature for each of them, P is the CW laser power density exciting at the saturation point of the emission. The measured result of $g^{(2)}(0)$ can be evaluated by fitting the normalized data with a typical second order auto-correlation function (Equation 3-1) as the red curves in the figures.

When the temperature is less than 30K, the measured $g^{(2)}(0)$ values are less 0.2, this is a very clear evidence reveals a single photon emission in such quantum dot. However, during raising the operation temperature, an uncorrelated broad background emission increasingly in the spectrum, degrading the purity with of single photon emission from the QD. When temperature raised up to 77K, the measured a $g^{(2)}(0)$ value can be approximately evaluated as much as 0.52. It can be inferred that the sub-Poissonian statistics of measured light, is not strong enough to claim the single photon emission property from this sample. This contaminating background emission is explained that it comes from the thermal broadening and increased carrier population of states related to the GaN quantum well that forms as part of the growth process of these QDs. [62, 106]

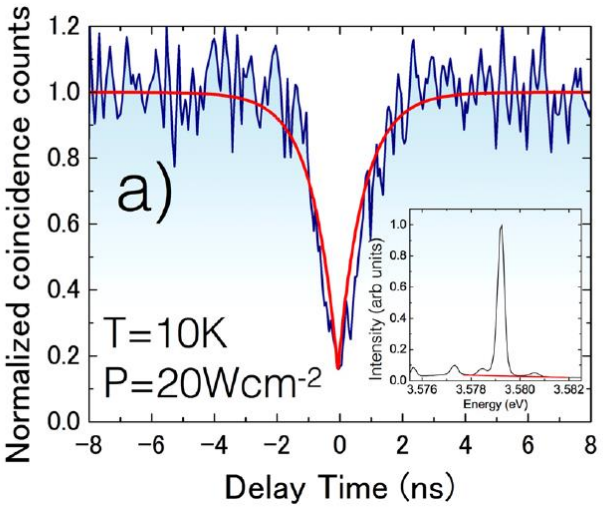
a)
T=10K
P=20Wcm-2
Normalized coincidence counts
Delay Time (ns)
Intensity (arb units)
Energy (eV)

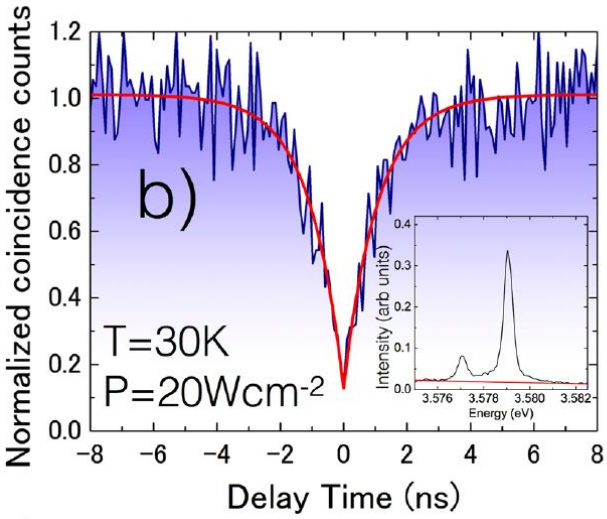
b)
T=30K
P=20Wcm-2
Normalized coincidence counts
Delay Time (ns)
Intensity (arb units)
Energy (eV)

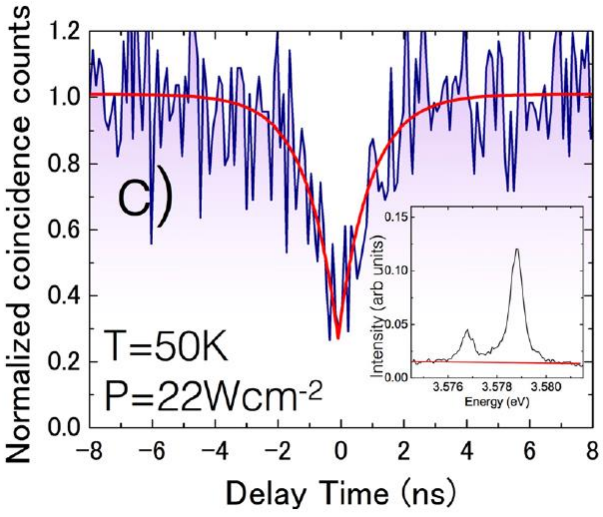
c)
T=50K
P=22Wcm-2
Normalized coincidence counts
Delay Time (ns)
Intensity (arb units)
Energy (eV)

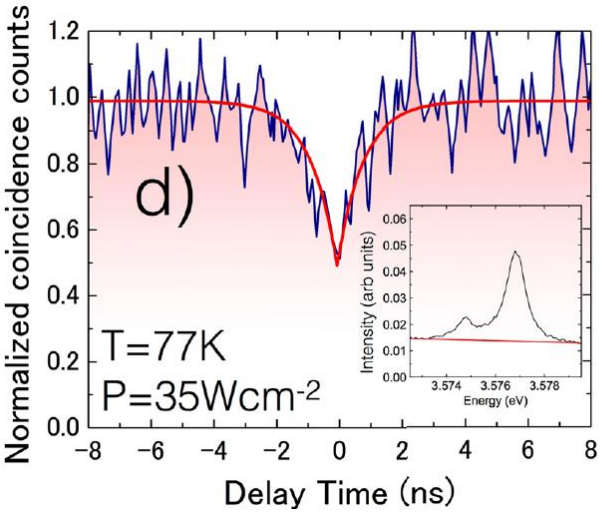

Figure 4-4. Photon auto-correlation measurements and their corresponding emission spectrum from the selected single interface fluctuation GaN quantum dot from 10K to 77K (a-d). [106]

The measurement of $g^{(2)}(0)$ provides us a lot of meaningful information of the characteristics of the interface fluctuation III-Nitride quantum dot system (including the quantum dot, surrounding material, and excitation/collection optics). And it shows the possibility to emit high purity single photon. It guides us to further study its single photon properties by investigating the extent to which the background emission is actually responsible for the purity of the single photon emission. In the next section, we will discuss the emission background effect of the single photon emission from our dot and its temperature dependence.

4.3 Single Photon Emission with Emission Background Effect

In order to investigate the emission background effect, a parameter called ρ is a key factor, which follows $\rho = \frac{S}{S+B}$, equals to the ratio between the measured single photon emission intensity S and the total measured signal (including the background emission B) inside the measured region, [107] as the spectrum shown in figure 4-5.

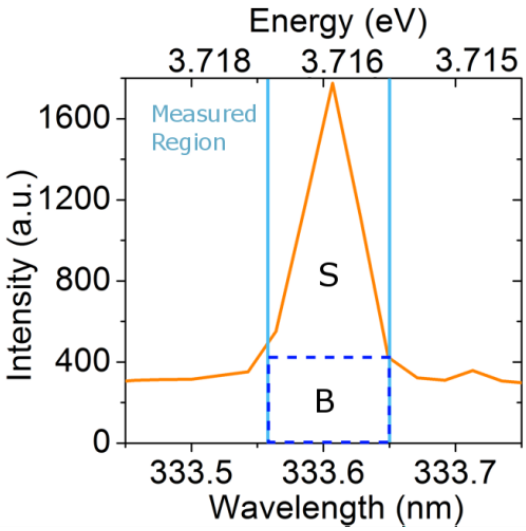

Figure 4-5. An illustration of the ratio ρ, background B and signal S on an emission spectrum. [103]

4.3.1 Influence of an Uncorrelated Background Emission

When taking account the effect of uncorrelated background-emission on a single photon emission candidate, it can be shown that the measured $g^{(2)}(0)$ will always be limited by:

$$g_l^{(2)}(0) = 1 - \rho^2 \tag{4-1}$$

This simple equation provides us a mathematical limitation of the value ρ required for the claim of single photon emission, that is $\rho > \sqrt{1/2}$.(if we want the measured $g^{(2)}(0)$ value is smaller than 0.5) In figure 4-6 we plot the measured $g^{(2)}(0)$ as a function of temperature compared to the background limited values, where the solid line is the background limited $g_l^{(2)}(0)$ value.

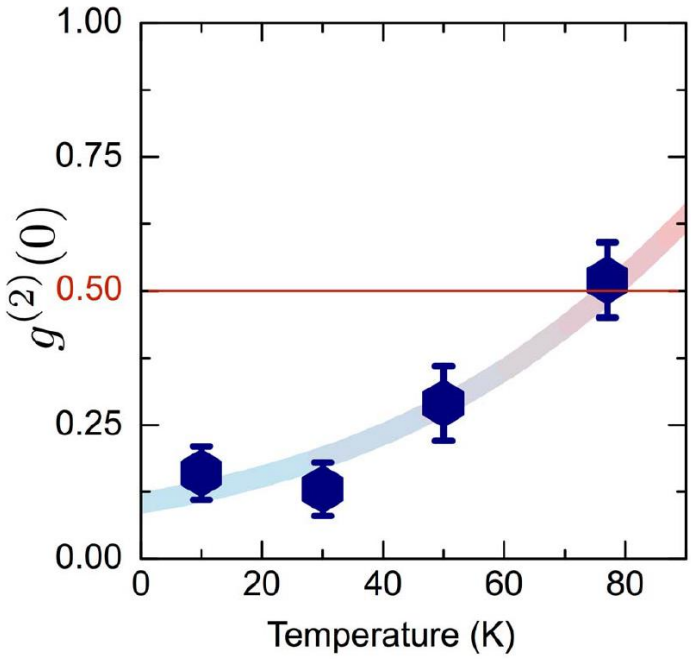

Figure 4-6. Temperature dependence of measured $g^{(2)}(0)$ extracted from figure 4-4(data point). The extrapolated curve is the background spectral contamination limited values $g_l^{(2)}(0)$. [106]

It is easy to find from figure 4-4 that the measured data compares well with temperature dependent background spectral contamination limited curve of $g_l^{(2)}(0)$, and reveal the fact that the background emission is actually the important limiting factor of the single photon emission. [41,105,106, 108–112]

In this experiment, we can clearly find the fact that the background emission of the quantum dot is the main reason degrading the measured $g^{(2)}(0)$ values. This result

shows that the quantum dots themselves are attractive candidates for high purity single photon emission sources towards the further high quality quantum sources for practical quantum applications.

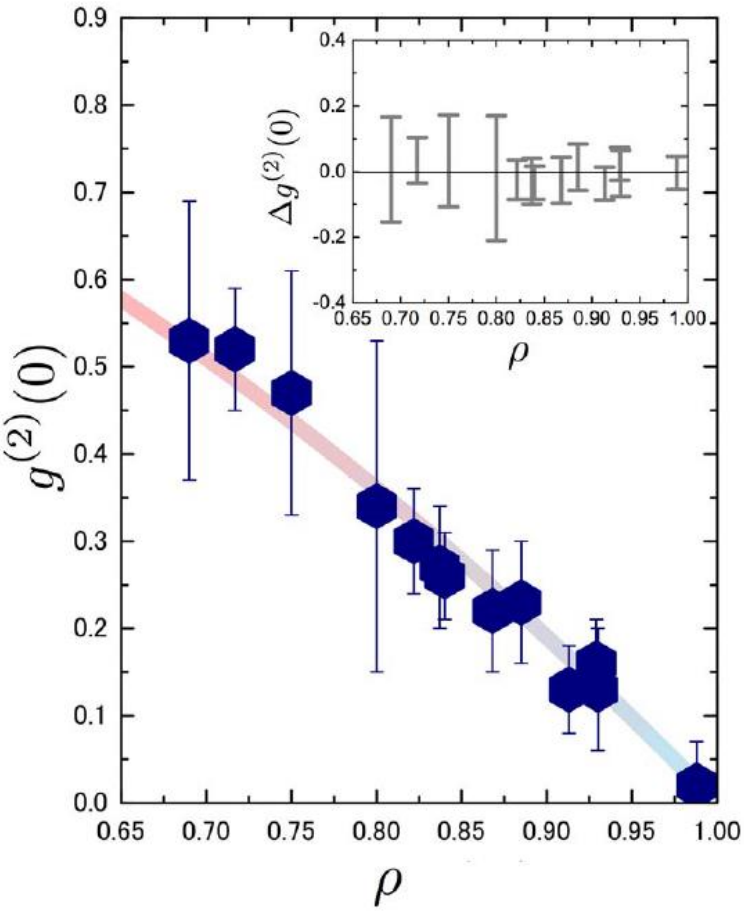

Figure 4-7. Measured $g^{(2)}(0)$ values from several quantum dots under various ambient conditions shown as a function of the measured value of ρ. The figure inset shows the residual values of $\Delta g^{(2)}(0)$. [106]

Furthermore, in order to confirm this relationship between the extent of the background emission to the single photon emission purity limitation, more measurements have been done by a large number of different other quantum dots under various excitation and ambient conditions. The measured $g^{(2)}(0)$ values are shown in

figure 4-7 as a function of measured background ratio values of ρ extracted from the spectrums.

The figure inset the figure 4-7 reveals the residuals of the $g^{(2)}(0)$ values between the measured and background limited values, $\Delta g^{(2)}(0) = g^{(2)}(0) - g_l^{(2)}(0)$ plotted as a function of ρ.

From all of these results, we can infer that measured $g^{(2)}(0)$ values follow the expected curve with a high purity single photon emitting quantum dot combined with uncorrelated background contamination in the emission spectrums, to within the experimental error for all measurements.

4.3.2 Optimization Towards High Purity Single Photon Emission

By the understanding of the background effect on the purity of the single photon emission we got. We try to optimization of the excitation conditions of such interface fluctuation GaN quantum dot.

Firstly, we measured the photoluminescence in the temperature range from 4.6K to 80K. The temperature dependence of the peak intensity was performed in figure 4-8. We found for this single quantum dot, the emission intensity reached its maximum around 10K. As a result, we set 10K a standard temperature for measuring.

Furthermore, we changed the excitation power to investigate the excitation power dependent photoluminescence peak intensity and background ratio as the results shown in figure 4-9.

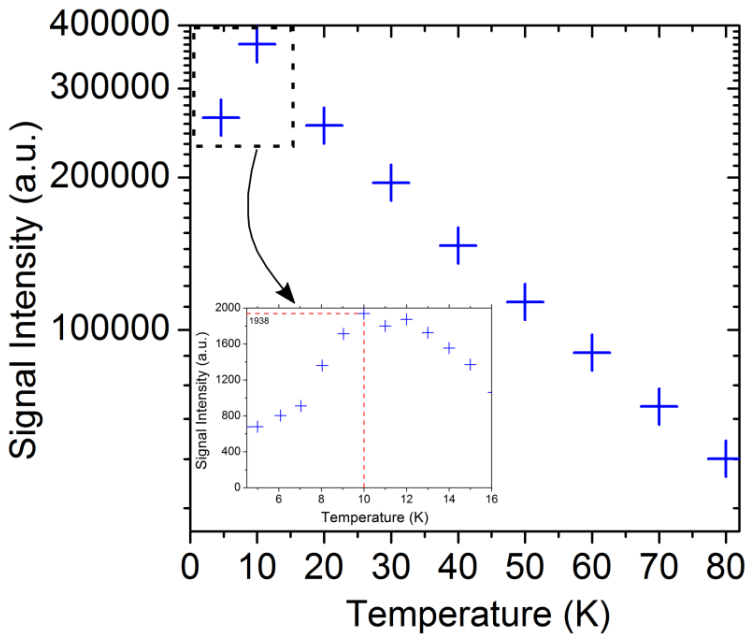

Figure 4-8. Temperature dependence of the photoluminescence intensity under an excitation power of 1 mW. Inset figure shows more data point around 10K. [103]

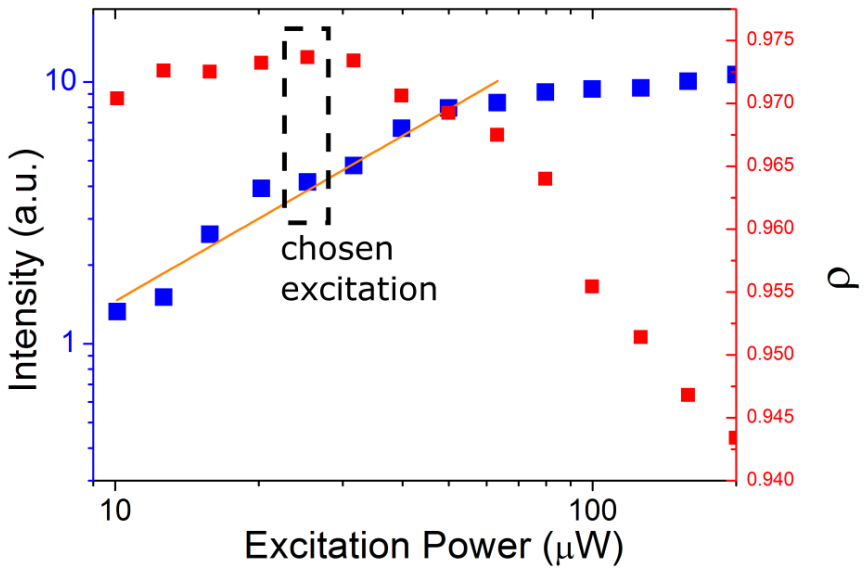

Figure 4-9. Excitation laser power dependence of the photoluminescence intensity and background ratio 10K. [103]

From figure 4-9 we can find the trend of power dependent peak intensity in the

blue data, and the red data shows the background ratio trend. It is easy to find the ratio got maximum (~0.973) when the excitation power is 25μW.

From equation (4-1), we can indicate the background spectral contamination limited values $g_I^{(2)}(0) \approx 0.053$.

4.4 High Purity of Single Photon Emission

We used the optimized operation condition (10K, 25μW) to measure our selected quantum dot.

The left figure in figure 4-10 shows the emission spectrum under CW excitation power of 25mW and temperature of 10K. The rectangle represents the spectral window we selected to guide to the HBT setup.

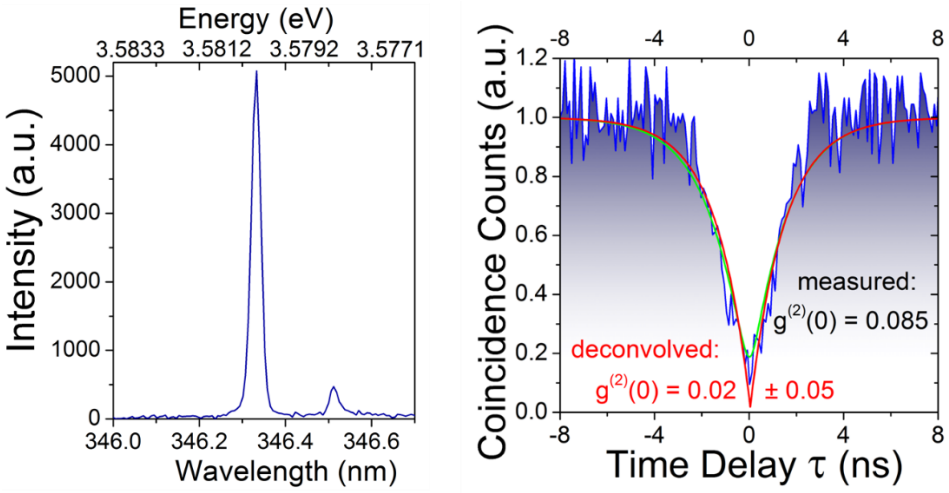

Figure 4-10. Left, the emission spectrum of the selected quantum dot in optimized operation condition. Right, auto-correlation histogram. [62,103, 113]

The photon auto-correlation result can be found in the right figure in figure 4-10.

The measured $g^{(2)}(0)$ value of 0.085, which is close to our indication. Fitting deconvolved $g^{(2)}(0)$ value (the red curve) can reach as low as 0.02±0.05. This value is the lowest ever reported for a III-nitride QD, and is, in fact, actually limited by the detector response function.

4.5 Concluding Remarks

In conclusion, we have shown the high purity single photon emission properties of interface-fluctuation GaN quantum dots for the first time. The measured $g^{(2)}(0)$ value of 0.085. Fitting deconvolved $g^{(2)}(0)$ value can reach as low as 0.02±0.05. This value is the lowest ever reported for a III-nitride QD, and is actually limited by the detector response function. This result shows that III-nitride quantum dots based high-quality optical properties are possible to be created.

Furthermore, we have shown the single photon emission properties of interface-fluctuation GaN quantum dots as a function of their operation temperature. The increased contamination in the emission spectrums due to uncorrelated background emission related to quantum-well states around the quantum dot positions, decreases the purity of single photon emissions up to the temperature of 77K.

5 Measurement of Emission Lifetime using Single Photon Emission Dynamics of III-Nitride Quantum Dots

In this chapter, we will focus on the experiment of the emission lifetime measurement of interface fluctuation GaN quantum dot by the evaluation of its power dependent single photon dynamics. By measuring the photon auto-correlation of such quantum dot under various excitation laser power, we would like to reveal the reason of the narrow emission linewidth and provide more information of the environment of such quantum dot. This work has been accepted by Physica Status Solidi A, [114] and will be published soon.

5.1 Motivation: Why is the Linewidth of Fluctuation Dots So Narrow?

In Chapter 2, we introduce the current limitation of the III-Nitride quantum dots is their induced linewidth broadening (which can result in emission linewidths of a few meV) suffering from spectral diffusion.

As the discussion in [80], the spectral diffusion occurs due to an interaction between the internal-field induced exciton permanent dipole moment [83, 84] and the fluctuating electric field of charges trapped in relatively large densities of surrounding defects [85], showing in equation (5-1)

$$\Delta E \propto Var\left[\vec{\mu} \bullet \sum \vec{F}_i\right]$$

(5-1)

where ΔE is the fluctuation of the photon energy, which represents the emission linewidth, $\vec{\mu}$ represents the permanent dipole moment, and $\sum \vec{F}_i$ is the composition of electronic forces caused by quantum dot environment.

The novel GaN interface fluctuation quantum dot can represent a narrow linewidth down to less than 100μeV. However, we need further evidence to explain the physical reason that caused such narrow linewidth.

In previous works all around the world, the emission lifetimes of III-Nitride quantum dots have been measured to be on time scales from hundreds of picoseconds to microsecond levels [92, 108, 115-120], but there have been no reports of measurements of the lifetimes of GaN interface fluctuation quantum dots.

Among these works, the results from S. Kako and M. Miyamura [92, 115] provide us an interesting relationship between the emission lifetime to the emission photon energy as shown in figure 5-1.

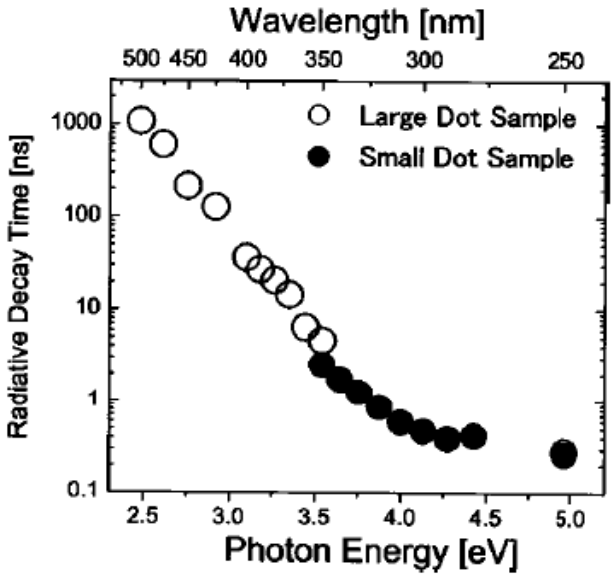

Figure 5-1. Radiative decay time of two different sizes of quantum dot samples as a function of emission energy and emission wavelength. [92]

Moreover, from the work by C. Kindel [81], we can find another relationship between the emission photon energy to the size of the dipole moment.

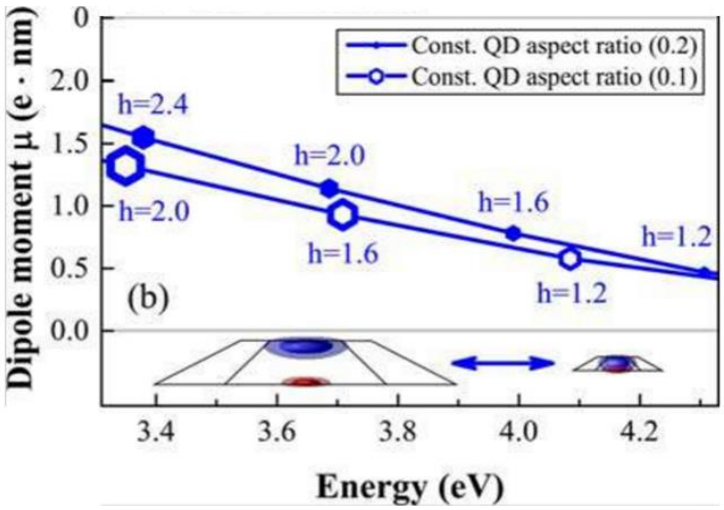

Figure 5-2. Decreasing trend ofr the dipole moments μ for two quantum dot aspect ratios. The symbol size scales with the quantum dot diameter. [81]

As a result, we can build an indirect relationship between the dipole moment and the emission lifetime, using the emission photon energy as a bridge between them. That means the dipole moments of the GaN interface fluctuation quantum dots are similar to the typical SK GaN dots when the lifetime (~1ns) and the photon energy (~0.1eV) are in the same order.

In general, time-resolved PL decay measurements are typically used to evaluate the exciton decay time. However, in our case, we found that pulsed excitation leads to emission spectra with an increased background, which affected our ability to perform lifetime (and indeed auto-correlation) measurements. We, therefore, used CW excitation to measure the lifetime at the same time as measuring the single photon emission [105, 121].

Moreover, when we measure the exciton decay indirectly via g2-measurements, we can also be sure of that the anti-bunching decay is due to the single quantum dot we measured (when the measured $g^{(2)}(0)$ less than 0.5).

In one word, by measuring the emission lifetime, we can hopefully get the information of the permanent dipole moment. We chose to measure the power dependence single photon dynamics to evaluate the lifetime of the GaN fluctuation quantum dot. This is the motivation of this research.

5.2 Power Dependence of Emission Spectrum

In this experiment, we use the side excitation setup for UV measurement as introduced previously.

The sample is held under vacuum in a continuous flow helium cryostat with a cryogenic temperature controller to ensure that the sample is held at a constant temperature of 10K in all of the measurements.

The excitation laser used is a 266nm continuous wave diode pumped laser, and an ND filter in the excitation path is used to control the excitation power onto the sample surface to enable power dependent measurements.

Micro-photoluminescence is collected using a near UV objective lens (40x, NA=0.6, Olympus, LUCPLFLN), and measured using a nitrogen cooled CCD array attached onto a 75cm monochromator with a 2400lmm-1 diffraction grating. The spectral resolution of the setup is ~200μeV. Photon auto-correlation of the emission from the quantum dot is performed using a home-made standard Hanbury Brown & Twiss type setup consisting of a beam splitter (BS) at the exit slit of the monochromator to split the light, and two PMTs to get the signal into the two arms from the BS. Time-correlated single photon counting was performed using a PC-mounted Becker & Hickl GmbH card.

5.2.1 Micro-Photoluminescence Intensity

Figure 5-3 shows the emission spectrum of an excitonic emission line from a selected interface fluctuation III-Nitride quantum dot excited by a laser power of 50μW (the corresponding excitation power density is ~32W/cm^2).

The quantum dot emission energy can be evaluated around ~3.58 eV. The Gaussian profile of the emission peak reveals the linewidth broadening is mainly due to the spectral diffusion coming from the stochastic jumps in the emission energy. The full width at half maximum (FWHM) of the emission peak from such quantum dot is relatively narrow (~400μeV), compared with typical GaN quantum dots in the literature that exhibit linewidths of a few meV.

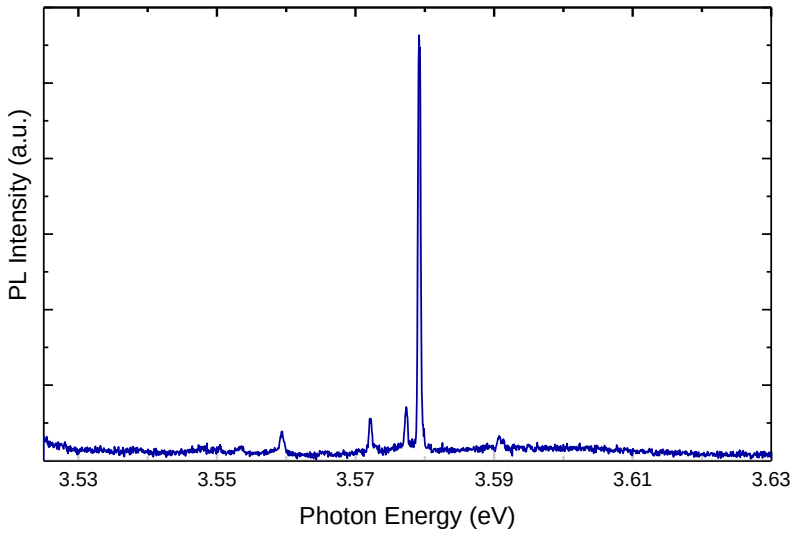

Figure 5-3. The emission spectrum of a selected single interface fluctuation quantum dot measured in 1 second. The emission photon energy is ~3.58 eV. [114]

By using the ND filter in the excitation laser path, we can investigate the emission spectrum under various laser powers (50, 100, 150 and 200 μW).

Firstly, it is easy to find that the emission line of such selected single interface fluctuation quantum dot does not move greatly while increasing the laser power.

Secondly, the height of emission peak increases with higher excitation power, while the emission linewidth (FWHM) keeping stable. We will discuss these in detail in the following section.

Moreover, the additional peaks in the spectrum of lower energy don't have so much change that leads to more evidence to support the assumption of the origin

relating to nearby quantum dots.

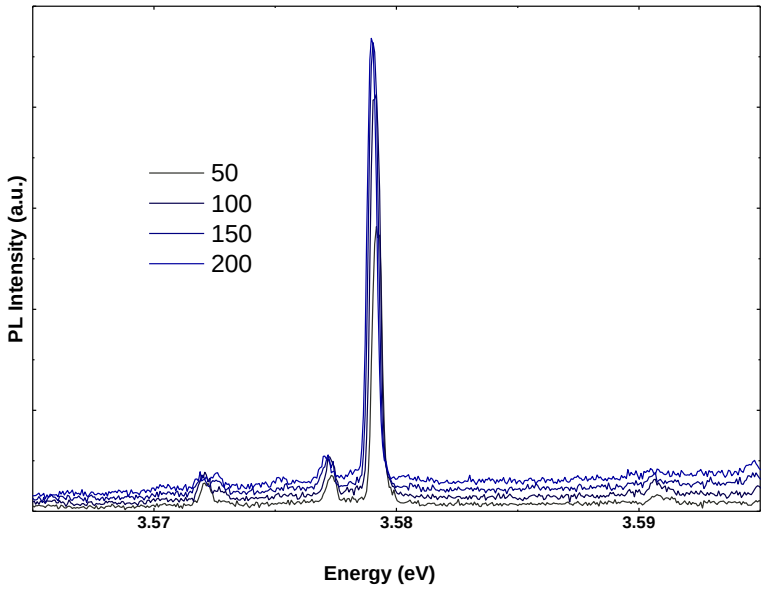

Figure 5-4. Emission spectrums of such single interface fluctuation quantum dot measured in 1 second under various excitation power. The emission photon energy is basically stable at ~3.58 eV. Their linewidths and photoluminescence Intensity will discuss in the following two figures.

5.2.2 Emission Linewidth of the Micro-Photoluminescence

Figure 5-5 shows and the emission linewidth as a function of excitation power. The data is extracted from the data in figure 5-4 by single peak fitting of the Gaussian profile.

In the analyze of the spectrum, we used the Gaussian and Lorentz profile to fit the emission spectrum. We found the Gaussian fitting is much better which support the origin of the emission linewidth is resulting from the spectral diffusion due to stochastic jumps in the emission energy.

We should say the emission linewidth is not such ideal down to less than 100μeV

but it still better enough comparing with typical emission linewidth of III-Nitride quantum dots. [80, 81]

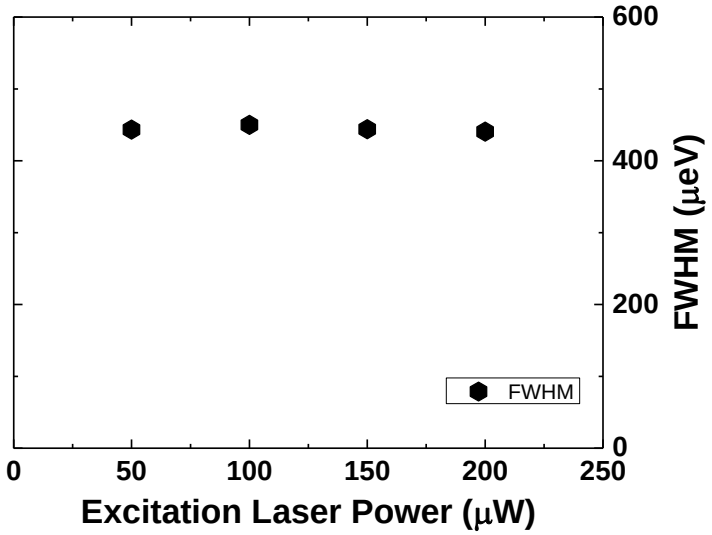

Figure 5-5. Emission linewidth (FWHM) of such single interface fluctuation quantum dot as a function of laser excitation power. This data is extracted from the data in figure 5-4 by single peak fitting of the Gaussian profile.[114]

Furthermore, we change the excitation power to get more information of the quantum dot emission. We changed the power from 7.5 to 200 μW by measuring its spectrums.

Figure 5-6 shows the photoluminescence intensities of such single interface fluctuation quantum dot as a function of excitation power. We can find the emission of such dot is saturated around the 150-200 μW, while the emission background doesn't have big change as shown in figure 5-5. Which can be explained as the clean environment surround that quantum dot.

Here we should add an important detail that in this figure we also present the density of excitation power. It is coming from the estimation of the laser spot to an ellipse with a major semi-axis of ~100 μm and minor semi-axis of 50 μm. Comparing with the estimation in Chapter 4, the situation of the optical path is better because we did some more alignment after previous experiment.

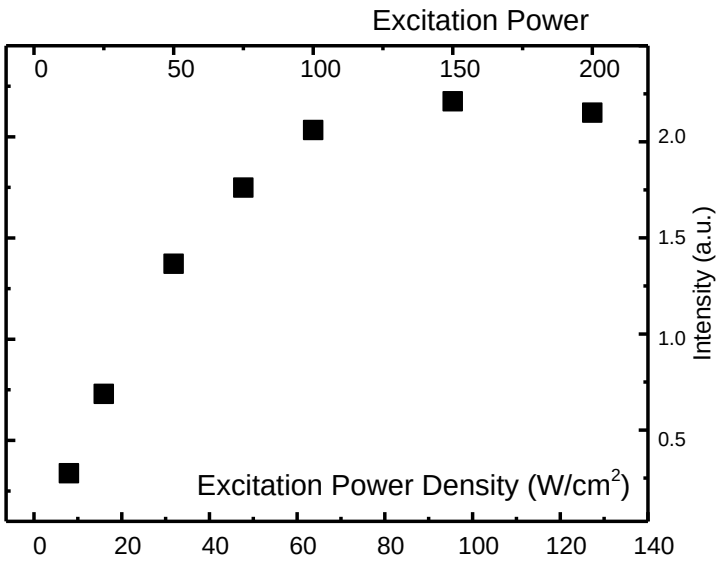

Figure 5-6. Photoluminescence intensities of such single interface fluctuation quantum dot as a function of excitation laser power.

5.3 Power Dependence of Auto-Correlation Measurements

The emission shown in figure 5-3 and 5-4 was filtered using the exit slit of the spectrometer, and the HBT setup was used to measure the second order intensity auto-correlation at time delay τ, $g^{(2)}(\tau)$ at various laser powers (50, 100, 150 and 200 μW).

5.3.1 Auto-Correlation Function with Excitation Power Effect

The auto-correlation measurement results have been shown in figure 5-7. In order to investigate the single photon emission dynamics as a function of the excitation power, the normalized measured data were fitted follows the second-order correlation function as we discussed in Chapter 3 (Equation 3-1):

$$g^{(2)}(t) = 1 - \beta \exp\left(\frac{-|t|}{\tau}\right) \tag{5-2}$$

Where $1/\tau$ is the anti-bunching rate, τ represents the decay time scale of the anti-bunching dip, t is the time delay of our home-made HBT setup. β is the factor related to fitted $g^{(2)}(0)$:

$$\beta = 1 - g^{(2)}(0) \tag{5-3}$$

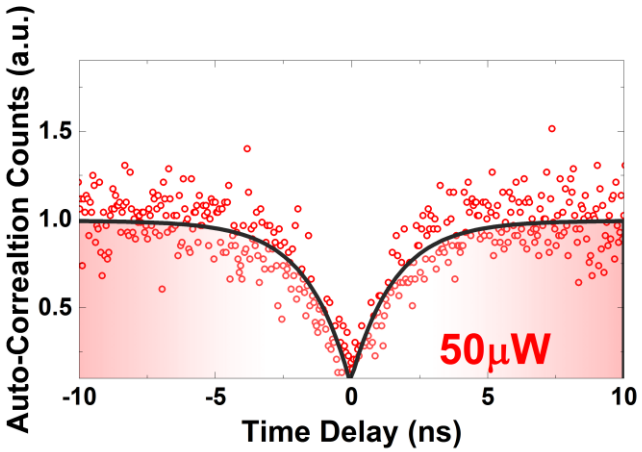
Auto-Correaltion Counts (a.u.)
1.5
1.0
0.5
-10
-5
0
5
10
Time Delay (ns)
50μW

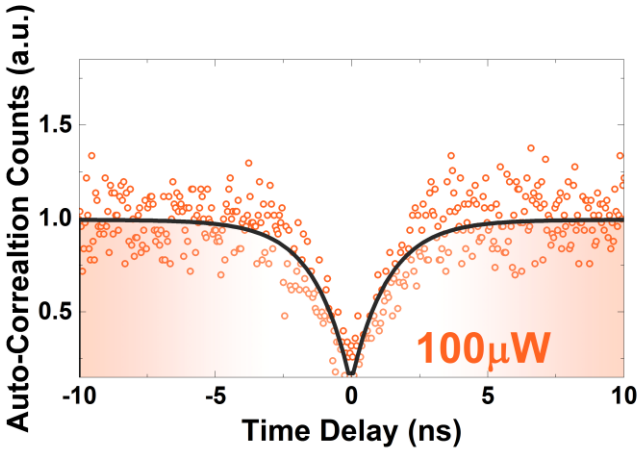
Auto-Correaltion Counts (a.u.)
1.5
1.0
0.5
-10
-5
0
5
10
Time Delay (ns)
100μW

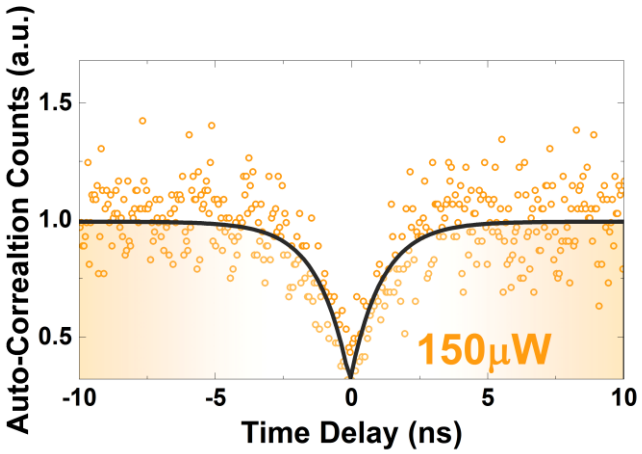
Auto-Correaltion Counts (a.u.)
1.5
1.0
0.5
-10
-5
0
5
10
Time Delay (ns)
150μW

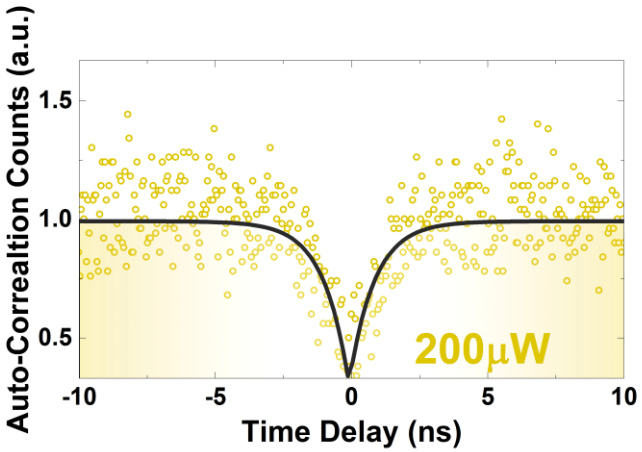

Figure 5-7. Photon auto-correlation of a single GaN fluctuation quantum dot under various excitation laser powers (50, 100, 150 and 200 μW). Black curves show the fitting curves based on equation (5-2), revealing single photon emission (all of the measured $g^{(2)}(0)$ values are below 0.5). [114]

We can clearly find that the measured and fitted (usually during the fitting these two values are always limited to be similar) $g^{(2)}(0)$ values are lower than 0.5 for all of the cases with different excitation laser powers. It reveals the fact of single-photon emission from such quantum dot. Basically, the value was getting worse while increasing the excitation laser power due to the background spectral contamination as shown in figure 5-4. (As the discussion in Chapter 4)

5.3.2 Anti-Bunching Rate of the Power Dependent Auto-Correlation

After the fitting by second-order correlation function (5-2) in the previous section, we extract the anti-bunching decay rate under different excitation conditions.

Figure 5-8 shows the extracted anti-bunching decay rate from the fittings as a

function of excitation laser power, and its linear fit follows [122]:

$$\frac{1}{\tau} = \frac{1}{\tau_0} + \alpha P \tag{5-4}$$

Where $1/\tau$ represents the anti-bunching decay rate, P is the pump power intensity, α is a constant relating to the carrier injection efficiency into the dot, and τ_0 is the exciton decay time. This equation (5-4) relies on the assumption that τ_0 is not directly depending on the excitation laser power.

The anti-bunching decay rate increased when we increased the excitation power. The physical meaning of this phenomenon is that the upper layers around the quantum dot are more possible to be excited while increasing the laser power, which leads to the narrower dip of the anti-bunching.

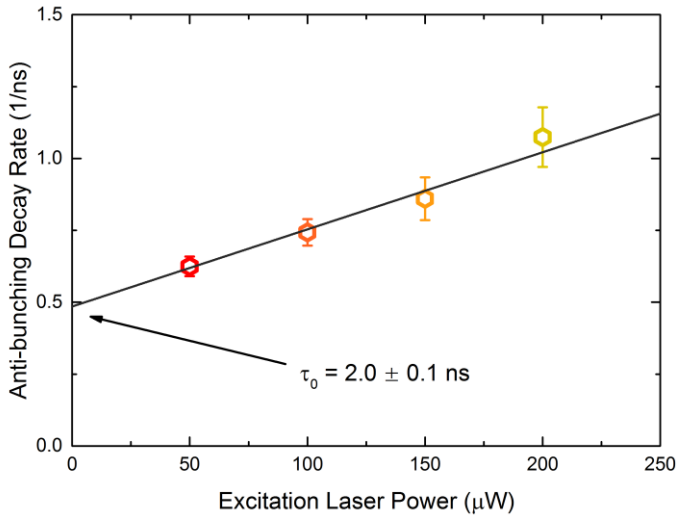

Figure 5-8. Power dependent anti-bunching decay rate of the confined exciton. The black line is the linear fit of the anti-bunching decay rate as a function of excitation laser power. From the y-intercept, the exciton decay time can be evaluated to be 2.0±0.1 ns. [114]

5.3.3 Evaluation of Recombination Time

The data fits well with the expected linear trend, and from the fitting result we can evaluate the exciton decay time of such quantum dot as 2.0±0.1 ns from the intercept of its linear fit.

It is worth noting here that in the literature quantum dot lifetimes are typically evaluated using time resolved photoluminescence studies with pulsed laser excitation. However, in the current study, we opted for CW excitation as it enabled us to achieve cleaner emission spectra with less background contamination.

By comparing this measurement to the literature results of typical III-nitride quantum dots [118,119], we find that the life-time measured for such an interface fluctuation quantum dot compares very well with that for typical Stranski-Krastanow (SK) GaN quantum dots emitting at around the same energy. As both the lifetime and permanent dipole moment depend in effect on the separation of the electron and hole wave-functions, we can infer that there is likely to be no large difference between the permanent dipole in the present dots and those of SK dots that emit at the same energy. Accordingly, it is therefore likely that the suppressed spectral diffusion in these fluctuation dots (when compared to typical GaN quantum dots emitting at the same energy) is due to a cleaner environment (i.e. a lower density of active charge traps), as opposed to any inherent difference in the quantum dots themselves.

Finally, we note that the 2ns lifetime that we measure would correspond to a lifetime limited linewidth of the order of ~1μeV by the calculation through the Heisenberg's uncertainty principle ($\Delta E \bullet \Delta t \approx \hbar$). It should be much smaller than actually measured in this case, revealing the extent of the spectral diffusion limited broadening.

5.4 Concluding Remarks

In summary, we have measured the exciton recombination time in a GaN interface fluctuation quantum dot using photon auto-correlation measurements.

The exciton decay time of such a dot is evaluated to be the order of ~2 ns by its power dependent single photon dynamics with an emission photon energy of ~3.58eV. By comparing with typical SK GaN QDs data in figure 5-1 from Ref. [118]. It is clear to find that the ~2ns lifetime measured data (the red spot in figure 5-9) for such an interface fluctuation quantum dot compares very well with the typical SK GaN QDs around the same energy.

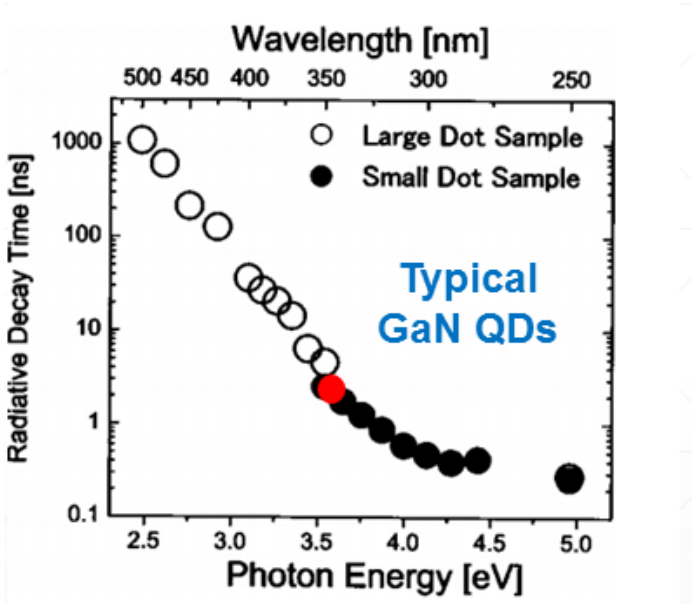

Figure 5-9. Radiative decay time of two different sizes of quantum dot samples as a function of photon energy or wavelength. [118]

The red spot inset is the similar typical GaN quantum dot to our interface fluctuation quantum dot in the photon energy and lifetime.

This result has been used to infer that the relatively narrow emission linewidths of these quantum dots are likely resulting from a comparatively cleaner environment around such a single quantum dot.

These GaN fluctuation quantum dots may become an important technical solution for III-nitride based quantum sources, but will also act as a good platform for the study of fundamental properties of III-nitride nanostructures.

This study also leads to the following work of the evaluation of the spectrum diffusion of such GaN fluctuation quantum dot which is the main reason caused the emission linewidth.

6 Nanosecond-scale Spectral Diffusion in the Single Photon Emission of a GaN Quantum Dot

As the introduction in Chapter 2, Spectral diffusion is an emission linewidth limiting phenomenon in quantum dots (QDs) involving random jumps of the emission line in the emission wavelength.

It usually occurs from electronic interactions between a confined exciton and its environment (such as charge fluctuations). [80-81, 118, 123] Such energy fluctuations will ultimately limit the indistinguishability of the emitted photons, and therefore have detrimental effects on the use of single photon emitters in future quantum applications. [124-128]

Typical III-Nitride semiconductors suffer from a large degree of spectral diffusion, which can broaden the emission linewidth up to a few meV [80-82]. In this chapter, we will focus on the investigation of the spectral diffusion in the single photon emissions of our interface fluctuation III-Nitride quantum dots. This work has been published in AIP Advances 7, 125216 (2017). [129]

6.1 Motivation: What is the Spectral Diffusion Time Scale?

Spectral diffusion which is well-known spectral wondering phenomenon is a result of random spectral jumps of a narrow line resulting from the fluctuating in the environment of the emitter.

Typically, the temporal variation of the photoluminescence on a relatively long-time scales is a typical method to investigate the spectral diffusion on such large energy

scales. Indeed, it has been used to evaluate temporal fluctuations in Nitride-based QDs [130,131], and also other materials such as CdTe QDs [132], CdSe QDs [133], and InAlAs QDs. [134]

As the examples shown in figure 6-1. [132, 133]

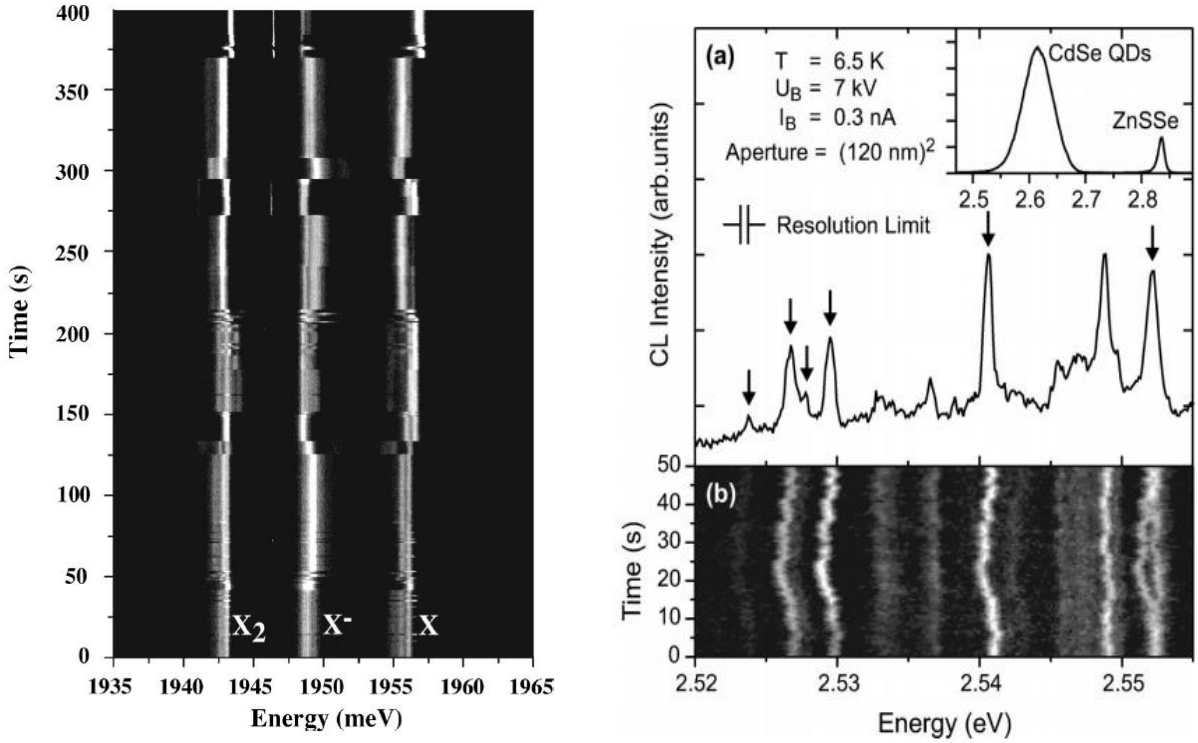

Figure 6-1. The temporal variation of the luminescence on long-time scales from different materials such as CdTe QDs, [132] CdSe QDs. [133]

However, fluctuations can occur on timescales in a big range from sub-nanosecond [135] levels to several seconds. [130] Which is usually considered to come from the different density of the defects around the emitter, or the distance between the emitter and other charges in its surroundings. [80]

The time resolution of this mothed by measuring of the temporal spectums is always limited to the order up to serval micro-seconds because of the required time to get the emission spectrum.

As a result, the measurement the spectral diffusions on fast time scales requires

more advanced measurement techniques such as photon auto-correlation measurement, [135] as shown in figure 6-2.

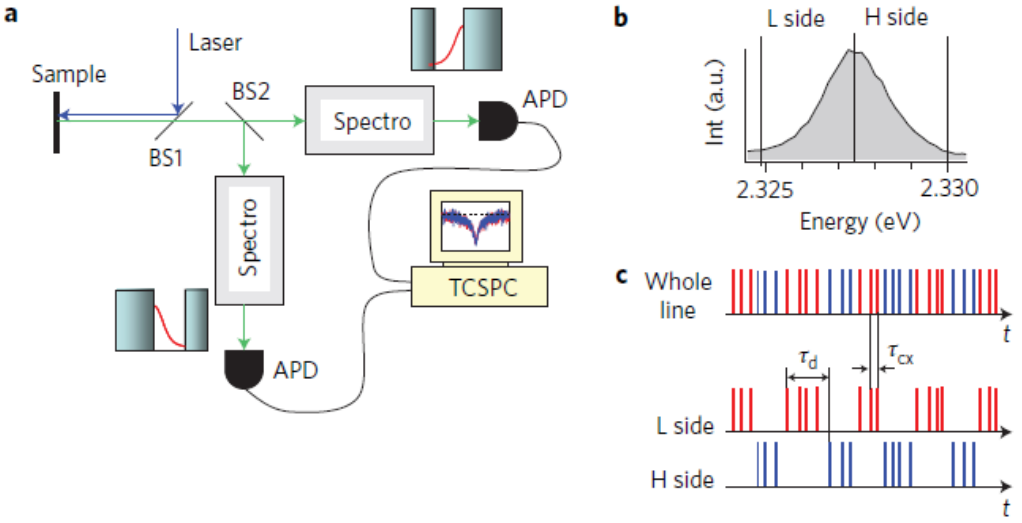

Figure 6-2. Spectral diffusion measurements.
(a) Experiment setup by using two spectrometers imbedded on two APD detectors, (b) Photoluminescence of a single CdSe QD, (c) repesentation of the photons selected by a spectral window as shown in (b). [135]

The auto-correlation measurement converts the spectral fluctuation into an intensity fluctuation and therefore improved time resolution up to sub-nanosecond levels thanks to the detectors used in a Hanbury Brown & Twiss type setup. [135]

By the selection of the spectral window as the L and H side in figure 6-2 (b), the photons emitting from the studied single CdSe QD embedded in ZnSe nanowire can be separated as shown in figure 6-2 (c).

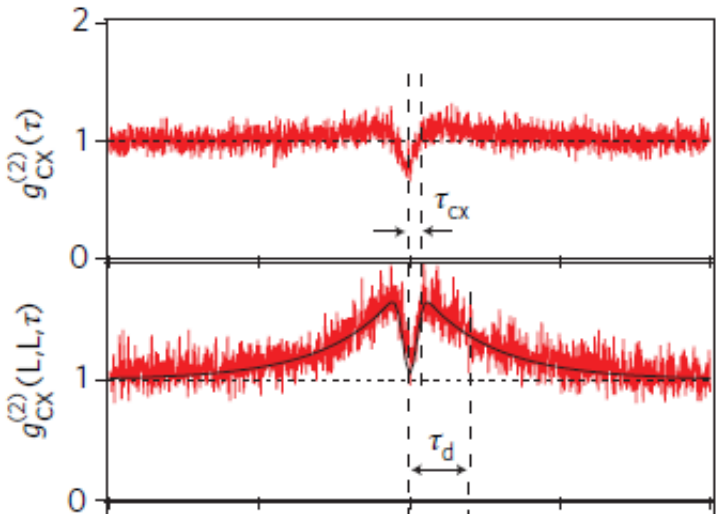

Figure 6-3. Upper, Photon auto-correlation of whole emission profile in figure 6-2 (b). Lower, Photon auto-correlation of one half of the emission profile showing the bunching effect. The characteristic spectral diffusion times (τ_D~4ns) provide local information on the environment of a single photon emitter.

As shown in figure 6-3 Upper, the photon auto-correlation of whole emission profile in figure 6-2 (b) shows the normal anti-bunching effect that results from the single photon emission from the studied single CdSe QD embedded in ZnSe nanowire.

Figure 6-3 Lower, the result of the photon auto-correlation of one half of the emission profile not only contribute by the anti-bunching effect from the single photon emission but also have the influence from spectral diffusion acted as an additional bunching effect. The mechanism of this effect we will discuss later in this chapter.

The characteristic time of the bunching effect, as well as the spectral diffusion times (τ_D~4ns), provide us the local information of the environment of the studied single photon emitter.

Although spectral diffusion in different materials has been investigated using this method, including CdSe QDs embedded in ZnSe nanowires, [135-137] nitrogen

vacancy centers in nano size diamonds[138] and oxidized tungsten disulfide multilayers,[139] the fast time scale of spectral diffusion in III-Nitride QDs has yet to be investigated.

6.2 Temporal Variation of Emission Spectrum

Here we used the side excitation UV setup to elucidate the spectral diffusion timescale of a single-photon-emitting GaN interface fluctuation QD via photon auto-correlation measurements, and furthermore, provide information on the characteristic spectral diffusion time as a function of excitation laser power.

The sample was hold into a continuous flow helium cryostat with a temperature controller, cooled to 10K, and the excitation source is a CW laser with 266nm emission wavelength.

Photoluminescence from the interface fluctuation III-Nitride quantum dot was collected by a UV objective lens. The emission spectrum was performed by a nitrogen cooled CCD array attached onto a 75cm-length spectrometer with a 2400lmm^{-1} diffraction grating. The spectral resolution of the setup has been evaluated around the order of ~200μeV.

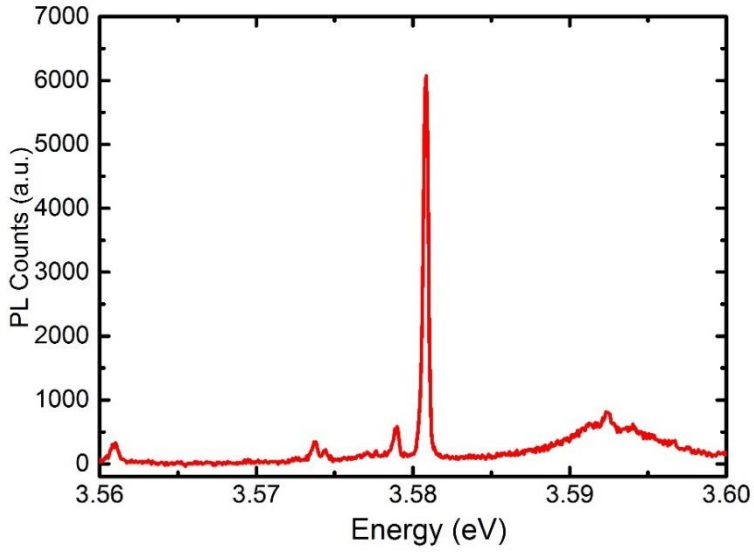

Figure 6-4. Emission profile from a selected GaN interface fluctuation QD.

First of all, we scan the surface of the sample and selected a single-like narrow linewidth quantum dot emission as shown in figure 6-4.

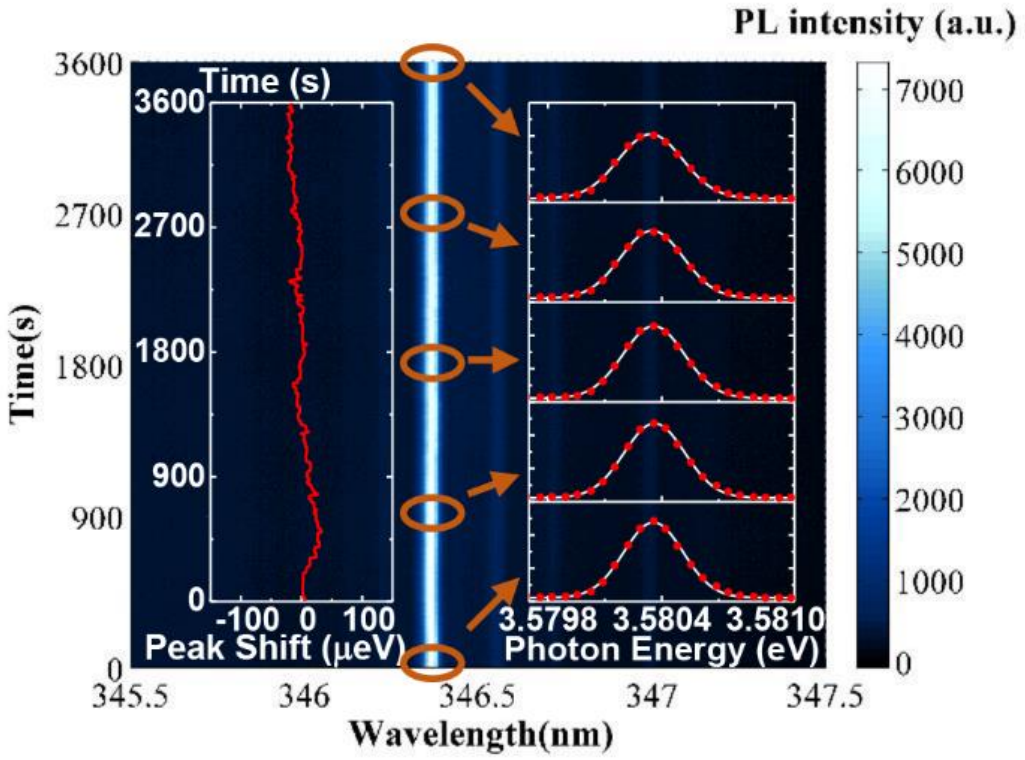

Figure 6-5. The temporal variation of the emission spectrum of a selected single GaN interface fluctuation quantum dot measured over a period of one hour.
The left inset shows the peak shift of the emission.
The right inset shows five representative spectra (data points) with Gaussian lineshape fits (white lines). [129]

To measure the spectral diffusion timescale of III-Nitride interface fluctuation QDs, we begin by investigating its temporal evolution of the emission spectrum. The single QD was excited under the laser power of 200μW, and its temporal evolution spectrums were measured for a 1-hour period. The integration time for each of the single spectrum was 5s. As figure 6-5, the emission is extremely stable even in a relatively long-time period of 3600 seconds.

Moreover, the left inset figure is the time evolution of the peak shift of the emission center. It clearly reveals that the extent of any spectral wandering is smaller than 100μeV, and it is even much smaller than the resolution limit.

Indeed, the right inset figure (five selected spectrums at different time points) reveals all the line shapes of the emission has a Gaussian profile leads to the assumption of the mechanism of the emission linewidth broadening due to its fast time scale spectral diffusion.

As a result, in order to further investigate the properties of this fast-spectral diffusion, a higher resolution method is necessary for its measurement.

Furthermore, we selected two more emission profiles from GaN interface fluctuation quantum dots and investigated their temporal evolution of the emission spectrums. We compared them to the emission properties from two more other kinds of III-Nitride quantum dot.

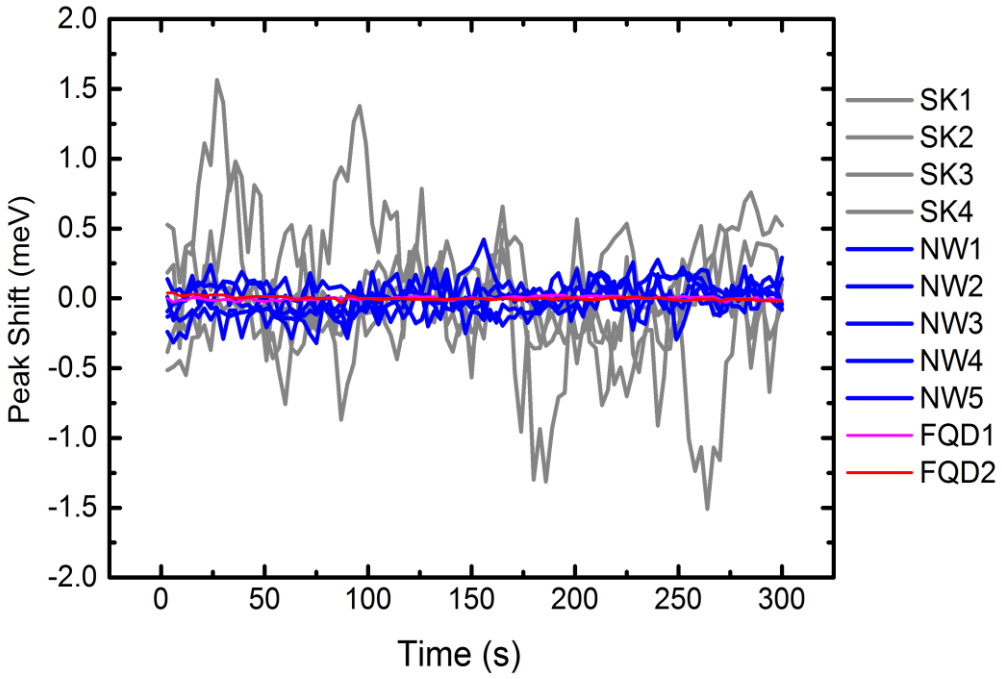

Figure 6-6. Comparison of emission spectral wandering of three kinds of III-Nitride QDs.

Figure 6-6 shows the time evolution of the emission peak center, where it is clear that the extent of any spectral wandering of the GaN interface fluctuation quantum dots (red lines) is much smaller than the SK QDs (grey lines) and nanowire QDs (blue lines). We can infer that this smaller jump of the emission line from our interface fluctuation QDs is in fact revealing a cleaner environment of the QDs with lower density of defects, which leads to longer average distance from the defects from the QDs to the defects, and smaller average electric forces.

This provides evidence that the environment around the GaN interface fluctuation quantum dots is relatively cleaner (with a low density of defects), which makes the in-built electric field in stable, led to a smaller long term spectral diffusion.

6.3 Spectral Diffusion Measurement based on Auto-Correlation Measurement

In order to investigate the properties of the fast time scale spectral diffusion of interface fluctuation III-Nitride quantum dots, a higher resolution method by using the auto-correlation of the emission was selected.

6.3.1 Auto-Correlation Function with Bunching Envelope due to Spectral Diffusion

The main mechanism of this high resolution of fast-spectral diffusion is coming from photon auto-correlation with two different spectral selection.

Firstly, we used the spectrometer to select the whole emission profile from the quantum dot and guided the photoluminescence into the HBT setup. In the whole profile photon auto-correlation measurement, a typical narrow antibunching ($g^{(2)}(0)<0.5$) in the photon statistics is expected to reveal the single-photon nature of the emission.

Secondly, we selected the half emission profile by the spectrometer from the quantum dot and did the half profile photon auto-correlation measurement. the spectral diffusion of the peak into and out of the measurement window induces an additional photon bunching in the auto-correlation.

In order to evaluate the bunching time scale, the measured auto-correlation data has been fitted with a second-order auto-correlation function including a bunching envelope to describe the spectral diffusion[135]:

$$g^{(2)}(\tau) = [1 - \alpha \exp(-\frac{|\tau|}{\tau_e})] \bullet [1 - \beta \exp(-\frac{|\tau|}{\tau_{SD}})] \quad (6\text{-}1)$$

where the factors α and β represent the extent of the antibunching dip and the visibility of the bunching peak, respectively. Here τ is the time delay of the auto-correlation measurement, τ_e is the time scale of the anti-bunching dip (in this case it is of the order of~1ns), and τ_{SD} is the time scale of the spectral diffusion that we focus on here.

6.3.2 Optical Setting to Select the Emission Profile

As we motioned before, we used the side excitation UV setup to evaluate the spectral diffusion timescale of a single-photon-emitting GaN interface fluctuation QD.

Figure 6-1 shows the emission spectrum from the selected GaN interface fluctuation quantum dot. The full width at half maximum (FWHM) of the emission peak of this particular dot is measured to be ~300 μeV.

We estimate the pixel number on the CCD that representing the emission profile, and calculated the total width that representing the emission angle of such narrow linewidth.

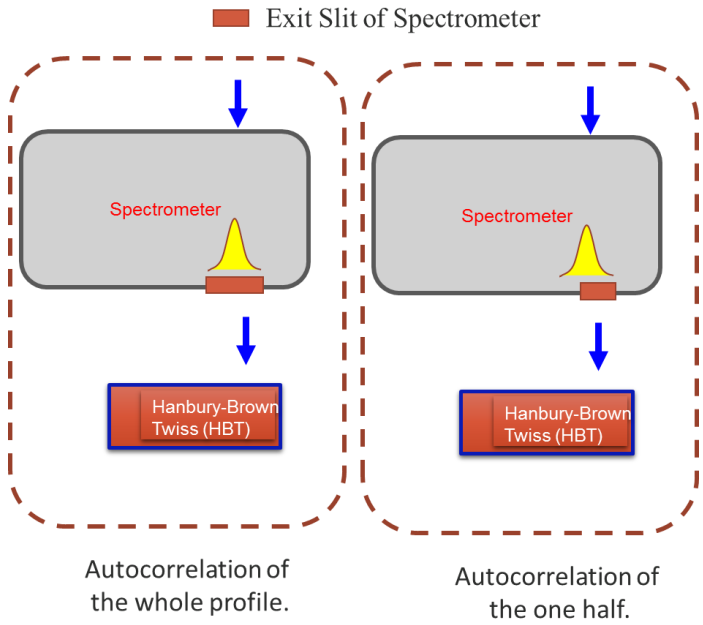

Figure 6-7. Selection of a spectral window for auto-correlation measurement. The size of the exit slit connecting the spectrometer and HBT setup in opened up representing to the whole and one half of emission profile.

By changing the angle of the grating in the spectrometer and the size of the exit slit connecting the spectrometer and HBT setup as shown in figure 6-7, we could freely select a spectral window representing whole or one half of the emission profile to do the auto-correlation measurement.

Auto-correlation of the emission was performed by using a standard UV HBT setup with two photomultiplier tubes (Hamamatsu H10682-210) combined at the exit slit of the spectrometer. The time resolution of our setup has been measured to be ~400ps.

6.3.3 The Nanosecond Time Scale of the Spectral Diffusion

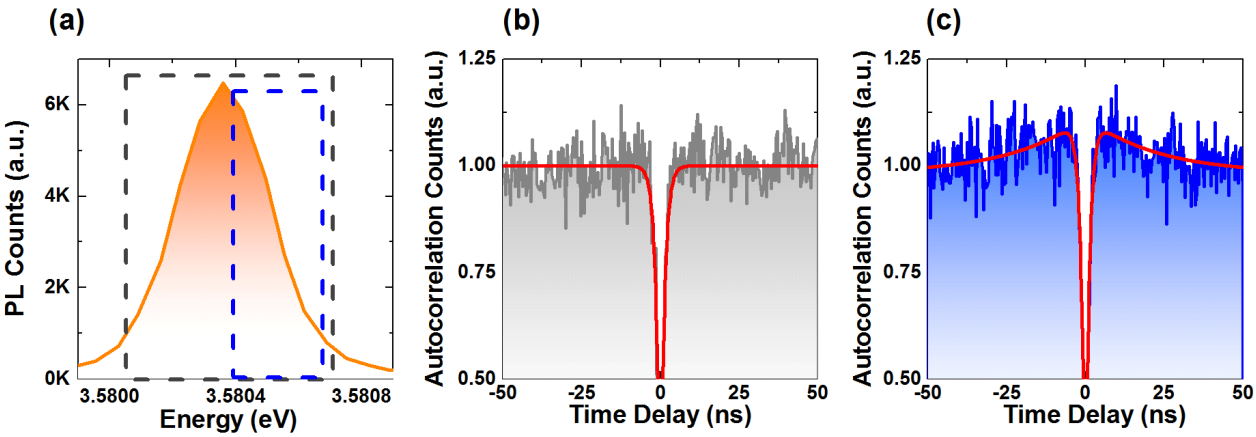

Figure 6-8. Spectral diffusion measurements using auto-correlation.
(a) Photoluminescence spectrum of a single GaN interface fluctuation QD (the same as figure 6-1). (b) Auto-correlation of the whole peak as the grey dash box in figure 6-8a. (c) Auto-correlation of high energy profile range as the blue dash box in figure 6-8a. The inset figures in (b) and (c) show a zoomed in region of the auto-correlation measurement such that the bunching effect can be clearly seen. [129]

Figure 6-8a shows the same emission spectrum of the GaN interface fluctuation QD integrated over 1s as figure 6-1.

Two dashed boxes in figure 6-8a represent different spectral windows that were selected for the auto-correlation measurements corresponding to figures 6-8b and 6-8c. Figure 6-8b represents the measurement of the whole peak (grey dashed box in figure 6-8a), which represents a ~700 μeV spectral window width. Figure 6-8c corresponds to the auto-correlation measurement of one high energy half of the emission profile (the blue dashed box in figure 6-8a) with a spectral range of ~300 μeV.

When the full peak is measured (figure 6-8b) a typical narrow antibunching ($g^{(2)}(0)<0.5$) appeared, and it clearly reveals the single-photon nature of the emission,

from such selected interface fluctuation III-Nitride quantum dot. However, while measuring only the high energy half of the emission peak as shown in figure 6-8c, the spectral diffusion of the peak jumping into and out of the selected spectral window induces an additional photon bunching.

The characteristic spectral diffusion timescale of this dot can be evaluated around ~22ns under these excitation conditions. The measured additional bunching characteristic spectral diffusion time (~22ns) reveals that fact that the homogeneous line does not move for timescales less than ~22ns. After the time scale of ~22ns, the QD loses memory of its spectral position and the auto-correlation reduce to 1.

We note that this value is comparable with previous reports of spectral diffusion in self-assembled CdSe QDs. [135]

6.4 Power Dependence of the Spectral Diffusion

The spectral diffusion phenomenon is always induced by the fluctuating Stark shifts [140] due to the charge environment. As a result, it is easy to be expected to exhibit an excitation laser power dependence that the diffusion rate increases with increased number of excited charges in the surrounding environment of the emitter while increasing the excitation laser power.

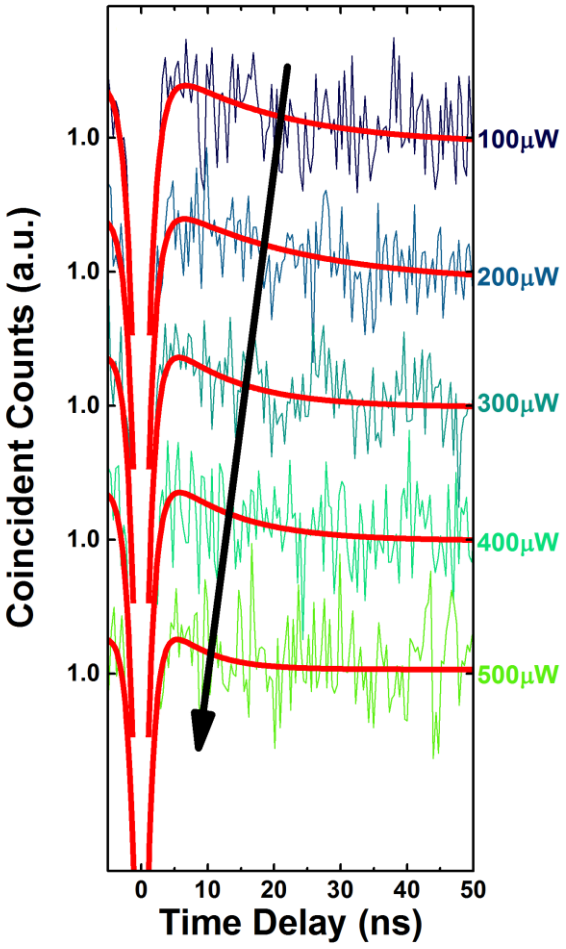

Figure 6-9. Power dependent photon auto-correlation data (log scale), offset for clarity. The black arrows are guides to the eye. [129]

In order to investigate excitation power dependent fast spectral diffusion of the interface fluctuation III-Nitride quantum dot, we changed the excitation power of the laser from 100μW to 500μW and made the spectral filtered auto-correlation measurements under different excitation laser powers.

The spectral diffusion characteristic rate (equals to the inverse of the spectral diffusion characteristic time) can be evaluated as a function of excitation laser power in figure 6-10. This trend can be explained that more and more carriers (the defects) around the quantum dot are excited while increasing the excitation laser power, which leads to the faster spectral jumps of the emission due to more complex fluctuating electrical filed.

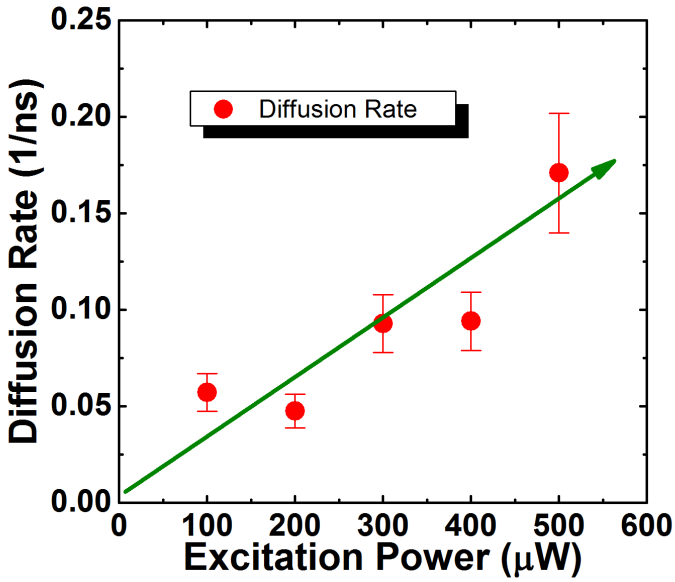

Figure 6-10. The nanosecond spectrum diffusion in a single interface fluctuation QD as a function of excitation laser power. [129]

The figure 6-11 also shows the emission linewidth of the single interface fluctuation GaN QD under various powers, revealing that it only changes by a small amount as the excitation power is increased. However, the measurement results show that the diffusion rate increases with increasing excitation power.

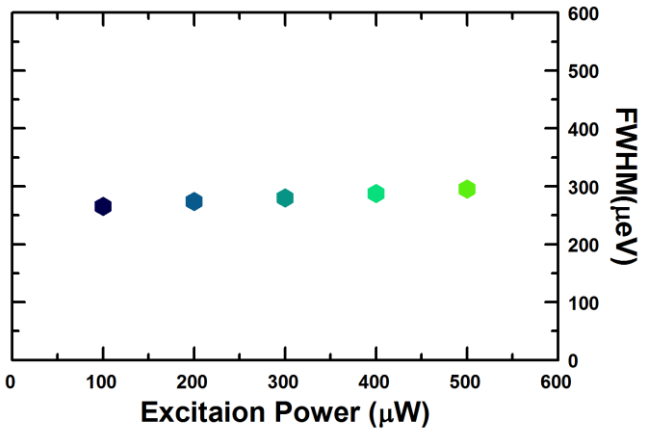

Figure 6-11. Emission linewidth of the single interface fluctuation GaN quantum dot as a function of excitation laser power. [129]

Such an increase of the spectral diffusion rate with increasing excitation power has been observed in other material systems [136,138,139]. In previous works, this relationship between the excitation power and the spectral diffusion rate has been observed with a linear dependence in diamond-based Nitrogen-vacancy centers [139] and with a sublinear dependence in CdSe QDs embedded in ZnSe nanowires [136]. However, in the present case, we do not observe any apparent saturation in the diffusion rate with increasing power over the studied excitation power range. The observed relationship between the excitation power and the diffusion rate can be approximated by a linear trend as shown by the black arrow in figure 6-11.

6.5 Concluding Remarks

In summary, we have reported a study of spectral diffusion in a GaN QD and revealed the characteristic spectral diffusion time, via measurement of the second-order auto-correlation, to be of order ~20ns. We have also presented the excitation power dependence of the spectral diffusion rate, showing the expected increase in rate as the excitation power is increased.

For single photon sources, this spectral diffusion phenomenon will affect the indistinguishability of the photon emission. Our results show here that it may be possible to generate indistinguishable photons using III-Nitride QDs under excitation with pulse pairs separated by times less than ~10ns.

Such information on the spectral diffusion times will be important for the generation of indistinguishable photons using this material system.

7 Conclusions and Outlook

7.1 Conclusions

Summary of the results.

The following are the main results presented in this thesis:

1. We have shown the temperature dependence of single photon emission properties from interface-fluctuation GaN quantum dots. The quantum nature of the emission is maintained up to 77K, although its purity gradually decreases, due to increased spectral contamination from uncorrelated background emission resulting from the environment surrounding the quantum dot. It is possible that improved temperature characteristics could be achieved by reducing the volume of measured material- perhaps via the fabrication of mesa-like structures, or by local resonant excitation. Furthermore, we have shown the high purity single photon emission properties of interface-fluctuation GaN quantum dots can be obtained by the optimizing the emission conditions. This result shows that III-nitride quantum dots based high-quality optical properties are possible to be created.

2. We have measured the exciton recombination time in a GaN interface fluctuation quantum dot using photon auto-correlation measurements. The decay time is evaluated to be ~2 ns by power dependent single photon dynamics. By comparing previous typical SK GaN QDs data, we can find that this ~2ns lifetime measured data for such an interface fluctuation QD compares very well with typical SK GaN QDs around the same energy. According to this result, we can provide further evidence that

the relatively narrow emission linewidths of these quantum dots are likely resulting from a comparatively cleaner environment around the QD. These GaN fluctuation quantum dots may become an important technical solution for III-nitride based quantum sources, but will also act as a good platform for the study of fundamental properties of III-nitride nanostructures.

3. We have reported a study of spectral diffusion in a GaN interface fluctuation QD. Initially, we found the emission line has a fairly static Gaussian profile, indicating that the emission energy fluctuations on time scales are faster than our previous studied SK QDs and nanowire QDs, even much faster than the shutter speed of our CCD. Then we used second order auto-correlation measurement to reveal the characteristic spectral diffusion time to be of order ~20ns. We have also presented the excitation power dependence of the spectral diffusion rate, showing the expected increase in rate as the excitation power is increased. Our results show here that it may be possible to generate indistinguishable photons using III-Nitride QDs under excitation with pulse pairs separated by times less than ~10ns. Such information on the spectral diffusion times will be important for the generation of indistinguishable photons using this material system.

7.2 Future Prospect

In order to investigate our understanding of the physics of the III-Nitride QD and apply them to our daily life, related works have already started and will keep continuing in our group. I present a brief outlook in the near future.

1. Towards to comparison of the characteristics with other III-Nitride quantum dots

By investigating the temperature dependent single photon emission, the power dependent single photon emission, and the nanosecond-scale spectral diffusion time from the interface fluctuation QD, we have built and maintained the experiment setup and gathered experience of various methods of experiment. Now we already have several samples in different types of III-Nitride materials such as InGaN quantum dots sample, hBN samples...

We would like to continue to map these samples and try to investigate their physical properties such as their time-scale spectrum diffusion, the excitation effect on their single photon emission. And try to do the comparison of their characteristics with other our result in interface fluctuation QDs.

2. Towards higher purity

As we discussed in Chapter 4, the background emission from the environment is an important factor that limited the purity of the single photon emission from the

interface fluctuation GaN QDs. In order to improve its purity, removing the bulk layer of GaN is a possible way towards higher purity, even for the higher temperate single photon operation because we believe the background emission in the spectrum is most likely resulting from this quantum well-like GaN structure.

Furthermore, quasi-resonant excitation could be another solution towards the higher purity of single photon emission, as their successes in other III-V material systems. If the carrier can be excited directly to the first excited state and then recombine to emit the single photons, an improvement in the purity of single quantum state can be obtained. It will lead to higher purity of the single photon emission.

However, considering our recent result has already reached the limitation of the detector response function, our UV setup need some future upgrade to face the future challenge of the ultra-pure single photon detections.

3. Towards bright single photon source

The brightness of the single photon emissions not only affects their practical applications but also causes difficulties in the experiment.

For example, if we can increase the efficiency of the single photon emission tenfold, the accumulation time for the second order auto-correlation will be 100 times faster. Therefore, engineering a structure design for our interface fluctuation quantum dot would lead a great improvement for the practice quantum source devices. In the Appendix, we provide a DBR bull's eye structure design, and the simulation results show a higher collection efficiency. In the future, more efficient structures could be discussed towards the bright single photon source from III-Nitride QDs.

Appendix

Design of an Efficient Structure for Collecting Emission from III-Nitride Quantum Dots Emissions: To Increase the Single Photon Extraction Efficiency

The III-Nitride interface fluctuation quantum dot has been proved as an ideal candidate to build a single photon source. However, our simulation result shows that the collection efficiency limits the measurement and the application of the QD based single photon source, which is less than 5% when the quantum dot is embedded in the bulk martial (when NA=0.7). Here we used the similar structure parameters according to our interface fluctuation GaN quantum dot.

There are some useful structures to achieve a highly efficient single photon source. For example, the QDs in trumpet-like and needle-like photonic wires [54], the QDs embedded in a mircopillar device [55], the QDs in a Bragg bullseye DBR structure [141] and so on.

2nd order Bragg bullseye DBR structure has been proved to be useful for increasing the extraction efficiency from Arsenide QDs [61, 141]. For typical Arsenide QDs, when emission wavelength is around 800nm, the size of the structure radial period (as displayed in fig A-1) is about 400nm.

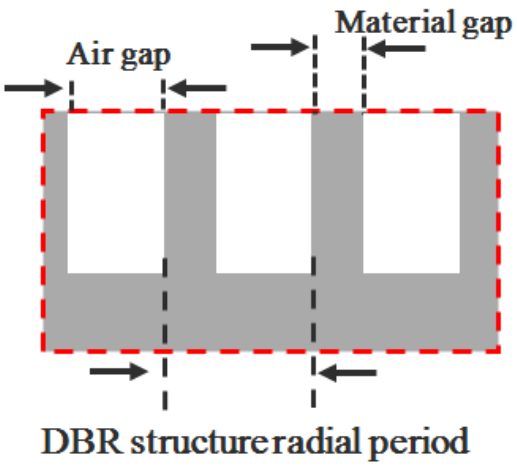

Figure A-1. Cross section of a DBR structure:

However, for Nitride QDs (the emission wavelength around 340nm), the size for a radial period of the DBR structure would be too small (reduce to 170nm) to easily fabricate.

The motivation of this research is to design a similar but alternative bullseye-like structure, based on radial 5quarters Nitride-Air gap DBRs around a central waveguide structure on a planar mirror to efficiently out-couple photon emission into the desired direction.

A.1 Simulation Method of the Extraction Efficiency

We use finite-difference time-domain (FDTD) [142, 143] method to simulate the collection efficiency of QD emission with commercially available software (RSoft).

In this simulation, we approximate the QD as a dipole emitter. As shown in figure A-2 we made a “Monitor Box” (MB) around the structure to calculate the power of the light emission from the QD.

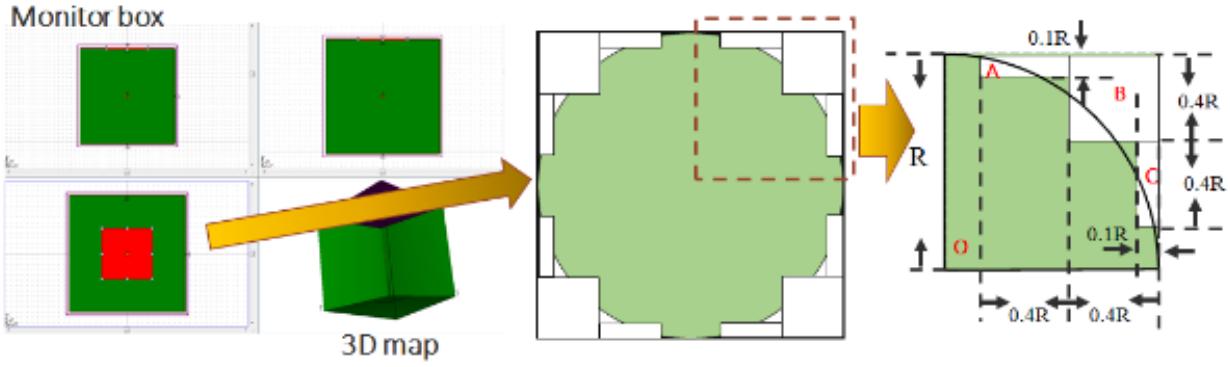

Figure A-2. monitor box in 3D map (left), small monitor group to estimate different NA (middle) and the quarter monitor group in the simulation (right).

We use a group of small monitors on the top surface of the MB to estimate a region corresponding to different Numerical Aperture (NA). Also, because of the symmetry of the structure, we use a quarter of the whole structure to simulate the efficiency.

As a result, the collection efficiency can be expressed as follows:

$$Efficiency = \frac{P_{small}}{P_{top} + P_{bottom} + 2P_{right} + 2P_{left}} \tag{A-1}$$

Here P represents the power of the emission from the dipole emitter reach to

different monitors on the surfaces of the monitor box, and the P_{small} is the total power results from the small monitor group.

We calculation the collection efficiency form the quantum dot emission when the QDs are in the free space, embedded in the AlGaN bulk material and in the nanowire structure as in [144]. The simulation results when light emission was collected by different numeral aperture illustrate as figure A-3.

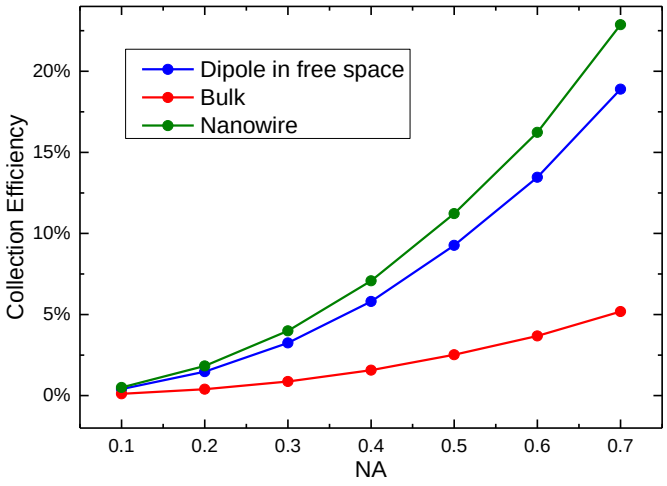

Figure A-3. The collection efficiency for QDs in the free space, embedded in the bulk material and in nanowire structure.

We can find that the efficiency for the QD in the free space is only 18.9% for NA=0.7, and it reduces to only 5.2% when the QD in bulk material (for NA=0.4, the efficiency is just 2%). In the nanowire structure, efficiency is still only 22.9%.

A.2 Efficient Structure Design and its Optimization

A.2.1 Bragg Bullseye DBR Structure

In order to raise the collection efficiency of single quantum dot emission, we design a Bragg bullseye DBR structure by etching from the bulk material embedded the quantum dot and the photon emission from the quantum dot will be collected from the top of the sample.

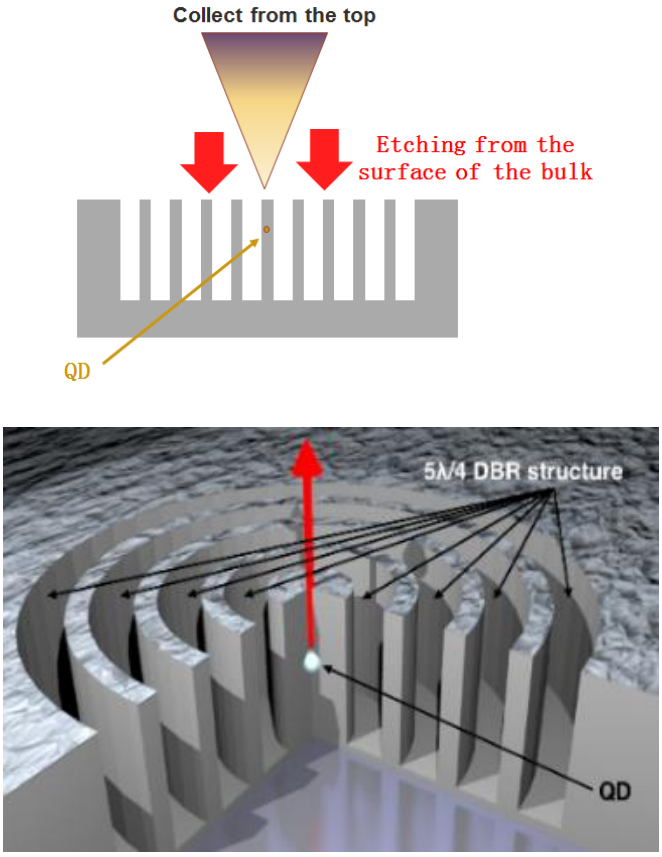

Figure A-4. Cross section (upper) and 3D- schematic (lower) of our Bragg bullseye DBR structure design.

The Nitride-Air gap is raised up to 5 quarters of the wavelength in this structure design for raising the structure radial period. It means the size for each radial period of such a structure raise to 582nm including 425nm width air gap and 157nm width Nitride gap. This structure as shown in figure A-4 would be much easier to fabricate than structures with a 170nm period.

This 5quarters size was chosen according to the calculation results of the 46nm stopband (from 318~364nm), and it will be suitable for our interface fluctuation QD emission spectrum compare with the other orders as figure A-5.

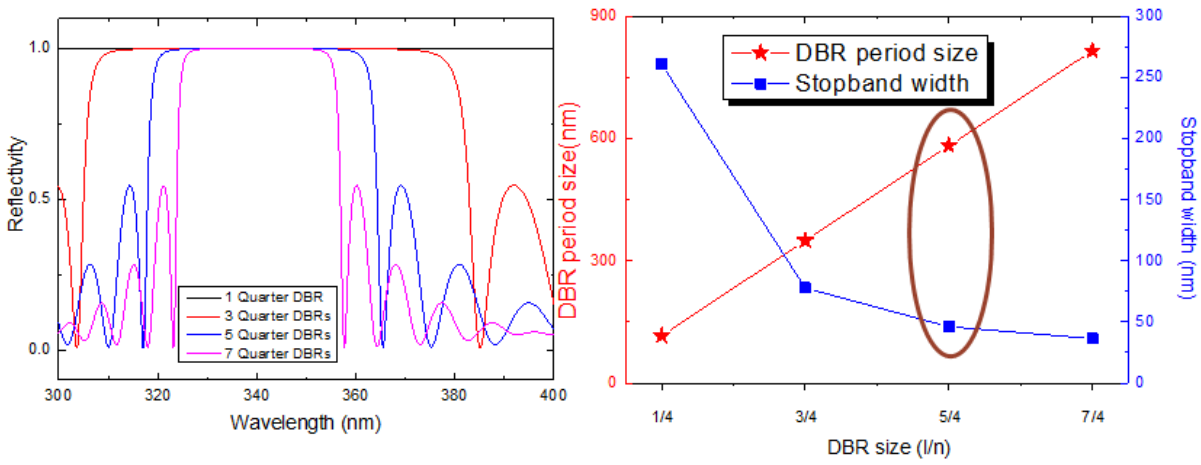

Figure A-5. Stopband (left) and period size (right) of the DBR structures.

In this structure the QD is located 100nm from the top surface as our GaN interface fluctuation quantum dot sample, the thickness of the whole bulk Ga/AlN material is 500nm and the height of the etched DBRs is set to 450 nm.

A.2.2 Optimization of the Efficient Bullseye DBR Structure Design

We optimized the central region by the simulations results with different center diameters of the DBR structures as shown in figure A-6 (left). Based on the simulation results, the highest efficiency appeared when the center Diameter equals to 160nm. That should be convinced because it is very close to the 5 quarters wavelength.

After that, we did the simulations with different numbers of the DBR period rings around the central region. The results are in figure A-6 (right). It seams that when the DBR number is around 5, there is almost no change of their collection efficiency. So we thought in this case, 5 rings are enough to optimize the DBR structure.

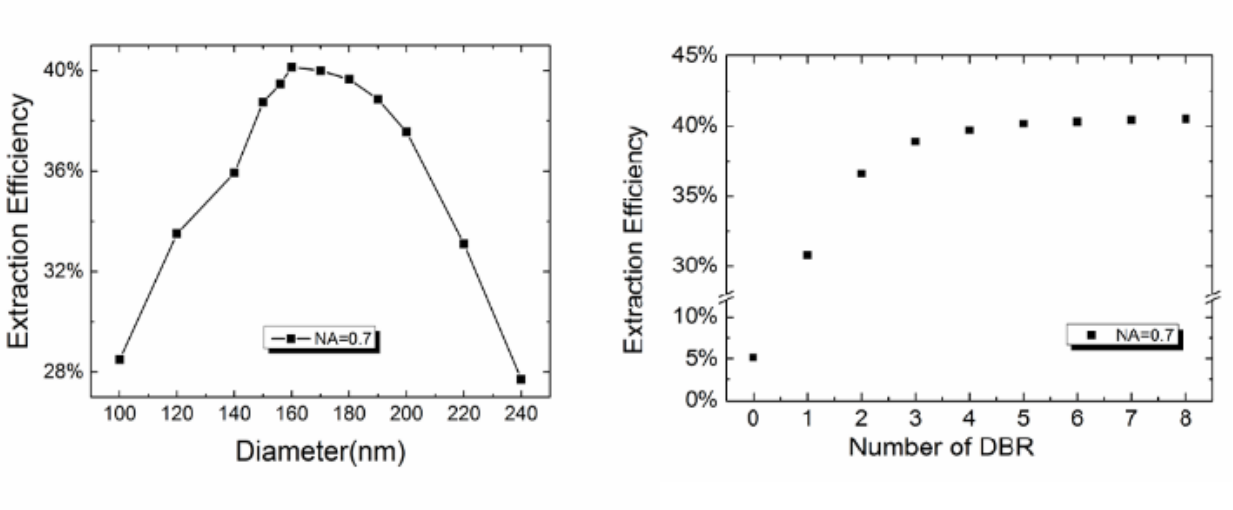

Figure A-6. Central region optimizing (left) and the DBR rings number optimizing (right) of the efficient structure design.

If we can attach a mirror on the bottom of the 5 rings DBR structure, even higher collection efficiency could be achieved as figure A-7. These simulation results show that we can achieve an optimized efficiency of 69.4% for collection in an NA of 0.7, which is comparable to the calculated values for the aforementioned 2nd order DBR structure [141] and the largest reported collection efficiencies to date using trumpet-

like photonic wires on mirrors. [54]

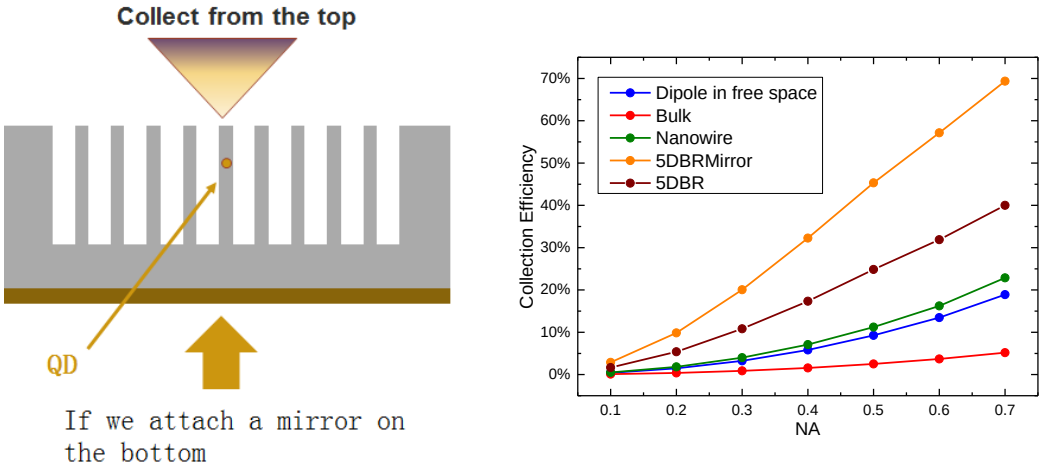

Figure A-7. The 5DBR structure with a mirror attached to the bottom (left) and the efficiency results of this structure with different numeral apertures (right).

Also, we simulate the structure shown in figure A-8. (left) with different etching depths of the DBR rings, and the results in figure A-8. (right) demonstrate that the collection efficiency of the 5DBR structure attached to a mirror can reach ~70% when the etching depth is larger than 150nm. These results provide an important guide to the future fabricate work.

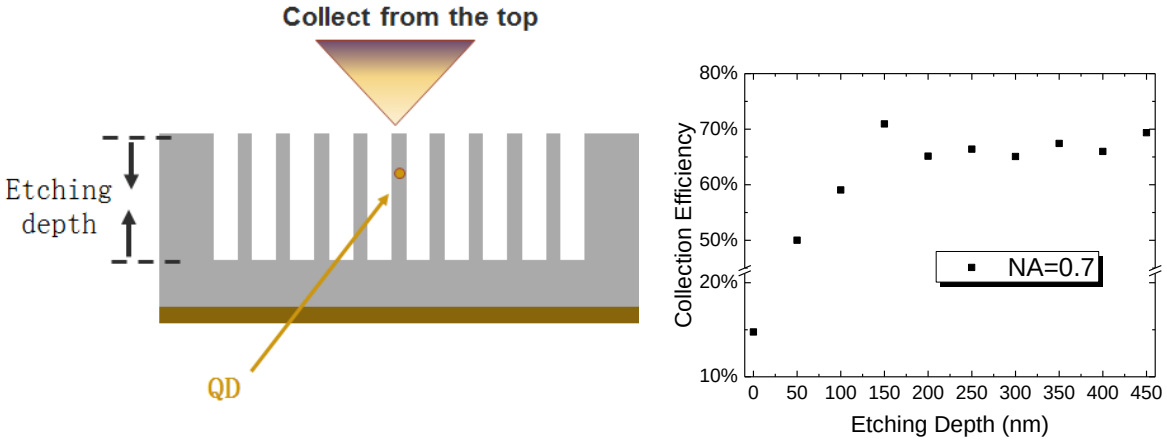

Figure A-8. The collection efficiency from the 5DBR structure attached a bottom mirror with different etching depth.

A.3 Tolerance for the Imperfect Fabrication

There are a lot of previous reports on the vertical etching fabrication of Nitride material. The most useful technique is called as hydrogen environment anisotropic thermal etching (HEATE). [145]

As those results demonstrated that it is possible to cause some kinds of imperfect fabrication during the vertical etching. So it is important to discuss the tolerance of the imperfect fabrication for the efficient structure we designed. This discussion including two probable imperfect fabrication, the imperfect alignment of the position of the quantum dot and the etching edge angle during vertical etching fabrication.

A.3.1 Imperfect Alignment of Quantum Dots

Before the fabrication of the efficient structure in the bulk material, we should locate the accurate position of the quantum dot, and target the center of the DBR rings to that. During this work, there would be a position shift from the quantum dot to the center of DBR rings. We named it as alignment error and calculated the efficiency with that.

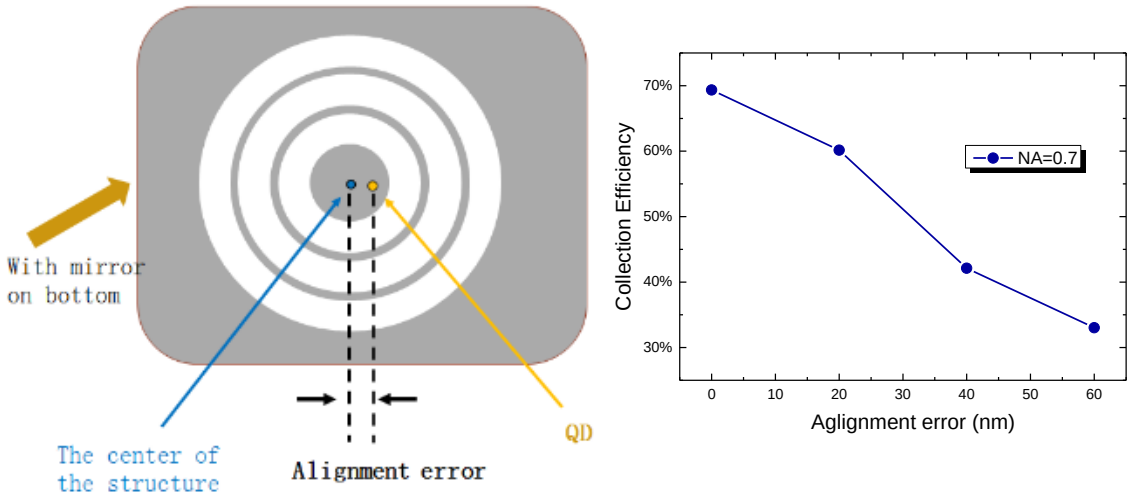

Figure A-9. The sketch map of the alignment error during the fabrication of our structure design (left), the collection efficiency with different alignment errors.

The results in figure A-9 illustrate that even the alignment error is 60nm (compared with the diameter of the central region equals to 160nm), the collection efficiency is still above 30%, which is also much efficient than the nanowire structure based on results in figure A-3.

A.3.2 Imperfect Vertical Etching Edges

On the other hand, after the vertical etching, there would be possible to have a small angle between the air-nitride surfaces of the DBR rings and the vertical direction as shown in figure A-10 (left), and this etching edge angle is usually positive. It should be useful to simulation the cases with small etching angle to consider the imperfect etching.

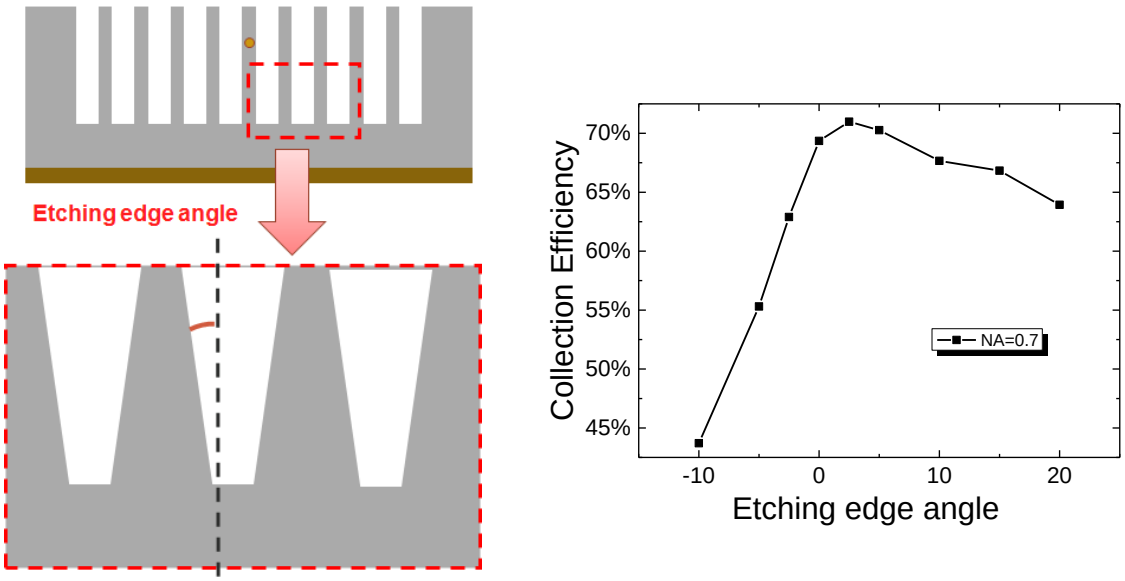

Figure A-10. The sketch map of the edge angle caused by the imperfect vertical etching of our structure design (left), the collection efficiency with different etching edge angle.

Figure A-10 illustrates the collection efficiency with different etching edge angles from -10 degree to +20 degree. The results demonstrate that small errors in the etching edge angle do not affect the efficiency too much. Even with small positive etching edge angle, which is the most probable imperfect vertical etching result, the efficiency seems a little better (more than 70%).

A.4 Concluding Remarks

We present the design of a bullseye-like structure to increase the collection efficiency of the single photon source based on III-Nitride interface fluctuation quantum dot considering fabrication issues, which is based on radial 5 quarters wavelength Nitride-Air gap DBRs around a central waveguide structure on a planar mirror to efficiently out-couple photon emission into the desired direction. These DBR structures are used as they are relatively large (582nm period size including 157nm width nitride section and 425nm width air section) and can, therefore, be fabricated more easily, whilst still presenting stop-band of width 46nm.

We use FDTD calculations to simulate the structures with commercially available software. Our simulation results show that we can achieve an optimized efficiency of 69.4% for collection in an NA of 0.7, representing a large increase from a QD embedded in bulk material or a nanowire structure as figure A-11.

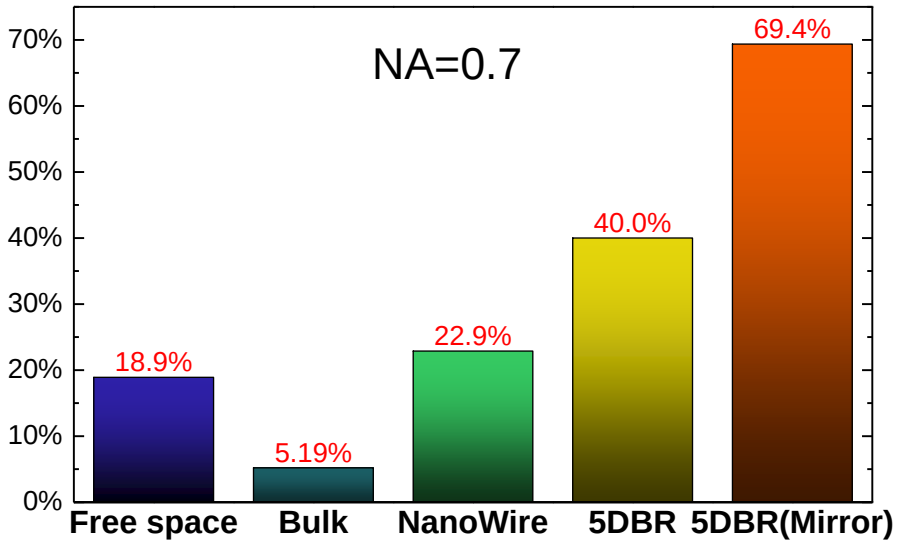

Figure A-11. The collection efficiency of the quantum dot emission from different structures in an NA of 0.7.

This value is comparable to the calculated values for the other efficient structures but should be more easily fabricated for III-nitride materials. This structure also shows a great tolerance with the different imperfect fabrications such as the alignment error and the small positive vertical etching edge angle. In the future, we will continue optimizing this efficient design and try to fabricate it.

Bibliograhpy

[1] N. Gershenfeld, Isaac L. Chuang, Quantum Computing with Molecules, Scientific American (1998).

[2] P. Benioff, The computer as a physical system: A microscopic quantum mechanical Hamiltonian model of computers as represented by Turing machines, Journal of statistical physics. 22 (5): 563–591 (1980).

[3] Y. Manin, Vychislimoe i nevychislimoe [Computable and Noncomputable], Sov. Radio. pp. 13–15. (1980).

[4] R. Feynman, Simulating physics with computers, International Journal of Theoretical Physics, 21(6): 467–488 (1982).

[5] D. Deutsch, Quantum Theory, the Church-Turing Principle and the Universal Quantum Computer, Proceedings of the Royal Society of London, A. 400 (1818): 97–117 (1985).

[6] C. Bennett, G. Brassard, C. Crépeau, R. Jozsa, A. Peres, W. Wootters, Teleporting an Unknown Quantum State via Dual Classical and Einstein-Podolsky-Rosen Channels, Physical Review Letters 70, 1895-1899 (1993).

[7] L. Vaidman, Teleportation of Quantum States, Physical Review A 49, 1473-1476 (1994).

[8] G. Brassard, S. Braunstein, R. Cleve, Teleportation as a Quantum Computation, Physica D 120 43-47 (1998).

[9] C. Bennett, G. Brassard, Quantum cryptography: Public key distribution and coin tossing. In Proceedings of IEEE International Conference on Computers, Systems and Signal Processing, 175 8. New York (1984).

[10] A. Ekert, Quantum cryptography based on Bell's theorem, Physical Review Letters, 67, pp. 661–663 (1991).

[11] S. Kako A three-stage quantum cryptography protocol, Foundations of Physics Letters, 19, 293–296 (2006).

[12] Y. Chen, et al., Embedded security framework for integrated classical and quantum cryptography in optical burst switching networks, Security and Communication Networks, 2, 546–554 (2009).

[13] I. Aharonovich, D. Englund, M. Toth, Solid-state single-photon emitters, Nature Photonics 10, 631-641 (2016).

[14] J. L. O'Brien, A. Furusawa, J. Vuckovic, Photonic quantum technologies, Nature Photonics 3, 687–

695 (2009).

[15] P. Lodahl, S. Mahmoodian, S. Stobbe, Interfacing single photons and single quantum dots with photonic nanostructures, Rev. Mod. Phys. 87, 347–400 (2015).

[16] A. Koenderink, A. Alù, A. Polman, Nanophotonics: shrinking light-based technology, Science 348, 516–521 (2015).

[17] W. B. Gao, A.Imamoglu, H. Bernien and R. Hanson, Coherent manipulation, measurement and entanglement of individual solid-state spins using optical fields, Nature Photonics 9, 363–373 (2015).

[18] T. Northup, R. Blatt, Quantum information transfer using photons, Nature Photonics 8, 356–363 (2014).

[19] M. Eisamana, J. Fan, A. Migdall, and S. Polyakov, Invited Review Article: Single-photon sources and detectors, Review of Scientific Instruments 82, 071101 (2011).

[20] T. Schmitt-Manderbach, et al., Experimental demonstration of free-space decoy-state quantum key distribution over 144 km, Physical Review Letters 98, 010504 (2007).

[21] H. Lo, X. Ma, K. Chen, Decoy state quantum key distribution, Physical Review Letters 94, 230504 (2005).

[22] K. Takemoto, et al., Quantum key distribution over 120 km using ultrahigh purity single-photon source and superconducting single-photon detectors, Scientific Reports 5, 14383 (2015).

[23] Y. Arakawa and H. Sakaki, Multidimensional quantum well laser and temperature dependence of its threshold current, Applied Physics Letters 40, 939 (1982).

[24] T. P. Pearsall, Quantum Semiconductor Devices and Technologies (KLUWER ACADEMIC PUBLISHERS 2000).

[25] Y. Toda, O. Moriwaki, et al., Efficient carrier relaxation mechanism in InGaAs/GaAs self-assembled quantum dots based on the exsistence of continuum states," Physical Review Letters, 82, 4114 (1999).

[26] C. Chunnilall, I. Degiovanni, S. Kück, I. Müller, A. Sinclair, Metrology of single-photon sources and detectors: a review, Optical Engineering, 53(8), 081910 (2014).

[27] M. Mucke, J. Bochmann, C. Hahn, A. Neuzner, C. Nölleke, A. Reiserer, G. Rempe, S. Ritter, Generation of single photons from an atom-cavity system, Physical Review A, 87, 063805 (2013).

[28] X. Ma, N. Hartmann, J. Baldwin, S. Doorn, and H. Htoon, Room-temperature single-photon generation from solitary dopants of carbon nanotubes, Nature Nanotechnology 10, 671–675 (2015).

[29] H. Eisele, A. Lenz, R. Heitz, R. Timm, M. Dähne, Y. Temko, T. Suzuki, K. Jacobi, Change of InAs/GaAs quantum dot shape and composition during capping, Journal of Applied Physics, 104, 124301

(2008).

[30] R. Brown, R. Twiss, et al., Correlation between Photons in two Coherent Beams of Light, Nature 177, 27–29 (1956).

[31] R. Brown, R. Twiss, The question of correlation between photons in coherent light rays, Nature 178, 1447–1448 (1956).

[32] S. Buckley, K. Rivoire, J. Vuckovic, Engineered quantum dot single-photon sources, Rep. Prog. Phys. 75, 126503 (2012).

[33] A. Shields, Semiconductor quantum light sources, Nature Photonics 1, 215-223 (2007).

[34] A. Ugur, S. Kremling, F. Hatami, S. Höfling, L. Worschech, A. Forchel, W. Ted Masselink, et al., Single-photon emitters based on epitaxial isolated InP/InGaP quantum dots, Applied Physics Letters 100, 023116 (2012).

[35] C. Santori, M. Pelton, G. Solomon, Y. Dale, Y. Yamamoto, et al., Triggered Single Photons from a Quantum Dot, Physical Review Letters 86, 1502 (2001).

[36] D. Bimberg et al., Quantum Dot Hetero structures (John Wiley and Sons, Chichester, 1999). For MBE growth of InAs self-assembled dots, Chap. 4.2.

[37] L. Landin, M. S. Miller, M.-E. Pistol, C. E. Pryor, L. Samuelson, et al., Optical Studies of Individual InAs Quantum Dots in GaAs: Few-Particle Effects, Science 280, 262 (1998).

[38] R. Warburton, et al., Optical emission from a charge-tunable quantum ring, Nature 405, 926 (2000).

[39] S. Kako, M. Holmes, S. Sergent, M. Bürger, D. As, and Y. Arakawa, Single-photon emission from cubic GaN quantum dots, Applied Physics Letters, 104, 011101 (2014).

[40] S. Kako, C. Santori, K. Hoshino, S. Götzinger, Y. Yamamoto, Y. Arakawa, A gallium nitride single-photon source operating at 200 K, Nature Materials 5, 887 - 892 (2006).

[41] M. Holmes, K. Choi, S. Kako, M. Arita, and Y. Arakawa, Room-Temperature Triggered Single Photon Emission from a III-Nitride Site-Controlled Nanowire Quantum Dot, Nano Letters 14, 982-986 (2014).

[42] M. Holmes, S. Kako, K. Choi, M. Arita, and Y. Arakawa, Single Photons from a Hot Solid-State Emitter at 350 K, ACS Photonics 3, 543-546 (2016).

[43] S. Deshpande, T. Frost, A. Hazari, and P. Bhattacharya, Electrically pumped single-photon emission at room temperature from a single InGaN/GaN quantum dot, Applied Physics Letters 105, 141109 (2014).

[44] K. Kao et al., Dielectric-fibre surface waveguides for optical frequencies, Proceedings of the

Institution of Electrical Engineers 113, 7, 1151 (1966).

[45] K. Takemoto, Y. Sakuma, S. Hirose, T. Usuki, N. Yokoyamaet, Japanese Journal of Applied Physics, Part 2, 43 3A (2004).

[46] C. Zinoni, B. Alloing, C. Monat, V. Zwillerb, L. H. Li, A. Fiorec, et al., Time-resolved and antibunching experiments on single quantum dots at 1300nm, Applied Physics Letters 88, 131102 (2006).

[47] M. Ward, O. Karimov, D. Unittb, Z. Yuan, P. See, D. Gevaux, and A. Shieldset, On-demand single-photon source for 1.3μm1.3μm telecom fiber, Applied Physics Letters 86, 201111 (2005).

[48] T. Miyazawa et al., the 25th International Conference on Indium Phosphide and Related Materials, MoC3-2 (Oral).

[49] Y. Sakuma, K. Taketomo, S. Hirose, T. Usuki, and N. Yokoyama, Controlling emission wavelength from InAs self-assembled quantum dots on InP (0 0 1) during MOCVD, Physica E (Amsterdam) 26, 81 (2005).

[50] T. Miyazawa, K. Takemoto, T. Nakaoka, T. Saito, S. Hirose, Y. Sakuma, N. Yokoyama and Y. Arakawa, Effect of electronic structure on single-photon emission in InAs/InP quantum dot with quasi-resonant excitation, Physica Status Solidi C 8, 2, 417 (2011).

[51] T. Miyazawa, K. Takemoto, Y. Nambu, S. Miki, T. Yamashita, H. Terai, M. Fujiwara, M. Sasaki, Y. Sakuma, M. Takatsu, T. Yamamoto, and Y. Arakawa, Single-photon emission at 1.5 μm from an InAs/InP quantum dot with highly suppressed multi-photon emission probabilities, Applied Physics Letters 109, 132106 (2016).

[52] A. Malko, M. H. Baier, K. F. Karlsson, E. Pelucchi, D. Y. Oberli, and E. Kapon, Optimization of the efficiency of single-photon sources based on quantum dots under optical excitation, Applied Physics Letters 88, 081905 (2006).

[53] H. Kumano, S. Kimura, M. Endo, H. Sasakura, S. Adachi, S. Muto, and I. Suemune, Deterministic single-photon and polarization-correlated photon pair generations from a single InAlAs quantum dot, J. Nanoelectron. Optoelectron. 1, 39 (2006).

[54] J. Claudon, J. Bleuse, N. Malik, M. Bazin, P. Jaffrennou, N. Gregersen, C. Sauvan, P. Lalanne and J. Gérard, A highly efficient single-photon source based on a quantum dot in a photonic nanowire, Nature Photonics 4, 174 (2010).

[55] T. Heindel, C. Schneider, M. Lermer, S. Hofling, S. Reitzenstein, L. Worschech and A. Forchel, Highly efficient electrically triggered quantum dot micropillar single photon source, J. Phys.: Conf. Ser. 245, 012005 (2010).

[56] M. Davanço, M. T. Rakher, D. Schuh, A. Badolato, and K. Srinivasan, A circular dielectric grating for vertical extraction of single quantum dot emission, Applied Physics Letters 99, 041102 (2011).

[57] J. Gérard et al., Very Efficient Single-Photon Sources Based on Quantum Dots in Photonic Wires. 2014 IEEE International Semiconductor Laser Conference.

[58] E. Moreau, I. Robert, J. M. Gérard, I. Abram, L. Manin, and V. Thierry-Mieg, Single-mode solid-state single photon source based on isolated quantum dots in pillar microcavities, Applied Physics Letters 79, 2865 (2001).

[59] M. Munsch, N. Malik, E. Dupuy, A. Delga, J. Bleuse, J. Gérard, J. Claudon, N. Gregersen, and J. Mørk, Dielectric GaAs Antenna Ensuring an Efficient Broadband Coupling between an InAs Quantum Dot and a Gaussian Optical Beam, Physical Review Letters 110, 177402 (2013).

[60] M. Munsch, N. Malik, E. Dupuy, A. Delga, J. Bleuse, J. Gérard, J. Claudon, N. Gregersen, and J. Mørk, Erratum: Dielectric GaAs Antenna Ensuring an Efficient Broadband Coupling between an InAs Quantum Dot and a Gaussian Optical Beam [Physical Review Letters 110, 177402 (2013)], Physical Review Letters 111, 239902 (2013).

[61] N. Livneh, M. Harats, D. Istrati, H. Eisenberg, and R. Rapaport, Highly Directional Room-Temperature Single Photon Device, Nano Letters 16, 2527-2532 (2016).

[62] M. Arita, F. Roux, M. Holmes, S. Kako and Y. Arakawa. Ultraclean single photon emission from a GaN quantum dot. Nano Letters 17, 2902-2907 (2017).

[63] "All Nobel Prizes in Physics". Nobelprize.org. Nobel Media AB. Retrieved 2016-01-19.

[64] J. Tatebayashi, S. Kako, JF. Ho, Y. Ota, S. Iwamoto, Y. Arakawa, Room-temperature lasing in a single nanowire with quantum dots, Nature photonics 9, 501-505 (2015).

[65] Y. Zhang, X. Zhang, K. Li, Y. Cheung, C. Feng, H. Choi, Advances in III-nitride semiconductor microdisk lasers, Physica Status Solidi A-Applications and Materials Science 212, 5, 960-973 (2015).

[66] A. Bao, Group III-nitride nanowires, A Materials Science and Technology 33, 7, 765-776 (2016).

[67] J. Su, G. Cui, M. Gherasimova, H. Tsukamoto, J. Hana, D. Ciuparu, S. Lim, and L. Pfefferle, Catalytic growth of group III-nitride nanowires and nanostructures by metalorganic chemical vapor deposition, Applied Physics Letters 86, 013105 (2005).

[68] G. Wang, A. Ling, X. Lv, J. Zhang, B. Zhang, III-Nitride-Based Quantum Dots and their Optoelectronic Applications, Nano-Micro Letters 3, 3, 200-207 (2011).

[69] D. Huang, Growth, Structures, And Optical Properties Of III-Nitride Quantum Dots, International Journal of High Speed Electronics and Systems, Int. J. Hi. Spe. Ele. Syst. 12, 79 (2002).

[70] N. Grandjean, B. Damilano, J. Massies, Group-III nitride quantum heterostructures grown by molecular beam epitaxy, J. Phys. Condensed Matter 13, 32, 6945–6960 (2001).

[71] J. Wierer Jr, N. Tansu, A. Fischer, and J. Tsao, III-nitride quantum dots for ultra-efficient solid-state lighting, Laser Photonics Review 10, No. 4, 612–622 (2016).

[72] A. Woolf, T. Puchtler, I. Aharonovich, T. Zhu, N. Niu, D, Wang, R. Oliver, and E. Hu, Distinctive signature of indium gallium nitride quantum dot lasing in microdisk cavities, PNAS, 111, 39, 14042–14046, doi: 10.1073/pnas.1415464111 (2014).

[73] H. Song, K. Takemoto, T. Miyazawa, M. Takatsu, S. Iwamoto, T. Yamamoto, Y. Arakawa, Design of Si/SiO2 micropillar cavities for Purcell-enhanced single photon emission at 1.55 μm from InAs/InP quantum dots, Optical Letters 38 (17), 3241-3244 (2013).

[74] D. Dalacu, K. Mnaymneh, J. Lapointe, X. Wu, P. Poole, G. Bulgarini, V. Zwiller and M. Reimer, Ultraclean Emission from InAsP Quantum Dots in Defect-Free Wurtzite InP Nanowires, Nano Letters 12, 5919-5923 (2012).

[75] M. Reimer, G. Bulgarini, R. Heeres, B. Witek, M. Versteegh, D. Dalacu, J. Lapointe, P. Poole, V. Zwiller, Overcoming power broadening of the quantum dot emission in a pure wurtzite nanowire, Physical Review B 93, 195316 (2016).

[76] B. Daudin, Polar and nonpolar GaN quantum dots, Journal of Physics: Condensed Matter, 20, 473201 (2008).

[77] H. Sekiguchi, K. Kishino, and A. Kikuchi, Emission color control from blue to red with nanocolumn diameter of InGaN/GaN nanocolumn arrays grown on same substrate, Applied Physics Letters, 96, 231104 (2010).

[78] B. Damilano, N. Grandjean, F. Semond, J. Massies, and M. Leroux, From visible to white light emission by GaN quantum dots on Si(111) substrate, Applied Physics Letters 75, 7, 962-964 (1999).

[79] S. Tomic, J. Pal, M. Migliorato, R. Young, and N. Vukmirović, Visible Spectrum Quantum Light Sources Based on InxGa1−xN/GaNQuantum Dots, ACS Photonics 2, 958-963 (2015).

[80] M. Holmes, S. Kako, K. Choi, M. Arita, and Y. Arakawa, Spectral diffusion and its influence on the emission linewidths of site-controlled GaN nanowire quantum dots, Physical Review B 92, 115447 (2015).

[81] C. Kindel, G. Callsen, S. Kako, T. Kawano, H. Oishi, G. Hönig, A. Schliwa, A. Hoffmann, and Y. Arakawa, Spectral diffusion in nitride quantum dots: Emission energy dependent linewidths broadening via giant built-in dipole moments, Physica Status solidi RRL 8, 5, 408-413 (2014).

[82] S. Sergent, S. Kako, M. Bürger, T. Schupp, D. As, and Y. Arakawa, Excitonic complexes in single zinc-blende GaN/AlN quantum dots grown by droplet epitaxy, Applied Physics Letters, 105, 14, 141112 (2014).

[83] I. Ostapenko, G. Honig, C. Kindel, S. Rodt, A. Strittmatter, A. Hoffmann, and D. Bimberg, Large internal dipole moment in InGaN/GaN quantum dots, Applied Physics Letters, 97, 063103 (2010).

[84] G. Honig, S. Rodt, G. Callsen, I. A. Ostapenko, T. Kure, A. Schliwa, C. Kindel, D. Bimberg, A. Hoffmann, S. Kako, and Y. Arakawa, Identification of electric dipole moments of excitonic complexes in nitride-based quantum dots, Physical Review B 88, 045309 (2013).

[85] C. Kindel, S. Kako, T. Kawano, H. Oishi, Y. Arakawa, G. Honig, M. Winkelnkemper, A. Schliwa, A. Hoffmann, and D. Bimberg, Exciton fine-structure splitting in GaN/AlN quantum dots, Physical Review B 81, 241309 (2010).

[86] L. Zhang, T. A. Hill, C.-H. Teng, B. Demory, P.-C. Ku, and H. Deng, Carrier dynamics in site- and structure-controlled InGaN/GaN quantum dots, Physical Review B 90, 245311 (2014).

[87] Tf.uni-kiel.de, “Zinc blende and wurtzite." 2015. 21.

[88] F. Bernardini, V. Fiorentini, and D. Vanderbilt, Spontaneous polarization and piezoelectric constants of III-V nitrides, Physical Review B, 56, R10024(R) (1997).

[89] S. Kako, Doctoral thesis, The University of Tokyo, Optical Properties of Gallium Nitride Self-assembled Quantum Dots and Application to Generation of Non-classical Light (2005).

[90] R. Bardoux, T. Guillet, B. Gil, P. Lefebvre, T. Bretagnon, T. Taliercio, S. Rousset, and F. Semond, Polarized emission from GaN/AlN quantum dots: Single-dot spectroscopy and symmetry-based theory, Physical Review B, 77, 235315 (2008).

[91] A. F. Jarjour, R. A. Oliver, and R. A. Taylor. Physica Status Solidi A, 206, no. 11, 2510-2523 (2009).

[92] S. Kako, M. Miyamura, K. Tachibana, K. Hoshino, and Y. Arakawa, Size-dependent radiative decay time of excitons in GaN/AlN self-assembled quantum dots, Applied Physics Letters, 83, 984, (2003).

[93] S. Schulz, M. A. Caro, E. P. O'Reilly and O. Marquardt, Piezoelectric properties of zinc blende quantum dots, Physica Status Solidi B, 249, 3, 521-525, (2012).

[94] S. Sergent, S. Kako, M. Burger, D. J. As, and Y. Arakawa, Narrow spectral linewidth of single zinc-blende GaN/AlN self-assembled quantum dots, Applied Physics Letters, 103, 15, 151109, (2013).

[95] D. Palmer, Electronic Energy Levels in Group-III Nitrides, Comprehensive Semiconductor Science and Technology, 4, 390-447 (2011).

[96] T. Schupp, T. Meisch, B. Neuschl, M. Feneberg, K. Thonke, K. Lischka, and D. As, Droplet epitaxy of zinc-blende GaN quantum dots, Journal of Crystal Growth 312, 3235 (2010).

[97] K. Hoshino, S. Kako, Y. Arakawa, Formation and optical properties of stacked GaN self-assembled. Applied Physics Letters 85, 1262–1264 (2004).

[98] Y. Arakawa, S. Kako, Advances in growth and optical properties of GaN-based quantum dots,

Physica Status Solidi A, 203, 14, 3512-3522 (2006).

[99] K. Choi, M. Arita, Y. Arakawa, Selective-area growth of thin GaN nanowires by MOCVD, Journal of Crystal Growth 357, 58-61 (2012).

[100] K. Choi, M. Arita, S. Kako, Y. Arakawa, Site-controlled growth of single GaN quantum dots in nanowires by MOCVD, Journal of Crystal Growth 370, 328-331 (2013).

[101] Ž. Gačević, A. Das, J. Teubert, Y. Kotsar, P. Kandaswamy, Th. Kehagias, T. Koukoula, Ph. Komninou, and E. Monroy, Internal quantum efficiency of III-nitride quantum dot superlattices grown by plasma-assisted molecular-beam epitaxy, Journal of Applied Physics, 109, 103501 (2011).

[102] G. Schmidt, C. Berger, P. Veit, S. Metzner, F. Bertram, J. Blasing, A. Dadgar, A. Strittmatter, J. Christen, G. Callsen, S. Kalinowski and A. Hoffmann, Direct evidence of single quantum dot emission from GaN islands formed at threading dislocations using nanoscale cathodoluminescence: A source of single photons in the ultraviolet, Applied Physics Letters 106, 252101 (2015).

[103] Florian Le Roux, Study on Single Photon Emission from GaN Interface Fluctuation Quantum Dots, The University of Tokyo (2016).

[104] J. Vuckovic, D. Fattal, C. Santori, G. S. Solomon, and Y. Yamamoto, Direct evidence of single quantum dot emission from GaN islands formed at threading dislocations using nanoscale cathodoluminescence: A source of single photons in the ultraviolet, Applied Physics Letters 106, 252101 (2015).

[105] T. Jemsson, H. Machhadani, P. Holtz, and F. K. Karlsson, PAPER Polarized single photon emission and photon bunching from an InGaN quantum dot on a GaN micropyramid, Nanotechnology, 26, 065702 (2015).

[106] F. Le Roux, K. Gao, M. Holmes, S. Kako M. Arita & Y. Arakawa, Temperature dependence of the single photon emission from interface-fluctuation GaN quantum dots, Scientific Reports 7, 16107 (2017).

[107] R. Brouri, A. Beveratos, J. Poizat & P. Grangier, Photon antibunching in the fluorescence of individual color centers in diamond, Optics letters 25, 1294 (2000).

[108] Z. Gacevic, M. Holmes, et al., Emission of Linearly Polarized Single Photons from Quantum Dots Contained in Nonpolar, Semipolar, and Polar Sections of Pencil-Like InGaN/GaN Nanowires, ACS Photonics 4, 657–664 (2017).

[109] J. Kim, Y. Ko, S. Gong, S, S. Ko & Y. Cho, Ultrafast single photon emitting quantum photonic structures based on a nano-obelisk, scientific reports. 3, 2150 (2013).

[110] S. Deshpande, J. Heo, A. Das & P. Bhattacharya, Electrically driven polarized single-photon emission from an InGaN quantum dot in a GaN nanowire, Nature Communications 4, 1675 (2013).

[111] S. Deshpande, A. Das & P. Bhattacharya, Blue single photon emission up to 200K from an InGaN quantum dot in AlGaN nanowire, Applied Physics 102, 161114 (2013).

[112] T. Jemsson, H. Machhadani, K. Karlsson, C. Hsu & P. Holtz, Linearly polarized single photon antibunching from a site-controlled InGaN quantum dot, Applied Physics 105, 081901 (2014).

[113] F. Roux, K. Gao, M. Holmes, M. Arita, S. Kako, Y. Arakawa, High Purity Single Photon Emission from a GaN Interface Fluctuation Quantum Dot, 77th JSAP Autumn Meeting 16p-A21-8 (September 2016), Niigata, Japan.

[114] K. Gao, M. Holmes, M. Arita and Y. Arakawa, Power dependence of single photon emission dynamics from a single GaN interface fluctuation quantum dot. Accepted by Physica Status Solidi A.

[115] M. Miyamura, K. Tachibana, and Y. Arakawa, High-density and size-controlled GaN self-assembled quantum dots grown by metalorganic chemical vapor deposition, Applied Physics 80, 21, 3937-3939 (2002).

[116] T. Zhu, F. Oehler, B. P. L. Reid, R.M. Emery, R. A. Taylor, M. J. Kappers, and R. A. Oliver, Non-polar (11-20) InGaN quantum dots with short exciton lifetimes grown by metal-organic vapor phase epitaxy, Applied Physics Letters 102, 251905 (2013).

[117] J. Robinson, J. Rice, A. Jarjour, J. Smith, R. Taylor, R. Oliver, G. Andrew, D. Briggs, M. Kappers, C. Humphreys, and Y. Arakawa, Time-resolved dynamics in single InGaN quantum dots, Applied Physics Letters 83, 13, 2674-2676 (2003).

[118] S. Kako, K. Hoshino, S. Iwamoto, S. Ishida, and Y. Arakawa, Exciton and biexciton luminescence from single hexagonal GaN⁄AlNGaN⁄AlN self-assembled quantum dots, Applied Physics Letters 85, 64 (2004).

[119] Z. Gačević, A. Das, J. Teubert, Y. Kotsar, P. K. Kandaswamy, Th. Kehagias, T. Koukoula, Ph. Komninou and E. Monroy, Internal quantum efficiency of III-nitride quantum dot superlattices grown by plasma-assisted molecular-beam epitaxy, Journal of Applied Physics 109, 103501 (2011).

[120] T. Bretagnon, P. Lefebvre, P. Valvin, R. Bardoux, T. Guillet, T. Taliercio, B. Gil, N. Grandjean, F. Semond, B. Damilano, A. Dussaigne, and J. Massies, Radiative lifetime of a single electron-hole pair in GaN⁄AlN quantum dots, Physical Review B 73, 113304 (2006).

[121] E. Chernysheva, Ž. Gačević, N. García-Lepetit, H. Meulen, M. Müller, F. Bertram, P. Veit, A. Torres-Pardo, J. Calbet, J. Christen, E. Calleja, J. Calleja and S. Lazić, Blue-to-green single photons from InGaN/GaN dot-in-a-nanowire ordered arrays, EPL 111, 24001 (2015).

[122] P. Michler, A. Imamoglu, M. Mason, P. Carson, G. Strouse, and S. Buratto, Quantum correlation among photons from a single quantum dot at room temperature, Nature 406, 968-970 (2000).

[123] A. Berthelot, I. Favero, G. Cassabois, C. Voisin, C. Delalande, P. Roussignol, R. Ferreira & J. Gérard, Unconventional motional narrowing in the optical spectrum of a semiconductor quantum dot, Nature Physics 2, 759 (2006).

[124] A. Thoma, P. Schnauber, M. Gschrey, M. Seifried, J. Wolters, J. Schulze, A. Strittmatter, S. Rodt, A. Carmele, A. Knorr, et al., Exploring Dephasing of a Solid-State Quantum Emitter via Time- and Temperature-Dependent Hong-Ou-Mandel Experiments, Physical Review Letters 116, 033601 (2016).

[125] T. Legero, T. Wilk, A. Kuhn & G. Rempe, Time-resolved two-photon quantum interference, Applied Physics B 77, 797 (2003).

[126]T. Santana, Y. Ma, R. Malein, F. Bastiman, E. Clarke & B. Gerardot, Generating indistinguishable photons from a quantum dot in a noisy environment, Physical Review B 95, 201410(R) (2017).

[127] J. Smith, D. McCutcheon, J. Mork & A. Nazir., Limits to coherent scattering and photon coalescence from solid-state quantum emitters, Physical Review B 95, 201305(R) (2017).

[128] J. Smith, D. McCutcheon, A. Nazir & J. Mork. Phonon scattering inhibits simultaneous near-unity efficiency and indistinguishability in semiconductor single-photon sources, Nature Photonics 11, 521 (2017).

[129] K. Gao, I. Solovev, M. Holmes, M. Arita and Y. Arakawa, Nanosecond-scale spectral diffusion in the single photon emission of a GaN quantum dot. AIP Advances 7, 125216 (2017).

[130] R. Bardoux, T. Guillet, P. Lefebvre, T. Taliercio, T. Bretagnon, S. Rousset, B. Gil & F. Semond, Photoluminescence of single GaN⁄AlN hexagonal quantum dots on Si(111): Spectral diffusion effects, Physical Review B 74, 195319 (2006).

[131] B. Reid, T. Zhu, T. Puchtler, L. Fletcher, C. Chan, R. Oliver & R. Taylor, Origins of Spectral Diffusion in the Micro-Photoluminescence of Single InGaN Quantum Dots, Japanese Journal of Applied Physics 52, 08JE01 (2013).

[132] L. Besombes, K. Kheng, L. Marsal & H. Mariette., Few-particle effects in single CdTe quantum dots, Physical Review B 65, 121314(R) (2002).

[133] V. Türck, S. Rodt, O. Stier, R. Heitz, R. Engelhardt, U. Pohl, D. Bimberg & R. Steingrüber, Effect of random field fluctuations on excitonic transitions of individual CdSe quantum dots, Physical Review B 61, 15, 9944 (2000).

[134] H. Robinson & B. Goldberg, Light-induced spectral diffusion in single self-assembled quantum dots, Physical Review B 61, 8, R5086 (2000).

[135] G. Sallen, A. Tribu, T. Aichele, R. André, L. Besombes, C. Bougerol, M. Richard, S. Tatarenko, K. Kheng & J. Poizat. Subnanosecond spectral diffusion measurement using photon correlation, Nature

Photonics 4, 696 (2010).

[136] G. Sallen, A. Tribu, T. Aichele, R. André, L. Besombes, C. Bougerol, M. Richard, S. Tatarenko, K. Kheng & J. Poizat, Subnanosecond spectral diffusion of a single quantum dot in a nanowire, Physical Review B 84, 041405(R) (2011).

[137] G. Sallen, A. Tribu, T. Aichele, R. André, L. Besombes, C. Bougerol, S. Tatarenko, K. Kheng & J. Poizat, Exciton dynamics of a single quantum dot embedded in a nanowire, Physical Review B 80, 085310 (2009).

[138] J. Wolters, N. Sadzak, A. Schell, T. Schröder & O. Benson, Measurement of the Ultrafast Spectral Diffusion of the Optical Transition of Nitrogen Vacancy Centers in Nano-Size Diamond Using Correlation Interferometry, Physical Review Letters 110, 027401 (2013).

[139] T. Tran, S. Choi, J. Scott, Z. Xu, C. Zheng, G. Seniutinas, A. Bendavid, M. Fuhrer, M. Toth & I. Aharonovich, Room-Temperature Single-Photon Emission from Oxidized Tungsten Disulfide Multilayers, Advanced Optical Materials. 1600939 (2017).

[140] S. Empedocles & M. Bawendi, Quantum-Confined Stark Effect in Single CdSe Nanocrystallite Quantum Dots, Science 278 (5346), 2114 (1997).

[141] M. Davanço, M. T. Rakher, D. Schuh, A. Badolato, and K. Srinivasan, A circular dielectric grating for vertical extraction of single quantum dot emission, Applied Physics Letters 99, 041102 (2011).

[142] A. Taflove, Review of the formulation and applications of the finite-difference time-domain method for numerical modeling of electromagnetic wave interactions with arbitrary structures, Wave Motion, 10, 6, 547-582 (1988).

[143] Understanding the finite-difference time-domain method[J]. School of electrical engineering and computer science, Washington State University.–URL: http://www. Eecs. Wsu. Edu/~ schneidj/ufdtd/, 2010.

[144] M. Holmes, S. Kako, K. Choi, P. Podemski, M. Arita, and Y. Arakawa, Probing the Excitonic States of Site-Controlled GaN Nanowire Quantum Dots, Nano Letters 15 (2), 1047 (2015).

[145] R. Kita, R. Hachiya, T. Mizutani, H. Furuhashi and A. Kikuchi, Characterization of hydrogen environment anisotropic thermal etching and application to GaN nanostructure fabrication, Japanese Journal of Applied Physics 54, 046501 (2015).

Publication List

Scientific Journals

Published：

1. K. Gao, I. Solovev, M. Holmes, M. Arita and Y. Arakawa. “Nanosecond-scale spectral diffusion in the single photon emission of a GaN quantum dot.” *AIP Advances* 7, 125216 (2017).

2. F. Le Roux, K. Gao, M. Holmes, S. Kako, M. Arita and Y. Arakawa. “Temperature dependence of the single photon emission from interface-fluctuation GaN quantum dots.” *Scientific Reports* 7, 16107 (2017).

Accepted:

3. K. Gao, M. Holmes, M. Arita and Y. Arakawa. “Power dependence of single photon emission dynamics from a single GaN interface fluctuation quantum dot.” Accepted by *Physica Status Solidi A*.

In preparation:

4. K. Gao, M. Holmes, M. Arita and Y. Arakawa. “An efficient structure design for single photon emitters from III-Nitride quantum dot.”

5. K. Gao, H. Springbett, T. Zhu, R. Oliver, M. Holmes, and Y. Arakawa. “Ultrafast and slow temporal scale of spectral diffusion in the single photon emission from a InGaN quantum dot.”

International Conference

1. K. Gao, M. Holmes, M. Arita and Y. Arakawa. “Lifetime measurement of a single GaN fluctuation quantum dot based on its power dependent single photon emission dynamics.” *The International Conference on Nano-photonics and Nano-optoelectronics* 3-3, 2017. Yokohama, Japan.

2. K. Gao, I. Solovev, M. Holmes, M. Arita and Y. Arakawa. “Nanosecond spectral diffusion in a single photon emitting GaN quantum dot.” *The 12th International*

Conference on Nitride Semiconductors B.02.37, 2017. Strasbourg, France.

3. K. Gao, M. Holmes, M. Arita and Y. Arakawa. “An efficient structure design to increase the single photon collection efficiency from III-nitride quantum dots.” *The 24th Congress of the International Commission for Optics* Th2E-05, 2017. Tokyo, Japan.

4. K. Gao, I. Solovev, M. Holmes, M. Arita, and Y. Arakawa. “Investigation of the spectral diffusion effect in GaN interface fluctuation quantum dots.” *The 7th International Symposium on Photonics and Electronics Convergence Advanced Nanophotonics and Silicon Device Systems* P-24, 2017. Tokyo, Japan.

5. F. Le Roux, K. Gao, M. Holmes, S. Kako, M. Arita and Y. Arakawa. “Pure single photon emission and its temperature dependence from interface-fluctuation GaN quantum dots.” *The 12th International Conference on Nitride Semiconductors* G.2.1, 2017. Strasbourg, France.

Domestic Conference

1. K. Gao, M. Holmes, M. Arita, Y. Arakawa. “Increasing the photon extraction efficiency from III-nitride quantum dots.” *The 77th JSAP Autumn Meeting* 16p-A21-9, 2016. Niigata, Japan.

2. K. Gao, M. Holmes, M. Arita, Y. Arakawa. “Power dependent single photon emission dynamics of a GaN fluctuation quantum dot.” *The 64th JSAP Spring Meeting* 16p-503-12, 2017. Yokohama, Japan.

3. K. Gao, I. Solovev, M. Holmes, M. Arita, Y. Arakawa. “Measurement of the temporal scale of the spectral diffusion of a GaN interface fluctuation quantum dot.” *The 78th JSAP Autumn Meeting* 5a-A301-5, 2017. Fukuoka, Japan.

4. 高 亢、F. Le Roux、I. Solovev、M. Holmes、有田 宗貴、荒川 泰彦。「GaN 界面揺らぎ量子ドットを用いた単一光子発生の光学特性に関する研究。」第８回、光電子融合ワークショップ、P-03、2017、東京、日本。

5. F. Le Roux, K. Gao, M. Holmes, M. Arita, S. Kako, Y. Arakawa. “High Purity Single Photon Emission from a GaN Interface Fluctuation Quantum Dot.” *The 77th JSAP Autumn Meeting* 16p-A21-8, 2016. Niigata, Japan.

6. H. P. Springbett, K. Gao, T. Zhu, M. Holmes, Y. Arakawa and R. A. Oliver. “Effect of excitation conditions on the purity of quantum emission from InGaN.” *Quantum Light-Matter Interactions in Solids: towards integrated quantum photonics* 14, 2017. London, UK.

7. M. Holmes, K. Gao, F. Le Roux, 有田 宗貴、荒川 泰彦。「窒化物半導体量子ドット、単一光子発生とデバイス物理」応用物理学会、第 13 回励起ナノプロセス研究会、2018、淡路市、日本。

8. M. Holmes, K. Gao, F. Le Roux, K. Choi, S. Kako, M. Arita, and Y. Arakawa. “III-Nitride Quantum Dots as Single Photon Emitters”.Berlin18, DPG Spring Meeting and EPS-CMD27, 2018, Berlin, Germany.

9. F. Le Roux, M. Holmes, M. Arita, K. Gao, S. Kako, Y. Arakawa. “Single Photon Emission from a GaN Interface Fluctuation Quantum Dot” *The 63rd JSAP Spring Meeting* 19p-H121-3, 2016. Tokyo, Japan.

10. “Single Photon Emission from a GaN Interface Fluctuation Quantum Dot” F. Le Roux, M. Holmes, M. Arita, K. Gao, S. Kako, Y. Arakawa, *Center for Photonics Electronics Convergence Symposium* 2016. Tokyo, Japan.